



UNIVERSITAT POLITÈCNICA
DE CATALUNYA
BARCELONATECH

PROGRAMA DE DOCTORAT EN ENGINYERIA BIOMÈDICA
DEPARTAMENT D'ENGINYERIA DE SISTEMES,
AUTOMÀTICA I INFORMÀTICA INDUSTRIAL
CENTRE DE RECERCA EN ENGINYERIA BIOMÈDICA

Tesis Doctoral por compendio de publicaciones

**Muscular pattern based on multichannel surface
EMG during voluntary contractions of the
upper-limb**

Mislav Jordanić

Setembre 2017

Directores:

Miguel Angel Mañas Villanueva
Mónica Rojas-Martínez

Abstract

Extraction of neuromuscular information is an important and extensively researched issue in biomedical engineering. Information on muscle control can be used in numerous human-machine interfaces and control applications, including rehabilitation engineering, e.g., prosthetics, exoskeletons and rehabilitation robots.

Neuromuscular information can be extracted at the brain level, peripheral nerves, or muscles. Among these options, muscle interface is the only viable way of information extraction in everyday life. Although brain and nerve recordings are promising, they usually require invasive measurement and achieve relatively low extraction speed which prevents real time control. But neuromuscular information can also be inferred from recorded electrical activity generated by contracting muscle (electromyography, EMG). Even though in EMG recordings information is not obtained directly from neural cells, it contains similar information as nerve recording. Given the fact that motoneuron induces action potentials of muscle fibers, information extracted from EMG is equivalent to information extracted from corresponding motor neurons. Moreover, muscles contain multiple motor units that activate simultaneously so their electrical activity sums on the surface of the skin, resulting in a relatively high amplitude compared to the other bio-electrical signals. Therefore, due to the richness of neural information, noninvasiveness and high signal-to-noise ratio, the surface EMG is extensively used for man-machine interfacing, especially in commercial/clinical upper-limb prosthetic control.

Motivation and merit of this thesis lies in the fact that information associated with muscular pattern during exercises can be very useful in different applications such as monitoring patients' control strategies during recovery, personalizing rehabilitation processes to increase their effectiveness or to provide information to be used for control of external devices (EMG based control of prosthesis or exoskeletons).

Within this Doctoral thesis a pattern recognition approach was used to assess neuromuscular information and to identify subjects' intended motion based on multichannel surface electromyographic recordings. Research was focused on control strategies of upper-limb, both in normal subjects and in patients with impaired mobility caused by incomplete spinal cord injury. Methods which are proposed can be used for the design and monitoring of rehabilitation therapies intended for patients with neuromuscular impairment, as well for the control of external devices like rehabilitation robots, exoskeletons, prostheses and even virtual games.

Resumen

La extracción de información neuromuscular es una problemática importante y extensivamente investigada en el campo de la ingeniería biomédica. La información sobre el control muscular puede ser utilizada en numerosas interfaces hombre-máquina y en aplicaciones de control, en las cuales se incluye la ingeniería de rehabilitación, que abarca la utilización de prótesis, exoesqueletos y robots para la rehabilitación.

La información neuromuscular puede ser extraída a nivel de cerebro, nervios periféricos, o músculos. Entre estas opciones, la interfaz muscular es la única forma viable de extraer información durante la vida diaria. A pesar de que los registros de señales cerebrales y nerviosas son prometedores, normalmente se necesitan medidas invasivas y su tiempo de extracción es relativamente bajo, previniendo el control en tiempo real. Sin embargo, la información neuromuscular puede ser inferida registrando la actividad eléctrica generada por la contracción del músculo (electromiografía, EMG). A pesar de que en los registros EMG la información no se obtiene directamente por las células neurales, ésta contiene información similar a la obtenida registrando los nervios. Dado el hecho que las motoneuronas inducen potenciales de acción de las fibras musculares, la información extraída por el EMG es equivalente a la información extraída por las correspondientes neuronas motoras. Por otra parte, los músculos contienen unidades motoras múltiples que se activan simultáneamente, de modo que su actividad eléctrica se suma en la superficie de la piel, lo que da como resultado una señal con una amplitud relativamente más elevada comparada a otras señales bioeléctricas. Por lo tanto, debido a la riqueza de información neural, la no invasividad y la elevada relación señal ruido, el EMG superficial se utiliza ampliamente en interfaces hombre-máquina, especialmente en sectores clínicos y comerciales en el control prostético de la extremidad superior.

La motivación y el mérito de esta tesis reside en el hecho de que la información asociada con los patrones musculares durante diferentes ejercicios puede ser muy útil en diversas aplicaciones tales como la monitorización de las estrategias de control de pacientes durante las terapias de recuperación, la personalización de los procesos de rehabilitación para aumentar su efectividad o para proveer información que pueda ser utilizada para el control de dispositivos externos (Control de prótesis o exoesqueletos basado en EMG).

Dentro de esta tesis doctoral se utilizó un enfoque de reconocimiento de patrones para evaluar la información neuromuscular y para identificar la intención de movimiento de los sujetos basado

en registros multicanal de EMG superficial. La investigación se centró en las estrategias de control de la extremidad superior, tanto en sujetos sanos como en pacientes con movilidad reducida causada por una lesión incompleta de la médula espinal. Los métodos propuestos pueden ser utilizados para el diseño y monitorización de terapias de rehabilitación para pacientes con deterioro neuromuscular, así como para el control de dispositivos externos tales como robots para la rehabilitación, exoesqueletos, prótesis e incluso videojuegos.

*To my family. I am who they made me to be.
For the good or the bad.*

Maybe it meant something. Maybe not, in the long run, but no explanation, no mix of words or music or memories can touch that sense of knowing that you were there and alive in that corner of time and the world. Whatever it meant.

Hunter S. Thompson

Contents

Abstract	i
Resumen	ii
List of Tables	xiii
List of Figures	xv
List of Acronyms	xxi
1 Introduction	1
1.1 Anatomy of a movement: Muscle	1
1.1.1 Muscle physiology	2
1.1.2 Muscle contraction	6
1.1.3 Muscle fatigue	8
1.2 Surface electromyography	11
1.2.1 Intramuscular vs. surface electromyography	11
1.2.2 Origin of surface electromyographic signal	12
1.2.3 Recording electrodes	15
1.3 Task identification using pattern recognition	18

1.4 Application to patients with neuromuscular impairment	23
1.5 Doctoral thesis overview	26
2 Problem statement	28
2.1 Motivation	29
2.2 Objectives	31
2.3 Thesis framework	32
3 Myoelectric patterns for task identification in patients with iSCI	34
3.1 Background	35
3.2 Method	38
3.2.1 Measurements	38
Instrumentation	38
Experimental setup	39
HD-EMG recordings	40
3.2.2 HD-EMG maps and feature extraction	40
HD-EMG maps calculation	40
Feature extraction	41
3.2.3 Identification of motion intention	42
Classification	42
Short-term identification	44
Influence of time- progress on identification	44
Influence of muscle fatigue on identification	45
Statistical methods	46

3.3 Results	46
3.3.1 Short-term identification	46
3.3.2 Influence of time on identification	49
3.3.3 Influence of time on identification	49
3.4 Discussion	51
3.5 Conclusion	54
3.6 Declarations	54
3.6.1 Acknowledgements	54
3.6.2 Open Access	55
3.6.3 Competing interests	55
3.6.4 Authors' contributions	55
4 Myoelectric patterns within the group of patients with iSCI	56
4.1 Introduction	57
4.2 Methodology	60
4.2.1 Experimental protocol	60
4.2.2 HD-EMG activation maps	62
4.2.3 Identification	63
4.3 Results	66
4.3.1 Activation maps	66
4.3.2 Identification of tasks	67
4.3.3 Identification of tasks and effort levels	71
4.3.4 Classification using smaller arrays of electrodes	74
4.4 Discussion	76

4.5 Conclusions	78
4.6 Acknowledgements	79
5 A Novel feature for task identification	80
5.1 Introduction	81
5.2 Materials and methods	84
5.2.1 Instrumentation and measurement protocol	84
5.2.2 HD-EMG processing	86
5.2.3 Feature extraction	86
5.2.4 Task identification	90
5.2.5 Statistical methods	91
5.3 Results	93
5.3.1 Bandwidth and time window selection	93
5.3.2 Short-term identification	94
5.3.3 Long-term identification	97
5.3.4 Identification during fatigue	98
5.4 Discussion	99
5.5 Conclusions	100
5.6 Acknowledgments	100
5.7 Author contributions	101
5.8 Conflicts of interest	101
6 Conclusion	102
6.1 Summary	102

6.2 Main conclusions	103
6.3 Main contributions	106
6.4 Future Work	107
6.5 Publications derived from the thesis	109
6.5.1 Journal papers	109
6.5.2 Conference papers	110
Bibliography	111
Appendices	121
A Mean shift algorithm	121
B Pattern recognition	124
B.1 Linear Discriminant Analysis	124
B.2 Support Vector Machine	128
C Isometric and non-isometric task identification	134
C.1 Introduction	135
C.2 Methodology	136
C.2.1 Experimental protocol	136
C.2.2 Signal processing	137
C.2.3 Movement classification	138
C.3 Results	140
C.3.1 Activation maps	140
C.3.2 Isometric task identification	140

C.3.3	Dynamic task identification	142
C.4	Conclusions	144
C.5	Acknowledgments	145

List of Tables

4.1	Relative standard deviation of activation maps for each muscle and effort level averaged between the group of all patients (top) and group of patients with C4 level of injury (bottom).	66
4.2	Percentages of the activation maps covered by the electrode arrays in each patient. Results are presented for each muscle as mean and standard deviation within the group of all patients (top) and group of patients with C4 level of injury (bottom).	69
4.3	Identification of tasks using LDA classifier	70
4.4	Identification of tasks using SVM classifier	70
4.5	LDA identification of tasks and three effort levels	72
4.6	LDA identification of tasks and low and moderate effort levels	72
4.7	SVM identification of tasks and three effort levels	73
4.8	SVM identification of tasks and low and moderate effort levels	73
4.9	Identification of tasks using a subset of electrodes: Classification indices using a 3×3 electrode grid located randomly in each muscle. Results are averaged within the group of all patients (top) and group of patients with C4 level of injury (bottom).	75
4.10	Identification of tasks and three effort levels using a subset of electrodes: Classification indices using a 3×3 electrode grid located randomly in each muscle. Results are averaged within the group of all patients (top) and group of patients with C4 level of injury (bottom).	75

5.1 Sensitivity and precision of identification of task using IMS features averaged between patients. Identification Indices for each patient were calculated as an average of hold-out repetitions ($N = 20$) and presented in terms of mean and standard deviation.	95
5.2 Sensitivity and precision of identification of task and effort level averaged between patients. Identification indices for each patient were calculated as an average of hold-out repetitions ($N = 20$) and presented in terms of mean and standard deviation.	96
C.1 Results of the identification of isometric tasks using the Ilog features and the combination of Ilog and CG features. The results are presented as the mean and the standard deviation calculated across five subjects.	141
C.2 Results of the identification of isometric tasks and effort levels using the Ilog features and the combination of Ilog and CG features. The results are presented as the mean and the standard deviation calculated across five subjects.	141
C.3 Identification of six dynamic contractions based on the intensity features, separately for slow movements and fast movements. The results are presented as the mean and the standard deviation calculated across five subjects.	143
C.4 Identification of six dynamic contractions based on the combination of intensity and spatial features, separately for slow movements and fast movements. The results are presented as the mean and the standard deviation calculated across five subjects.	143

List of Figures

1.1	Figure describes a) hierarchical organization of the neural system for motor control and b) side view and cross section of the brain showing motor control centers. Retrieved from Widmaier et al. (2014)	3
1.2	Figure represents a schematic representation of the motor control mechanisms. Idea of a movement is conceived in the brain, and is getting to the spinal cord by neural pathways. Motor neurons exiting the spinal cord activate muscle contraction. Simultaneously, sensory information is being transmitted to the higher controlling mechanisms. Retrieved from Merletti and Parker (2004).	4
1.3	Figure shows a) cross-section of a skeletal muscle with attachment to a bone, and a) a detailed cross-section of a skeletal muscle from myofibrils to the entire muscle.	5
1.4	Figure shows a) a single motor unit with motoneuron and muscle fibers it innervates, and b) two motor units. It can be seen that muscle fibers of different motor units are intermingled. Retrieved from Widmaier et al. (2014).	5
1.5	Figure describes characteristics of different types of muscle fibers. In a) is a diagram of different muscle fibers in muscle cross section (top), and muscle tension produced by recruitment of different types of muscle fiber (bottom), whereas in b) is the illustration of the time interval during which specific muscle fibers can remain tension. It can be noted that type I fibers are activated first, generate low force level, and are resistant to fatigue. On the other hand, type IIb fibers are activated last, generate high forces, and develop fatigue fastest. Retrieved from Widmaier et al. (2014).	7

1.6 Illustration of depolarization/repolarization of the muscle fiber. Adopted from Nazmi et al. (2016).	8
1.7 Illustration of the generation of the muscle fiber action potential. Retrieved from Widmaier et al. (2014).	9
1.8 Illustration of the force and the myoelectric signal recorded on the surface of the skin during fatiguing exercise (top), and the frequency spectra of the corresponding signal (bottom) recorded at the beginning of the exercise (a), and at the time when the force started decreasing (b). Retrieved from De Luca (1984).	10
1.9 The sEMG signal is a superposition of motor unit action potentials recorded on the electrodes convoluted by the belonging motor neuron spike train. Retrieved from Farina et al. (2014a).	13
1.10 Four types of recording surface EMG signal: monopolar, bipolar, linear electrode array, HD-EMG. Figure was modified from Merletti et al. (2010).	15
1.11 Estimating the location of the innervation zone (IZ) and the conduction velocity (CV) using averaged MUAPs recorded using linear electrode array. Figure was retrieved from Merletti and Parker (2004).	16
1.12 The figure represents HD-EMG electrode that was used for recording of the database used in this thesis.	17
1.13 The figure represents the HD-EMG activation map recorded on the biceps brachii muscle during flexion. Distinct activation of the two heads can be noticed in the map. Modified from Rojas-Martínez (2012).	18
1.14 Figure shows a) dorsal view of the spinal cord. Parts of the skull and vertebrae have been cut away. In subfigure b) ventral view of the section of the spinal cord can be seen. The direction of transmission of neural activity is noted by arrows. Subfigure c) shows magnetic resonance imaging scan of cervical spine of patient with SCI. There is a fracture and dislocation at C4 vertebra, compressing spinal cord.	25

3.1 Experimental setup. a) Positioning of the electrode arrays A1-A3 during the recording. b) Anatomical landmarks and paths used for the positioning of the arrays: A1 (6 rows, 16 columns) was placed over the forearm covering Anconeus, Brachioradialis and Pronator Teres muscles, where the most proximal row of electrodes was placed 2 cm bellow the elbow crest (EC) covering all three muscles, according to Kendall et al. (1993); A2 (6 rows, 12 columns) was placed in the distal part of the upper arm with respect to the center of the line connecting fossa cubit (FC) and acromion (AC), and covering Biceps Brachii muscle; A3 (6 rows, 12 columns) was placed in the proximal part with respect to the center of the line connecting EC and AC, over Triceps Brachii. Both A2 and A3 arrays were located in accordance with SENIAM recommendations (Hermens and Freriks, 1999). Reference electrodes (R) were placed on the clavicle, wrist and shoulder of the active arm. c) Detail of the electrode arrays used in the experiment	38
3.2 HD-EMG recording flow chart: Flow chart describes recording protocol of each task. Note that the recordings order was randomly selected in each part of the protocol.	41
3.3 Identification of tasks: Average classification indices (Acc, S, P, SP) are shown for classifiers based on different sets of features (I + CG, I, and Diff). Symbol “*” indicates statistical significance ($p < 0.05$).	47
3.4 Joint identification of tasks and effort levels: Average classification indices (Acc, S, P, SP) are shown for classifiers based on different sets of features (I + CG, I, and Diff). Symbols “*” and “**” indicate statistical significance $p < 0.05$ and $p < 0.01$, respectively.	48
3.5 Identification of tasks at specific levels of effort: Sensitivity and precision are shown for classifiers based on different sets of features (I + CG, I, Diff). Each classifier was trained using contractions of all effort levels, and evaluated on contractions of specific effort levels. Symbol “*” indicates statistical significance ($p < 0.05$).	48

3.6 Time influence on the identification of tasks: Average classification indices (Acc, S, P, SP) are shown for the classifier based on the I + CG features. In blue bars "A", training and validation sets were recorded during the first part of the protocol, whereas in red bars "B" training and validation sets were recorded during first and second part of the protocol, respectively. Symbol "*" indicates statistical significance ($p < 0.05$).	49
3.7 Influence of time effect on the identification: Figure shows average classification indices (Acc, S, P, SP) for classifiers based on different feature sets (I + CG, I, Diff). Training set was recorded during the first part of the protocol, and the validation set was recorded during the second part of the protocol. Symbols "*" and "***" indicate statistical significance $p < 0.05$ and $p < 0.01$, respectively.	50
3.8 Fatigue influence on identification based on I + CG feature set: Average classification indices (Acc, S, P, SP) are shown along the endurance contraction for the classifier based on the I + CG feature set.	51
3.9 Fatigue influence on sensitivity using different sets of features: Average sensitivity along the endurance contraction is shown for classifiers based on different sets of features (I + CG, I, Diff). Symbol "*" indicates statistical significance $p < 0.05$	51
3.10 Fatigue influence on precision using different sets of features: Average precision along the endurance contraction is shown for classifiers based on different sets of features (I + CG, I, Diff). Symbol "*" indicates statistical significance $p < 0.05$	52
4.1 Experimental protocol	61
4.2 Schematic diagram of identification	65
4.3 Activation maps of different tasks at 50% MVC averaged among patients with C4 level of injury	67
4.4 Relative standard deviation maps of different tasks at 50% MVC averaged among patients with C4 level of injury	68
4.5 LDA classification within a group of all patients using intensity features.	68
4.6 LDA classification within a group of C4 patients using intensity features	69

4.7	LDA classification within a group of all patients using intensity and spatial features	71
4.8	LDA classification within a group of C4 patients using intensity and spatial features	71
5.1	Figure shows (a) the position of the arm in the mechanical brace during the recording with the marked outlines of the electrode arrays; and (b) an electrode array.	85
5.2	Feature extraction flowchart.	88
5.3	Figure shows average processing time (a) and number of estimated modes (b) of mean shift algorithm given the specific bandwidth factor in the range from 0.2 to 1.	93
5.4	Sensitivity and precision of short-term identification of (a) identification of task and (b) identification of task and effort level using bandwidth factors 0.5 and 1.0 in mean shift algorithm.	94
5.5	Sensitivity (S) and precision (P) of (a) identification of task and (b) identification of task and effort level for time windows of 50 ms, 100 ms, 150 ms, and 200 ms.	94
5.6	Sensitivity (S) and precision (P) of short-term identification of task using (a) IMS, ICG, I, and TD features, and (b) using Diff features. Results of the identification using Diff is showed in a different scale.	95
5.7	Sensitivity (S) and precision (P) of short-term identification of task and effort level using (a) IMS, ICG, I, and TD features, and (b) using Diff features. Results of the identification using Diff is showed in a different scale.	96
5.8	Figure shows sensitivity (a) and precision (b) of short-term identification of task recorded at specific effort level using IMS, ICG, I, and TD features.	97
5.9	Figure shows sensitivity (S) and precision (P) of short-term identification of task recorded at specific effort level using Diff features.	97
5.10	Sensitivity (S) and precision (P) of long-term identification of task using IMS, ICG, I, TD, and Diff features.	98
5.11	Influence of fatigue on (a) sensitivity and (b) precision of the identification of task using IMS, ICG, I, TD, and Diff features.	98

C.1	Figure shows A) measurement equipment and the position of the subject during the experimental protocol, and B) experimental plane in which the tasks were performed. Position sensors are marked by dashed rectangles.	137
C.2	Activation maps of <i>pectoralis major</i> of one of the subjects. Up. Movement from the central point a) forward, b) rightward, and c) leftward. Down. Movement toward the center from d) ahead, e) right, and f) left.	142

List of Acronyms

ANOVA	Analysis of variance
AC	Acromion
Acc	Accuracy
BCI	Brain-computer-interface
CG	Center of gravity
CV	Conduction velocity
Diff	Intensity of single differential channel
DoF	Degree-of-Freedom
EC	Elbow crest
EMG	Electroencephalography
EMG	Electromyography
FC	Fossa cubit
HD-EMG	High-density electromyography
I	Intensity of HD-EMG map
ICG	Intensity and center of gravity
iEMG	Intramuscular electromyography
IMS	Intensity and mean shift points
iSCI	Incomplete spinal cord injury
IZ	Innervation zone
LDA	Linear discriminant analysis
MS	Mean shift
MUAP	Muscle unit action potential
MVC	Maximal voluntary contraction
NoAct	No activity class
sEMG	Surface electromyography
iEMG	Intramuscular electromyography
P	Precision
PCA	Principal component analysis
RMS	Root-mean-square
RSD	Relative standard deviation
S	Sensitivity
SNR	Signal-to-noise ratio
SP	Specificity
SVM	Support vector machine
TD	Time-domain features
TDR	Total duration of contraction

Chapter 1

Introduction

1.1 Anatomy of a movement: Muscle

Performing a locomotion task is a complicated process that involves many physiological entities working in high coherence. It involves bones, tendons, nerves, and many other systems working in perfect harmony, from basic cellular and electrochemical level to highest organizational levels of the organism. Even the simplest movements are rarely performed using just one muscle. Everything we do involves high muscular coordination and constant and precise regulation. While standing, for example, muscles of the legs and the trunk are constantly simultaneously co-contracting, maintaining balance.

The neural system has an important controlling function, but the actual force required to perform a movement is generated in the muscles. A muscle is a body tissue capable of transforming chemical energy to force. There are several muscle types: smooth, building internal organs, cardiac, building the heart, and skeletal. Only skeletal muscles can be controlled voluntarily and are used in locomotion. They are usually connected to bones with tendons (collagen fibers).

The neurons controlling the movement are organized in a hierarchical fashion (Widmaier et al., 2014). In the highest level of hierarchy, a movement is conceived. Very little is known about the exact location of neurons and brain centers responsible for this task. These centers transmit the command to the middle level structures, where the task is elaborated. Simultaneously, these

middle level neurons receive the information from the receptors in muscles, skin, tendons, and joints, but also from the visual system. All this information is taken into account when deriving a movement. Planning of the movement that is about to be executed is performed with respect to the space this movement will occupy, and control signals for each muscle involved in the movement are generated. The centers involved in these tasks are located in the cerebral cortex, the cerebellum, the subcortical nuclei, and the brain stem. The information is then transmitted to the lowest level of the motor hierarchy: the spinal cord and the brain stem. At this level the information is transmitted through the motor neurons to the muscles. The selection of the exact motor neurons and the exact timings of their activations are planned. The organization and the locations of the neural system for motor control can be seen in figure 1.1, whereas the overall figure of motor control can be seen in figure 1.2.

1.1.1 Muscle physiology

The elementary building block of a muscle is a muscle cell, or a muscle fiber - *myocyte*. Each myocyte is ensheathed by *endomysium*, a connective tissue that contains nerves and capillaries. Myocytes are organized in bundles of ten to hundred fibers, which are called *fascicles*, and they are surrounded by a sheath of connective tissue, *perimysium*. A group of fascicles is finally grouped together and enveloped by connective tissue, *epimysium*, forming a muscle. Cross-section of a muscle can be seen in figure 1.3.

Sarcolema is the cell membrane of a myocyte, consisting of a lipid bilayer that contains intracellular liquid, *myoplasma*. In the myoplasma, thin and thick filaments are serially connected, forming *sarcomeres*, which are longitudinally connected in *myofibrils* that extend through entire length of the myocyte. During the shortening of muscle fibers, thin and thick filaments of sarcomeres are pulled together by cross-bridges between them. Total shortening of a myofibril is the summation of shortenings of sarcomeres of which it is composed.

Each motor neuron at the neuromuscular junction innervates several muscle fibers, forming the smallest functional unit called *motor unit*. It was firstly defined by Liddell and Sherrington in 1925 (Liddell and Sherrington, 1925; Sherrington, 1925) and is composed of a motor neuron with axon and dendrites, and muscle fibers that the axon innervates, as seen in the figure 1.4

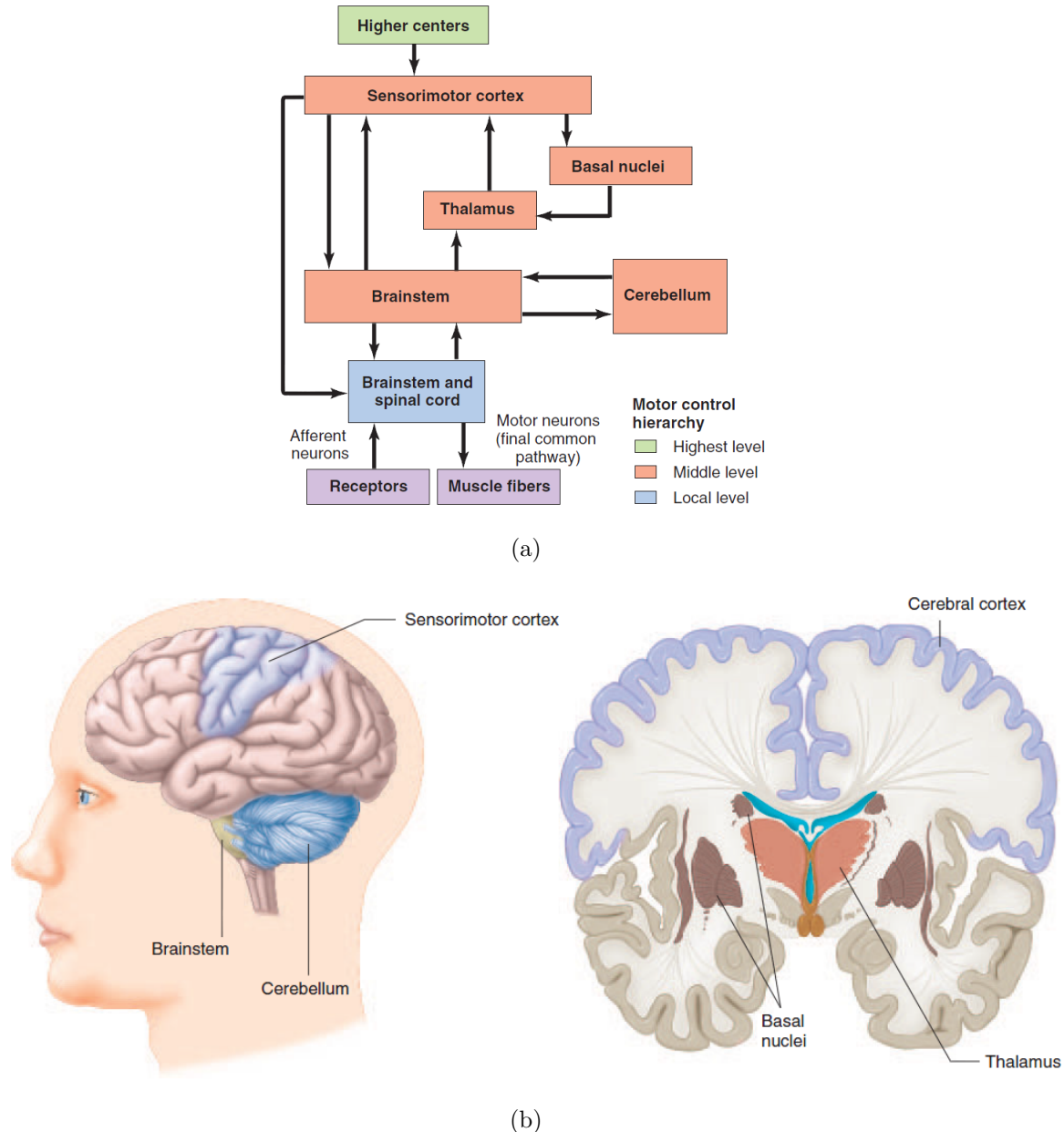


Figure 1.1: Figure describes **a)** hierarchical organization of the neural system for motor control and **b)** side view and cross section of the brain showing motor control centers. Retrieved from Widmaier et al. (2014).

(Duchateau and Enoka, 2011). Since a motor neuron with a single action potential usually evokes action potentials simultaneously in all belonging muscle fibers, by observing the action potentials of the muscle fibers, information on activity of the motor neurons in the spinal cord or the brain stem can be inferred (Merletti and Farina, 2016). However, muscle fibers belonging to the same motor neuron are not grouped together within a muscle, but are intermingled with muscle fibers belonging to other motor units (see figure 1.4b). The pool of motor neurons that

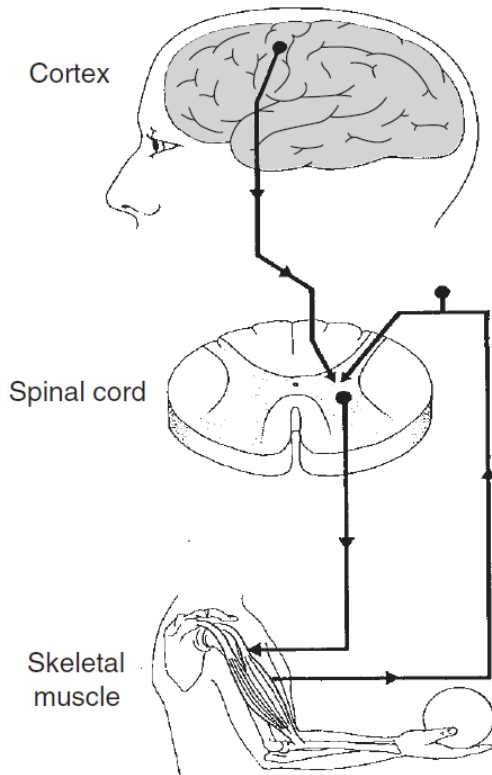


Figure 1.2: Figure represents a schematic representation of the motor control mechanisms. Idea of a movement is conceived in the brain, and is getting to the spinal cord by neural pathways. Motor neurons exiting the spinal cord activate muscle contraction. Simultaneously, sensory information is being transmitted to the higher controlling mechanisms. Retrieved from Merletti and Parker (2004).

innervates an entire muscle generally ranges from ten to a thousand, depending on the muscle (Merletti and Farina, 2016). Muscles controlled by a higher number of motor neurons can achieve finer and more precise movements, e.g. hand movements.

By the characteristics of a muscle fiber, there are three main types of muscle fibers:

Fast twitch, fatigable fibers (FF, or type IIb): These fibers have high levels of ATP (source of energy) for anaerobic energy supply, and are dominantly present in pale muscles. They are of glycolytic type and work well in ischemic or low oxygen conditions. Regarding contraction properties, they are characterized by a fast twitch, large forces, and a high nerve conduction velocity, but they get fatigued faster than the other muscle fiber types.

Fast twitch, fatigue-resistant (FR, or type IIa): These are oxidative glycolytic fibers, characterized by a fast twitch and are resistant to fatigue. They have an intermediate conduc-

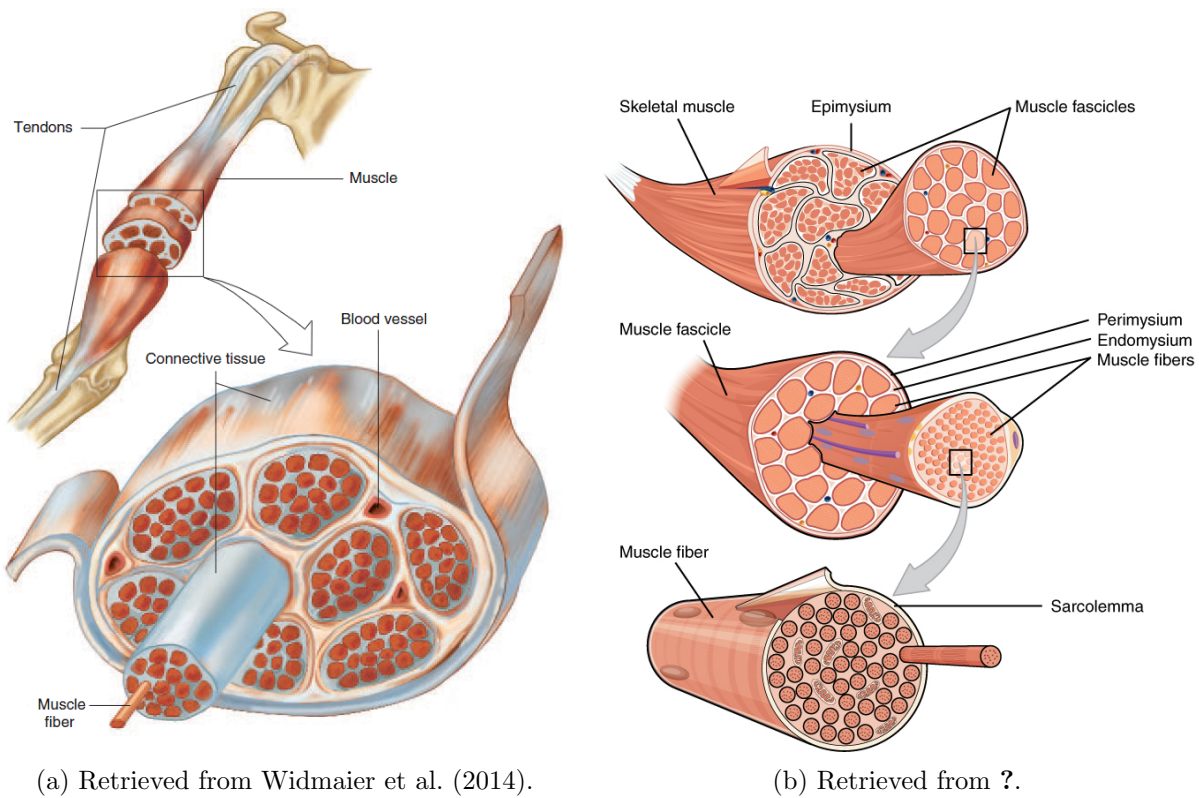


Figure 1.3: Figure shows a) cross-section of a skeletal muscle with attachment to a bone, and b) a detailed cross-section of a skeletal muscle from myofibrils to the entire muscle.

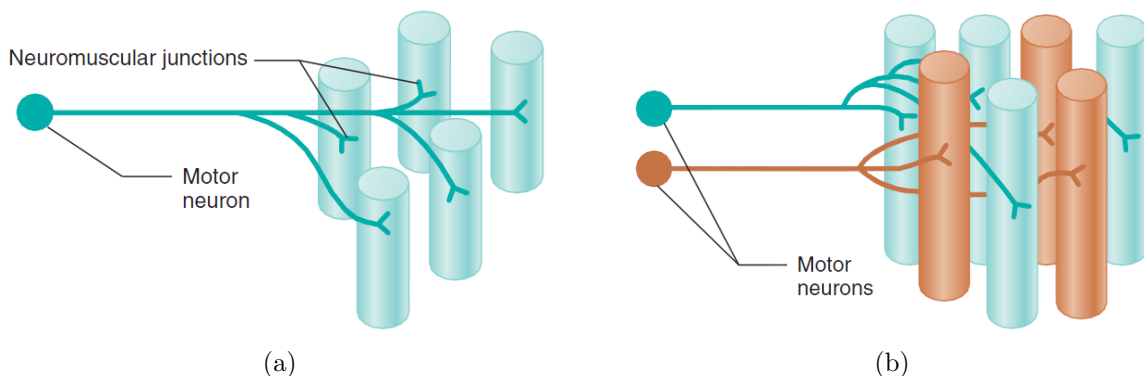


Figure 1.4: Figure shows a) a single motor unit with motoneuron and muscle fibers it innervates, and b) two motor units. It can be seen that muscle fibers of different motor units are intermingled. Retrieved from Widmaier et al. (2014).

tion velocity.

Slow twitch, very resistant to fatigue (S, or type I): They are slow oxidative fibers and do not work well in low oxygen conditions. They generate small forces, have a slow twitch, and are characterized by a lower nerve conduction velocity. This fiber type is very resilient to fatigue because of the high oxidative metabolism and energy efficiency. They are present

in a high percentage in red muscles, such as soleus.

Muscle fibers innervated by the same motor neuron have similar histochemical and contractile characteristics, and can be said that a motor unit is composed of muscle fibers of the same type (Merletti and Parker, 2004).

A force that muscle fibers generate depends on the firing frequency of the action potentials innervating the neuromuscular junction (rate coding), and the recruitment strategy by which the motor units are activated, i.e., the number of activated motor units. Therefore, the firing frequency and the recruitment strategy depend on the speed and the force of contraction. Usually type I muscle units with a low activation threshold are activated firstly, resulting in a low force and high endurance, i.e., resistance to fatigue. If a greater force is required, type II muscle units with a higher activation threshold are activated. They generate higher forces, but are also prone to fatigue (Freund et al., 1975; Merletti and Parker, 2004). This activation principle was firstly proposed by Henneman et al. in 1965, who state that the order of recruitment of motor neurons is based on the size principle, that is, neurons with smaller axons are recruited at lower effort levels and with an increase in force, larger motoneurons are recruited (Henneman et al., 1965). Therefore, type I muscle units, which have the smallest motoneurons are recruited firstly, followed by type IIa units, and finally type IIb units. The recruitment strategy and resistance to fatigue can be seen in figure 1.5.

1.1.2 Muscle contraction

Skeletal muscles are activated voluntarily by electrochemical impulses of motor neurons. The process is described in this chapter in a summarized version. For a more detailed description, the reader is pointed to medical literature (e.g. Widmaier2014).

During the stable state when there are no stimuli, i.e., in the resting state, the interior of the myocyte is at a higher electrical potential than the exterior. This difference in potential is usually around 80 mV and it is caused by the higher concentration of positive ions, namely Na^+ , outside of the sarcolemma (Nazmi et al., 2016), as shown in figure 1.6.

Motor neurons transfer nerve impulses that control the muscles from the spinal cord to the

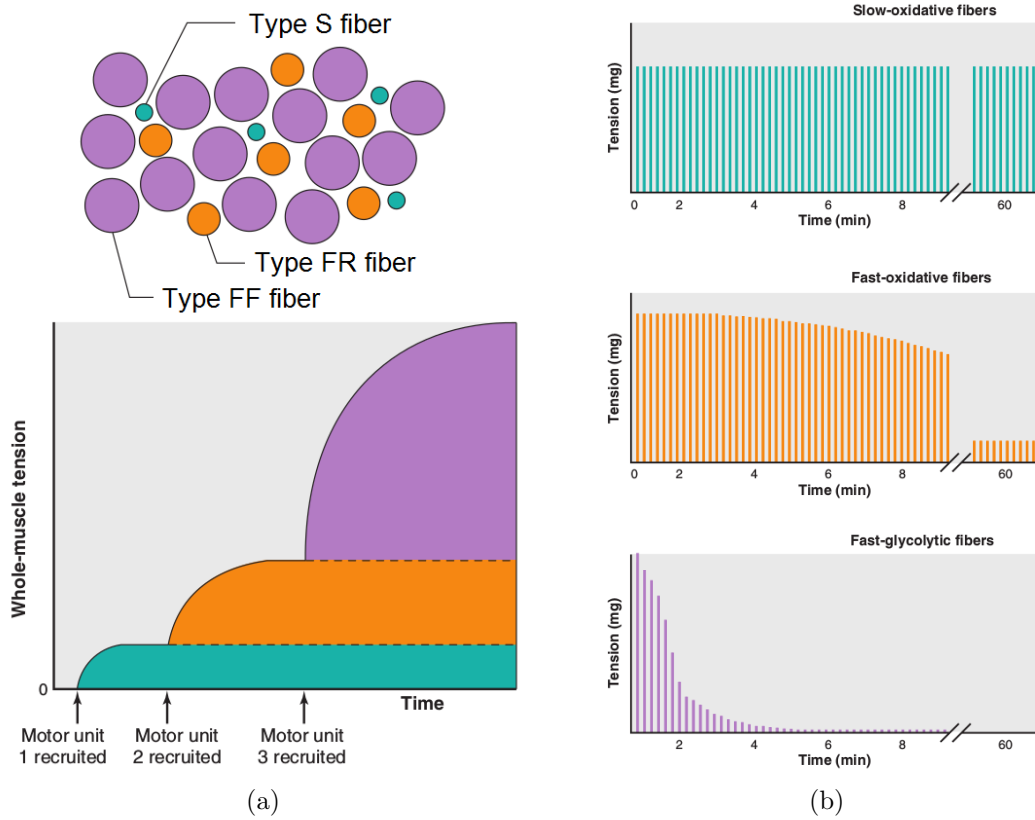


Figure 1.5: Figure describes characteristics of different types of muscle fibers. In **a**) is a diagram of different muscle fibers in muscle cross section (top), and muscle tension produced by recruitment of different types of muscle fiber (bottom), whereas in **b**) is the illustration of the time interval during which specific muscle fibers can remain tension. It can be noted that type I fibers are activated first, generate low force level, and are resistant to fatigue. On the other hand, type IIb fibers are activated last, generate high forces, and develop fatigue fastest. Retrieved from Widmaier et al. (2014).

neuromuscular junction. At the nerve endings, action potentials induce the opening of calcium channels, which enables calcium from extracellular fluid to enter the axon terminals and trigger the release of the neurotransmitter *acetylcholine*. Acetylcholine is released to the narrow space between the axon and the sarcolemma of the myocyte, and causes the sodium channels in sarcolemma to open and allow the flow of Na^+ and K^+ ions in both directions. Na^+ ions now flow into the myoplasm by diffusion due to the higher concentration of Na^+ ions outside of the membrane, but because of the similar gradient, concentrations of the K^+ ions do not change a lot. This process causes depolarization of the sarcolemma during which the outside potential of the muscle cell is at a lower voltage than the inside potential by around 30 mV. Depolarization is immediately followed by repolarization, a process during which the electrochemical balance and the resting potential of the cell are restored. It is achieved by flushing the Na^+ ions outside

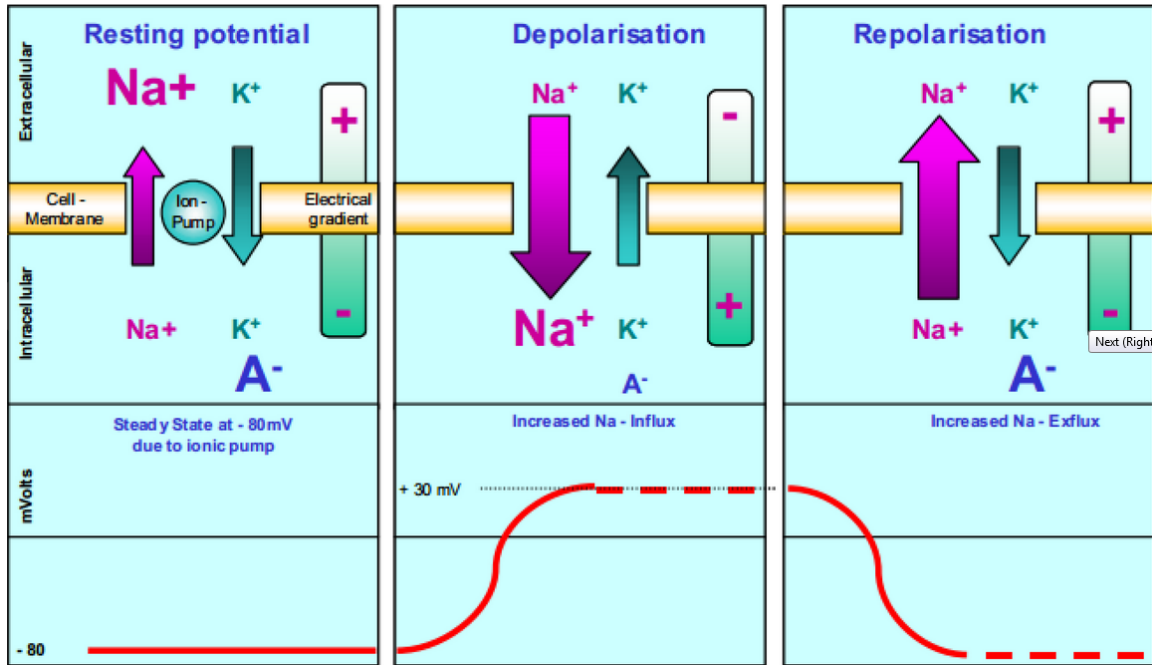


Figure 1.6: Illustration of depolarization/repolarization of the muscle fiber. Adopted from Nazmi et al. (2016).

of the sarcolemma by the *ion pump*. The process can be seen in figures 1.6 and 1.7.

If the amount of acetylcholine is sufficient for the excitation, depolarization/repolarization wave, that is, action potential, propagates longitudinally from the neuromuscular junction towards the ends of the muscle fiber causing contraction (Henneberg, 1999). Speed of the action potential propagation is called *conduction velocity* and typically ranges around 4 m/s.

Detailed analysis of muscle physiology can be found elsewhere (Squire, 1986; Widmaier et al., 2014).

1.1.3 Muscle fatigue

According to Widmaier et al. (2014), muscle fatigue is a decline in muscle tension as a result of a previous contractile activity. It is also characterized by a decreased relaxation rate and a lower shortening velocity of muscle fibers. Muscle fatigue is a continuous process that starts at the moment when the muscle unit activates. If a muscle keeps contracting long enough, eventually it will stop contracting because of the electrophysiological inability to maintain the contraction. This moment is called the *failure point* (De Luca, 1984). The failure point depends on many

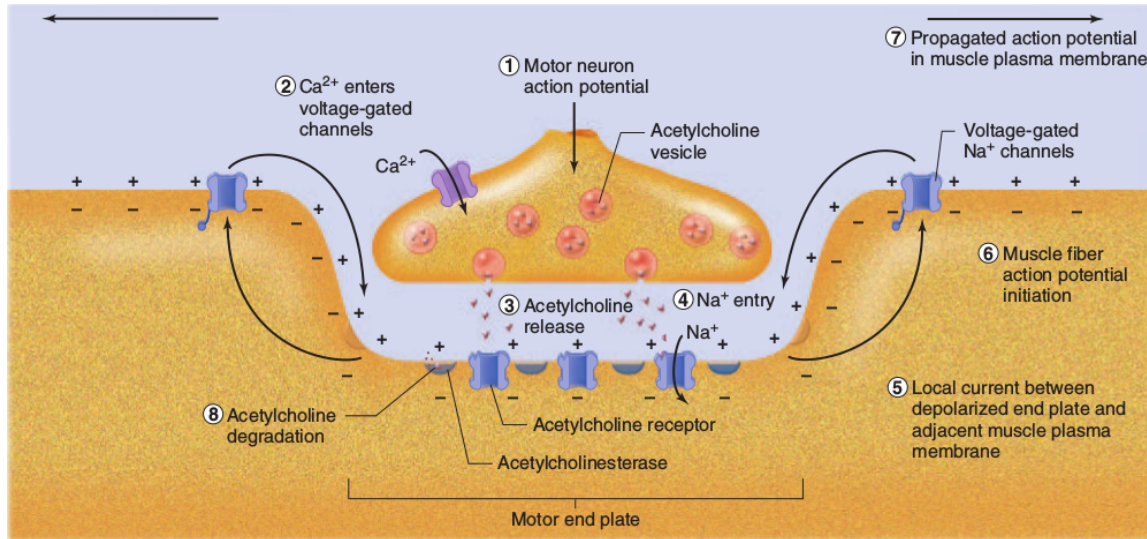


Figure 1.7: Illustration of the generation of the muscle fiber action potential. Retrieved from Widmaier et al. (2014).

different physiological characteristics, but also on the number of muscle fibers and the proportion of Type I and Type II muscle fibers. Muscles with a higher proportion of Type I fibers do not fatigue easily and recover sooner than muscles composed of type II fibers. However, type II fibers are able to generate higher forces, but are also prone to fatigue (Kupa et al., 1995), as explained in section 1.1.2.

With respect to the source of impairment, the muscle fatigue can be:

Peripheral fatigue

Peripheral fatigue occurs in the muscle itself, when muscle contraction is prevented because of an electrochemical imbalance. There are three main sources of peripheral fatigue:

- During sustained contraction, sarcolemma of the muscle fibers become acid, and this acidification lowers the muscle fiber conduction velocity (De Luca, 1984).
- High concentration of K^+ ions prevents generation of action potentials in muscle fiber (Widmaier et al., 2014).
- Buildup of adenosine diphosphate, a byproduct of muscle contraction, slows the rate of cross-bridge cycling, affecting the relaxation, and reducing the shortening velocity (Widmaier et al., 2014).

Central fatigue

Central fatigue occurs in the central nervous system that controls the movement. It is manifested as the synchronization of neural spike trains of different motor units. This synchronization occurs because the activation of more muscle units simultaneously increases the total output force of a muscle

Muscle fatigue changes characteristics of the myoelectric signal. Due to the decrease of the muscle fiber conduction velocity, caused by peripheral fatigue, and due to the synchronization of the firing times caused by central fatigue, there is a shift of energy in the frequency spectrum of the myoelectric signal towards lower frequency, as shown in figure 1.8 (De Luca, 1984). Another indicator of muscle fatigue is the increase of amplitude of the surface electromyographic signal.

This increase occurs due to two main reasons:

- The tissue between muscle fibers and the recording electrodes positioned on the surface of the skin (e.g. fat layers, skin, etc.) has low-pass filtering properties. The propagating electrical wave caused by the action potential is low pass filtered before it is recorded by the electrodes mounted on the surface of the skin. Since the power of the propagating wave shifts towards lower frequencies because of the fatigue, the amplitude of the recorded signal increases.
- Due to the synchronization of firing patterns caused by the central fatigue, the amplitude of the recorded signal increases.

There are many studies exploiting these changes in the myoelectric signal to estimate and monitor muscle fatigue. Most of the approaches are based on monitoring frequency characteristics of the signal. One of the simplest measures is the number of zero-crossings (Hägg, 1981), but because it is very sensitive to noise, it is rarely used. Mean and median frequencies are often used in literature (Lindstrom and Magnusson, 1977; Merletti and Lo Conte, 1997; Stulen and De Luca, 1981), as are more advanced time-frequency processing methods (Knaflitz and Bonato, 1999; Cifrek et al., 2000; Georgakis et al., 2003; Srhoj-Egekher et al., 2011).

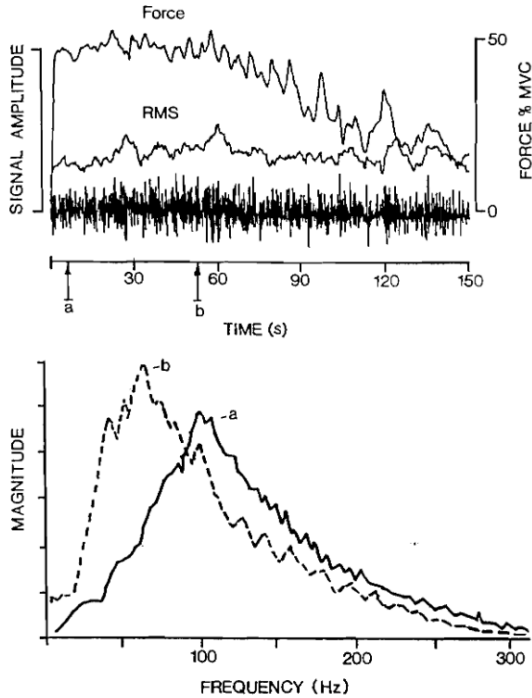


Figure 1.8: Illustration of the force and the myoelectric signal recorded on the surface of the skin during fatiguing exercise (top), and the frequency spectra of the corresponding signal (bottom) recorded at the beginning of the exercise (a), and at the time when the force started decreasing (b). Retrieved from De Luca (1984).

1.2 Surface electromyography

The muscle unit action potential (MUAP) is a combination of action potentials generated by all muscle fibers belonging to that motor unit, whereas the electromyographic signal (EMG) is a superposition of electrical activity (propagating action potentials) produced by all muscle units.

1.2.1 Intramuscular vs. surface electrmymography

There are two main types of electromyographic measurements:

Surface EMG (sEMG) This is a non-invasive type of EMG measurement where electrodes are positioned on the surface of the skin. Two types of electrodes are used: wet electrodes, which are used in combination with a conductive gel that provides high signal quality, and dry electrodes, which can be applied directly to the skin. Although wet electrodes are mostly used, the signal quality deteriorates during recording because of drying of the gel.

Since this effect is not present with dry electrodes, some authors recommend using this type of electrodes for long-term recordings (Merletti et al., 2009; Hakonen et al., 2015).

Intramuscular EMG (iEMG) This is an invasive type of recording which implies insertion of a needle or a wire electrode under the skin (Marateb et al., 1999). This type of recording is used for a precise measurement of a narrow volume, for example couple of muscle fibers. It has a high signal-to-noise ratio, but causes discomfort in subjects. It is often used in clinical practice because it can detect abnormal functionalities. For example, action potentials of spontaneously contracting single muscle fibers can be measured. These potentials are an important sign of deinnervation, but cannot be recorded using sEMG (Merletti and Parker, 2004).

Although iEMG signal usually has higher quality (in terms of signal-to-noise ratio), it was shown that similar results in the identification of upper-arm motor tasks can be obtained using both approaches (Hargrove et al., 2007). Since sEMG is non-invasive, it is usually the preferred method in myocontrol and has become a gold standard of the upper-limb prosthetics (Kamavuako et al., 2013). Moreover, although the narrow volume scope of iEMG can often be beneficial, especially in clinical applications regarding activation of a single muscle unit, it does not provide information on other parts of the muscle. For that reason, sEMG can be more appropriate because it simultaneously records action potentials of a large muscle area. Depending on the application, that can also be a serious drawback because if there are several active muscles in a small volume, myoelectric activity of both muscles will be recorded, i.e., there will be *crosstalk* between muscles.

1.2.2 Origin of surface electromyographic signal

The surface electromyographic signal is the sum of the electrical activity of muscle units recorded on the surface of the skin. From the statistical point of view, the EMG signal can be considered as a non-stationary stochastic process whose probability density function is a Gaussian function. (De Luca, 1984; ?). Since muscle fibers are activated by the impulse train of the innervating motor neurons, i.e. neural drive to the muscle, sEMG is the convolution of the motor neuron

spike trains by the motor unit action potential recorded on the electrodes (Farina et al., 2010, 2014a):

$$sEMG(t) = \sum_{i=1}^M \sum_{j=-\infty}^{+\infty} MUAP_i(t) \delta(t - t_{i,j}) \quad (1.1)$$

, where M is the number of active motor units, $MUAP_i(t)$ is the action potential waveform of the i^{th} motor unit recorded by the electrodes, and $t_{i,j}$ is the time of the discharge of the i^{th} motor neuron. This model assumes there is no interference and that the neuromuscular junction never fails, which is not the case. In the equation, $MUAP_i(t)$ is related to the electrophysiological state of the muscle fiber membranes and the conduction properties of the tissue through which the potential propagates, whereas neural information is contained in motor neuron spike trains $\delta(t - t_{i,j})$ (Farina et al., 2014b). With respect to the muscle fatigue explained in the previous section (section 1.1.3), peripheral fatigue affects $MUAP_i(t)$, whereas central fatigue has an effect on $\delta(t - t_{i,j})$ term. It is important to notice that following this model, sEMG reflects all motor control information that is present in the motor neurons. For that reason, it is more appropriate to extract motor control information carried by motor neurons using sEMG, than directly by invasive measurement of the electrical potential of the motor neuron. The advantage of the sEMG is that multiple fibers are activated simultaneously, generating a bioelectrical signal with a relatively high SNR, which can be measured on the surface of the skin. In this context, sEMG can be considered as the amplified neural signal, whereas the muscle can be considered as a biological amplifier of nerve activity (Farina et al., 2014a). Origin of the sEMG signal can be seen in figure 1.9.

Described in the frequency domain, the motor unit action potential spike train also provides the neural and the peripheral information:

$$P_{sEMG}(f) = \sum_{i=1}^M P_{ST_i}(f) |\Phi_{MUAP_i}(f)|^2 \quad (1.2)$$

, where $P_{sEMG}(f)$ is the power spectrum of the sEMG signal, $\Phi_{MUAP_i}(f)$ is the Fourier transform of the $MUAP_i$, and $P_{ST_i}(f)$ is the power spectrum of the neural spike train that innervates it, where it is assumed that spike trains are uncorrelated processes (Farina et al., 2014a).

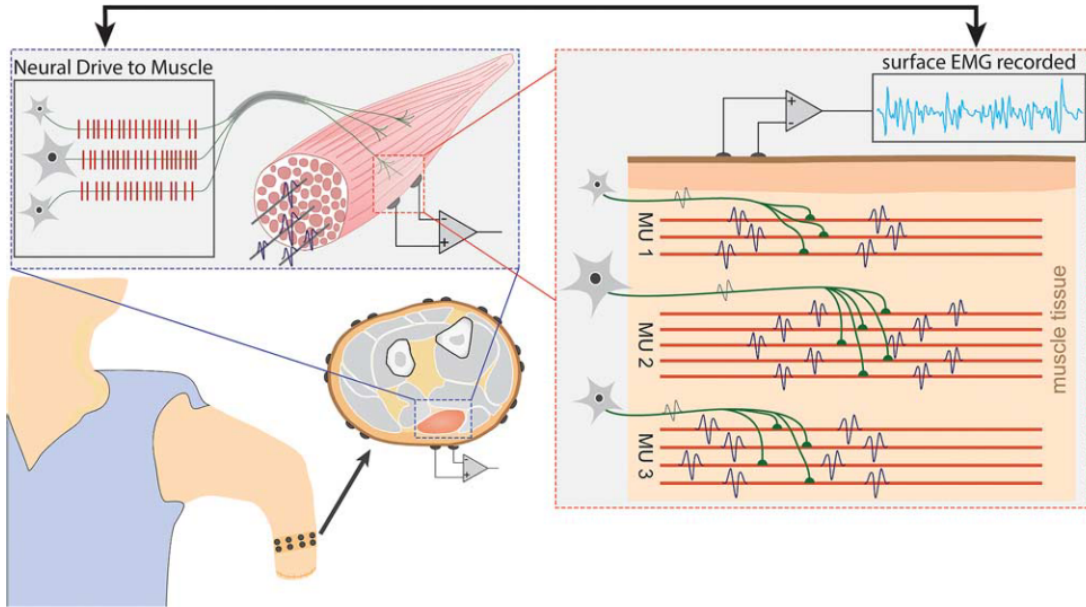


Figure 1.9: The sEMG signal is a superposition of motor unit action potentials recorded on the electrodes convoluted by the belonging motor neuron spike train. Retrieved from Farina et al. (2014a).

In case of a constant average discharge rate of spike trains, assuming that it is a stationary process, the spike train power spectrum can be calculated as (Farina et al., 2014a):

$$P_{ST_i}(f) = DR_i \left[1 - |Q_i(f)|^2 \right] + DR_i^2 |Q_i(f)|^2 \sum_{n=-\infty}^{+\infty} \delta(f - nDR_i) \quad (1.3)$$

, where DR_i is the average discharge rate, and $Q_i(f)$ is the Fourier transform of the probability density function of the inter-spike interval variability. The first term in the equation is dominant and equal to DR_i for frequencies greater than 10 - 20 Hz, as proven previously (Farina et al., 2014a). Therefore, the power spectrum of the sEMG signal can be estimated as:

$$P_{sEMG}(f) \approx \sum_{i=1}^M DR_i |\Phi_{MUAP_i}(f)|^2 \quad (1.4)$$

Power of the sEMG signal P can be obtained in the frequency domain as:

$$P = \int_0^{+\infty} P_{sEMG}(f) df \approx \sum_{i=1}^M DR_i \int_0^{+\infty} |\Phi_{MUAP_i}(f)|^2 df \approx \sum_{i=1}^M DR_i E_i \quad (1.5)$$

, where E_i is the energy of $MUAP_i$. It can be noted that the power of the sEMG is the sum of energies of action potentials of motor units weighted by their discharge rate. When the force of a contraction is increased, the power of the sEMG increases also because of the activation of additional motor units (M increases) and because of the increase of the average discharge rate of motor neuron action potentials (DR_i increases). On the other hand, when the muscle is fatigued, the conduction velocity of muscle fibers decreases and the power spectrum of the muscle fiber action potentials shifts towards lower frequencies, as explained in section 1.1.3. Due to this effect, energy of MUAPs recorded on the electrodes can increase, leading to an increase of sEMG power (E_i increases).

Given the fact that there is a large variability between shape, and amplitude of MUAP with respect to the electrode position and the tissue conduction characteristics, the association between the power of the sEMG and the neural drive can also have a very high variability, depending on the individual subject and the muscle (Farina et al., 2014a).

1.2.3 Recording electrodes

Depending on the number of electrodes used for the recording, the following classification exists: single-channel recording in a monopolar mode, single channel recording in a bipolar mode (differential recording), recording using a linear electrode array, and high-density EMG, as shown in figure 1.10.

In the single-channel monopolar recording, a single electrode is positioned over the muscle, whereas the reference electrode is positioned over the place that does not generate electrical activity. On the other hand, the single-channel bipolar electrode configuration is often used, in which a signal is the difference of potential between the two electrodes. This configuration is traditionally preferred because of the lower interference and a higher signal-to-noise ratio (Merletti and Parker, 2004). General recommendation is that the inter-electrode distance is around 20 cm (Hermens and Freriks, 1999), but the optimal distance depends on many factors, as briefly explained in (Hakonen et al., 2015). For both monopolar and bipolar single channel recordings it is recommended that the electrodes are positioned between the innervation zone and the tendon. Exact recommendations can be found in the findings of the SENIAM project

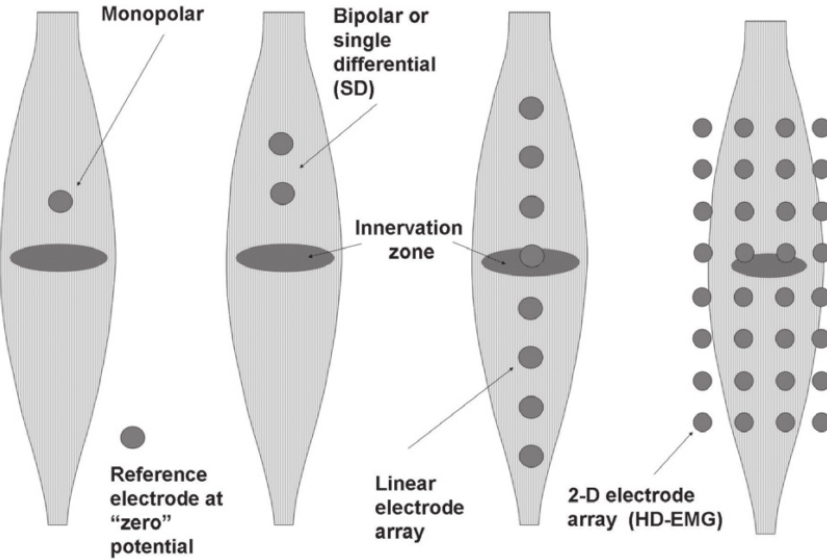


Figure 1.10: Four types of recording surface EMG signal: monopolar, bipolar, linear electrode array, HD-EMG. Figure was modified from Merletti et al. (2010).

(Hermens and Freriks, 1999).

The linear electrode array consists of multiple electrodes positioned at an equal distance along the line of muscle fibers, following the direction of the propagation of the action potentials. Measurements recorded using this type of electrodes provide more information on the muscle than a single channel recording. For example, it can be used for the estimation of the conduction velocity, as shown in figure 1.11 (Merletti and Parker, 2004).

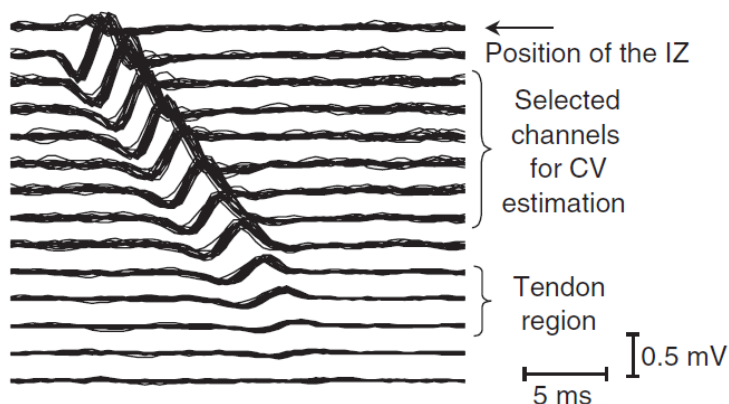


Figure 1.11: Estimating the location of the innervation zone (IZ) and the conduction velocity (CV) using averaged MUAPs recorded using linear electrode array. Figure was retrieved from Merletti and Parker (2004).

Technological advancement of the EMG acquisition systems enables the use of high-density

electromyography (HD-EMG) (Zwarts et al., 2004). Using an array of closely spaced electrodes organized in a quadrature grid, multiple EMG channels are recorded over the wide area of the muscle. The electrodes used for the HD-EMG recording can be seen in figure 1.12. This type of a recording is more reliable because it can record activations in different parts of the muscle and increase redundancy. HD-EMG is the only EMG recording approach that allows insights into the spatial distribution of motor units in a muscle. By observing the amplitude or the intensity of signals recorded in different channels, it is possible to analyze how different muscle regions activate depending on the joint position (Vieira et al., 2010), the contraction level (Holtermann et al., 2005), and the duration of movement and fatigue (Tucker et al., 2009; Staudenmann et al., 2014). Moreover, since muscles do not activate homogeneously, sEMG recorded using a single channel has some serious drawbacks, which can be overcome by using 2D electrode arrays. For example, Zwartz and Stegeman pointed out that the single channel EMG disregards important spatial aspects of MUAP propagation, which are essential for the force-generating capacity of the muscle, and, if not well addressed, can lead to incorrect conclusions (Zwarts and Stegeman, 2003).

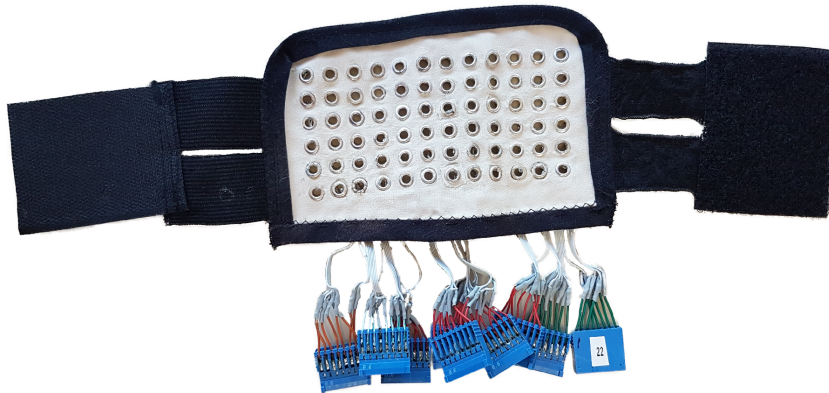


Figure 1.12: The figure represents HD-EMG electrode that was used for recording of the database used in this thesis.

In addition, the activation of individual motor units, i.e. individual motor neuron spike train, can be extracted from the HD-EMG recordings using blind source separation methods (Holobar and Zazula, 2007; Holobar et al., 2010), which can be a valuable information in the force estimation because the motor unit recruitment and the firing frequency depend primarily on the force level (Merletti and Parker, 2004). Several authors have used this approach instead of the traditional

one based on the intramuscular (invasive) EMG. One of the obvious advantages of this method is that it is safe and not painful. Using this technique, Holobar et al. were able to extract 6 to 7 motor units starting from contractions at 5% of maximal voluntary contraction (MVC) and up to 20% MVC with associated discharge rates between 10 pps and 12 pps (Holobar et al., 2010). However, one of the current limitations is that it can only be performed during isometric contractions and the intensity of isometric contraction must remain constant during the measurement.

HD-EMG recordings also allow calculation of two-dimensional activation maps where intensity of each pixel represents the intensity of a corresponding EMG channel (see figure 1.13). Consequently, the information on spatial distribution of the EMG intensity over the muscle is provided. Recent studies show that changes in the spatial activation pattern are related to the duration of movement and fatigue (Tucker et al., 2009; Staudenmann et al., 2014), the position of joint (Vieira et al., 2010) and the level of contraction (Holtermann et al., 2005). Furthermore, these HD-EMG activation maps can also be used to determine multiple innervation zones (Marateb et al., 2016).

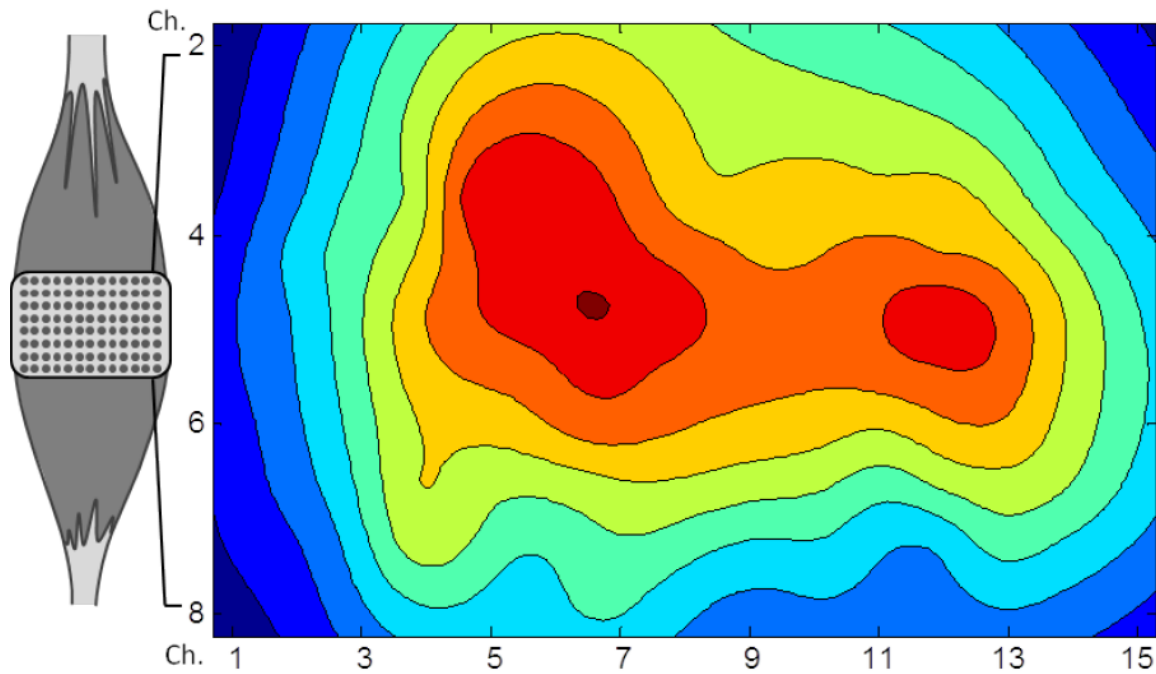


Figure 1.13: The figure represents the HD-EMG activation map recorded on the biceps brachii muscle during flexion. Distinct activation of the two heads can be noticed in the map. Modified from Rojas-Martínez (2012).

Moreover, these HD-EMG activation maps also proved to be valuable in the task identification using pattern recognition. Spatial characteristics of HD-EMG change depending on the task, but also depending on the force the subject is applying, and form repeatable muscle activation patterns that can be used in the identification of the motion intention (Rojas-Martínez et al., 2012).

However, HD-EMG can be corrupted by low quality channels, which are a common issue in measurements due to well-known artifacts, such as: electrode displacement, bad electrical contact between skin and the electrode, movement of cables, electromagnetic interference, etc. (Clancy et al., 2002). Affected channels differentiate themselves in amplitude and spectral content. To cope with this problem, Rojas-Martínez et al. developed an expert system for detection, removal and interpolation of HD-EMG channels corrupted by artifacts (Rojas-Martínez et al., 2012). On the other hand, Ghaderi and Marateb used image inpainting and surface reconstruction methods to reconstruct the corrupted activation map (Ghaderi and Marateb, 2017).

1.3 Task identification using pattern recognition

Given the one to one relationship between the neural commands and the activation of motor units in the muscles, surface electromyography (sEMG) has been used for more than a half of century as a noninvasive and natural way of extracting motor control information for identification of motion intention. Such information can be used in numerous applications in rehabilitation engineering, e.g., prosthetics (Li et al., 2010; Young et al., 2013; Stango et al., 2015), exoskeletons (Vaca Benitez et al., 2013) and rehabilitation robots (Dipietro et al., 2005; Marchal-Crespo and Reinkensmeyer, 2009; ?).

Ideally, a system for the identification of motion intention should fulfill the following criteria (Farina et al., 2014a):

- should provide simultaneous activation of multiple degrees of freedom
- should provide proportional control
- should be insensitive to changes in electrode - skin impedance,

- should be adaptive to changes during the use, i.e. fatigue, electrode-skin impedance change due to sweating and drying of conductive gel
- should be insensitive to precise position of electrodes
- should have fast and easy training procedure (ideally none)
- should provide real time identification, i.e. time delay less than 300 ms (Oskoei and Hu, 2007)
- should have low computation complexity which enables implementation in a battery-powered device

In most of the commercial prosthesis (Parker and Scott, 1986), sEMG of two muscles is recorded. In this simple scheme a single Degree-of-Freedom (DoF) can be controlled: the EMG amplitude of one muscle controls the output of one direction, whereas the EMG amplitude of the other muscle controls the other direction. If a prosthesis needs to operate in multiple DoFs, a subject needs to switch between active DoFs either by co-contraction, or by pressing a switch button. In any case, the method is not intuitive nor efficient for the user (Farina et al., 2014a).

Pattern recognition is an alternative to conventional control algorithms and has been extensively used in research institutions during the last decades (Hakonen et al., 2015; Farina et al., 2014a; Nazmi et al., 2016). The prerequisite of using pattern recognition for task identification is the presence of a pattern that can be extracted from the EMG signal. Major advancement over conventional switching myocontrol is the possibility of instant selection of any of the predefined movements.

However, although pattern recognition improves the possibilities of extraction of motion intention, it has several serious limitations. Therefore, there is still a large gap between use of pattern recognition in research and in practice in rehabilitation institutes and in users' homes (Jiang et al., 2012). The pattern recognition approach does not support proportional and simultaneous control for multiple motor tasks. Any task that requires more than one DoF must be performed sequentially. This type of control prevents the user from achieving a fluid movement, but also demands planning of movement execution. However, several authors recently proposed solutions which enable simultaneous control (Young et al., 2013; Kamavuako et al., 2013; Baker et al.,

2010). For example, Young et al. propose a system of parallel classifiers that use conditional probabilities to separate between combination of tasks (Young et al., 2013). On the other hand, there are also publications proposing solutions for the proportional control. Fougner et al. prepared a review on the topic (Fougner et al., 2012). The main idea behind this approach is that the muscle force can be estimated using the EMG signal (Staudenmann et al., 2010).

On the other hand, one of the disadvantages of pattern recognition is the fact that in spite of the high accuracy, an error could lead to a completely unwanted task. Furthermore, although the identification rate is usually very high during the stationary task, errors often occur during transition between tasks. These problems can be partially prevented by, for example, employing the majority voting principle (Englehart and Hudgins, 2003), or the decision-based velocity ramp that attenuates the velocity of a movement after the change of a task (Simon et al., 2011).

Although crosstalk is usually considered as a negative interference in electromyography, if it is consistent and repeatable, some authors argue that it can provide a discriminative power in task identification (Farina et al., 2014a). However, for some approaches it has a negative influence (He et al., 2015). To resolve this issue, source separation methods can be used to separate EMG activity of adjacent muscles (Farina et al., 2004; Holobar and Farina, 2014). This can be a powerful tool in task identification (Naik et al., 2007), because it could separate contributions of individual muscles in the myoelectric signal, and, therefore, minimize crosstalk effect from nearby muscles. Consequently, extracted features would characterize only the target muscles.

According to Oskoei et al. pattern-recognition-based task identification approach includes four main modules (Oskoei and Hu, 2007):

Data segmentation:

Comprises various techniques and methods that are used to handle data before feature extraction. Recording must be divided in time segments on which identification will be performed. Selection of duration of time segment has an effect on the identification. Features calculated on wider segments usually have lower variability, and, consequently, higher repeatability and a stronger pattern, which increases the identification rate. On the other hand, the output of the classifier should be as fast as possible in order to be used in real time. Therefore, the shorter the window, the shorter the response time will

be. General recommendation is that the total delay of the system should be less than 300 ms (Oskoei and Hu, 2007; Englehart and Hudgins, 2003).

Feature extraction:

This module computes preselected features for classification. Selection and extraction of features is one of the most critical stages in myoelectric control design and there are many features suggested in the literature.

Classification:

A classification module recognizes signal patterns, and classifies them into predefined categories. Due to the complexity of biological signals, and the influence of physiological and physical conditions, the classifier should be adequately robust.

Controller:

Generates output commands based on the output of the classifier and control schemes. Post-processing methods are often included in this module. For example, majority voting is often applied after classification to eliminate destructive jumps and to make a smooth output.

Many studies agree that the selection of the pattern recognition technique does not have a big influence on the task identification (Hakonen et al., 2015). Therefore, simple and fast classifiers are preferred. Linear discriminant analysis has become the 'gold standard' in the field of myoelectric control because of these properties (Tkach et al., 2010; Li et al., 2014; Hakonen et al., 2015). Although this classifier assumes multivariate normal distribution of classes, experiments proved that it performs well even if the normality assumption has not been met (Grouven et al., 1996).

Features, on the other hand, have a major influence on the identification results (Englehart et al., 1999; Tkach et al., 2010). Therefore, there are many features proposed in the literature focused on improving the rate of identification of motion intention:

Time domain features:

Mean absolute value (Hudgins et al., 1993), integrated EMG (Park and Lee, 1998), variance (Park and Lee, 1998; Zardoshti-Kermani et al., 1995), root mean square (Farrell and Weir,

2008), waveform length (Hudgins et al., 1993), zero crossing (Hudgins et al., 1993), log detector (Tkach et al., 2010), Wilson amplitude (Zardoshti-Kermani et al., 1995), slope sign change (Hudgins et al., 1993), autoregressive coefficients (Hargrove et al., 2007), cepstral coefficients (Park and Lee, 1998), mean absolute value slope (Phinyomark et al., 2012a), histogram of EMG (Phinyomark et al., 2012a; Zardoshti-Kermani et al., 1995)

Frequency domain features:

Mean frequency (Phinyomark et al., 2012b), median frequency (Phinyomark et al., 2012b), modified mean frequency (Phinyomark et al., 2009)

Time-frequency domain features:

Short time Fourier transform (Englehart et al., 2003, 2001), continuous wavelet transform (Englehart et al., 2003, 2001), discrete wavelet transform (Englehart et al., 2003), stationary wavelet transform (Englehart et al., 2003), wavelet packet transform (Englehart et al., 2003, 2001; Chu et al., 2006)

Spatial domain features:

Experimental variogram (Stango et al., 2015), center of gravity (Rojas-Martínez et al., 2012, 2013)

Time domain features are commonly used because they achieve high identification accuracy and are computationally efficient (Hakonen et al., 2015).

Since spatial distribution contains a lot of information on the muscle, features derived from this information are acknowledged as valuable in the identification of motion intention (Stango et al., 2015; Hakonen et al., 2015; Rojas-Martínez et al., 2013). For example, Stango et al. (Stango et al., 2015) used spatial characteristics of HD-EMG recording of the forearm muscles to identify 8 hand and wrist tasks (4 degrees of freedom). They fed the support vector machine classifier with a statistical measure of spatial correlation, i.e. variogram and achieved high identification results (95% accuracy). Furthermore, they proved that proposed spatial features are robust to the electrode shift.

Most of the pattern recognition identification methods are subject-specific. They usually achieve very high identification results, but require a time consuming training procedure for every patient

individually. This could be avoided by building a single identifier for a group of patients, i.e. a group-specific identifier. However, inter-subject variability is a big concern in the design of a group-specific pattern recognition-based identifier. Individuals differ from each other in a lot of physiological parameters, e.g., conductivity of subcutaneous tissue, and limb dimension. Nevertheless, by comparing HD-EMG activation maps between normal subjects it has been shown that inter-subject activation patterns exist for different tasks and levels of contraction (Rojas-Martínez et al., 2012).

Rojas-Martínez et al. demonstrated that by using intensity and spatial features extracted from activation maps it is possible to construct an inter-subject identification method based on the LDA classifier not only for different tasks, but also for different effort. Authors reported that in healthy subjects identification performance improves by adding spatial features in the identification, which proves that spatial distribution is less sensitive to inter-subject variability. They achieved a sensitivity higher than 75% for identification of four upper-limb tasks at three different effort levels and more than 90% sensitivity when identifying only four tasks, regardless of the effort level. Also, they reported higher classification results when using classification in two steps (in the first step the task is classified, and in the second step the level of effort), rather than a single step classification.

1.4 Application to patients with neuromuscular impairment

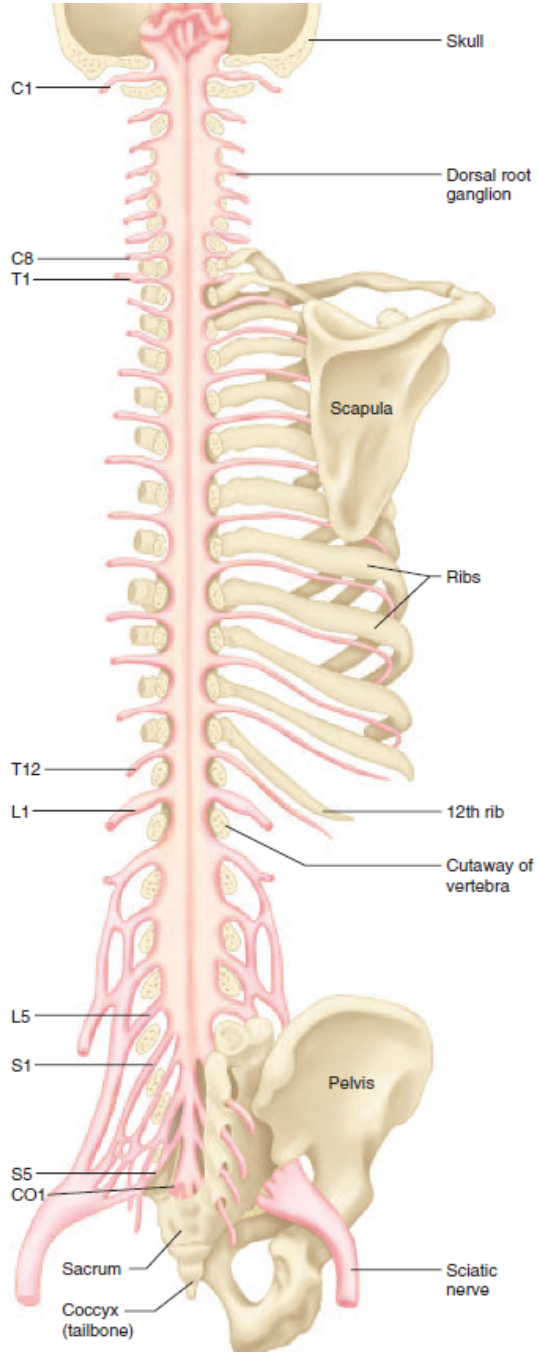
Physical injury to the brain, spinal cord, or nerves, is usually the cause of neurological disorders. According to World Health Organization, each year there are 500 000 spinal cord injuries and 15 million strokes (of which 5 million result with death and 5 million with permanent disability) every year. Furthermore, the number of people who are older than 60 years will increase to 22% of the world population by 2050 and will count 2 billion people. Unfortunately, in affected patients motor control can be impaired as a result of damaged nerves and they often suffer from uncoordinated movements, lack of force, and spasticity. Common manifestations of upper extremity motor impairment include muscle weakness, impaired motor control, and changes in muscle tone. These impairments induce disabilities in common daily life tasks like reaching and holding objects. During the recovery process, rehabilitation robots that stimulate neuroplas-

ticity are commonly used (Vaca Benitez et al., 2013; Dipietro et al., 2005; Marchal-Crespo and Reinkensmeyer, 2009; ?).

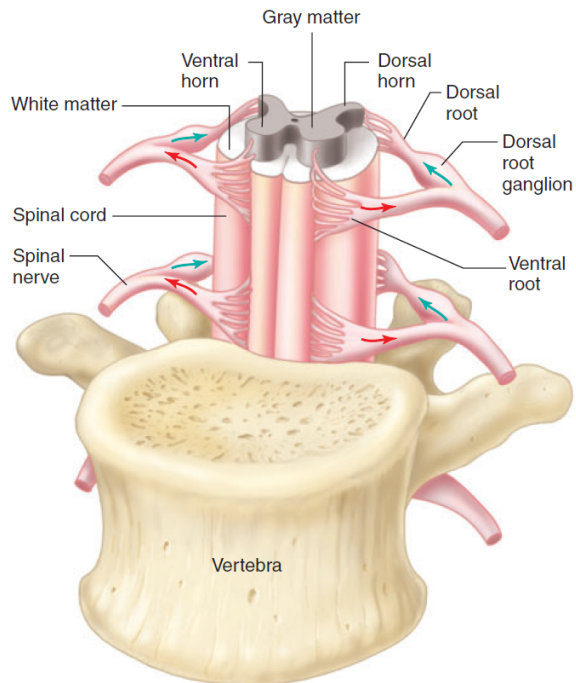
Spinal cord is a slender cylinder of soft tissue, lying protected within the vertebral column (Widmaier et al., 2014). In the center is gray matter, the butterfly-shaped cross section area composed of interneurons, the cell bodies and dendrites of efferent and afferent neurons, the entering fibers of afferent neurons, and glial cells. It is surrounded by white matter, consisted of groups of myelinated axons. At each vertebra and at each side of the spinal cord, efferent nerves leave the cord at ventral side, whereas afferent nerves enter the spine at the dorsal side (see figure 1.14b). A short distance from the cord, the dorsal and ventral roots from the same level combine to form a spinal nerve, which innervates a specific part of the body and carries motor control information to muscles. In general, the eight cervical nerves (C) control the muscles and glands and receive sensory input from the neck, shoulder, arm, and hand (see figure 1.14a). The 12 thoracic nerves (T) are associated with the chest and abdominal walls. The five lumbar nerves (L) are associated with the hip and leg, and the five sacral nerves (S) are associated with the genitals and lower digestive tract.

A spinal cord injury is the damage to the spinal cord usually caused by trauma (an example can be seen in figure 1.14c). The part of the spinal cord that was damaged affects the functionality of the spinal nerves at that level and below. Therefore, injuries located at higher vertebrae are more severe and cause greater loss of functionality. Classified by the level of injury, spinal cord can be cervical 1–8 (C1–C8), thoracic 1–12 (T1–T12), lumbar 1–5 (L1–L5), or sacral (S1–S5). Depending on the location and the severity of the injury, the symptoms can vary from pain and numbness to paralysis. While in complete spinal cord injury all functionality below the injury is lost, in incomplete spinal cord injury patients can preserve sensations or motor functions. Patients can still have uncoordinated movements, and a lack of force, or, in more difficult cases, they can weakly activate their muscles, but cannot perform the movement. If their motion intention could be extracted in real time, it would allow them to control assistive devices and maximize the benefits of robotic-aided therapies where it has been proved that the active participation improves the medical condition of the patient (Hogan et al., 2006).

It was already shown that intensity-related and task-specific activation patterns exist in patients



(a) Retrieved from Widmaier et al. (2014).



(b) Retrieved from Widmaier et al. (2014).



(c) Retrieved from ?.

Figure 1.14: Figure shows **a)** dorsal view of the spinal cord. Parts of the skull and vertebrae have been cut away. In subfigure **b)** ventral view of the section of the spinal cord can be seen. The direction of transmission of neural activity is noted by arrows. Subfigure **c)** shows magnetic resonance imaging scan of cervical spine of patient with SCI. There is a fracture and dislocation at C4 vertebra, compressing spinal cord.

with neurological disorders and that motion intention can be extracted from EMG. In other words, a movement that a patient is trying to perform can be predicted using the recorded myoelectric activity. Liu and Zhou were able to successfully perform identification of tasks using time domain and autoregressive model features in patients with incomplete spinal cord injury (Liu and Zhou, 2013), whereas Zhang and Zhou identified tasks in patients with stroke using a similar feature set (Zhang and Zhou, 2012).

After the neurological disorder, rehabilitation treatment should start as soon as possible, only days after injury in the case of stroke, whereas in the case of spinal cord injury, after the inflammation. Early interventions can achieve incredible results and patients can either regain control of limbs, which is known as *true recovery*, or can learn new compensatory movements, which is called *restitution*.

In spite of the correct neuromuscular activation, patients sometimes cannot achieve a movement because of insufficient contraction force, or spasticity (Liu et al., 2016b). These patients have a good chance of recovery, but therapists are often unaware of their state. On the other hand, rehabilitation robots are mostly based on force and inertia, and, therefore, cannot be of assistance either. Since these patients have the ability to generate EMG signals, they could control a rehabilitation robot and maximize their chance of recovery by individualizing rehabilitation.

1.5 Doctoral thesis overview

This doctoral thesis is presented as the compendium of three publications. The topic of the thesis is the analysis of muscular patterns of upper-limb muscles during isometric contractions and its relationship to incomplete spinal cord injury. Furthermore, the method for the identification of motion intention is developed based on the pattern recognition approach and the muscle co-activation patterns.

The doctoral thesis is organized by chapters as follows:

Chapter 1: Introduction

In this chapter background of the muscle physiology and origin of surface myoelectric signal is explained. Also, state-of-the-art of task identification approaches is briefly explained.

Chapter 2: Problem statement

This chapter states the problem and provides the motivation and objectives of the doctoral thesis.

Chapter 3: Myoelectric patterns for task identification in patients with iSCI

This chapter represents the first publication of the compendium of publications titled “Spatial distribution of HD-EMG improves identification of task and force in patients with incomplete spinal cord injury”. Using spatial distribution of myoelectric intensity, task identification was performed on patients with incomplete spinal cord injury. This work proves the positive contribution of spatial features in pattern recognition for identification of motor tasks. Not only that the identification performance increases, but the features show resilience to slow time dependent changes in the myoelectric signal, such as fatigue and drying of electrolytic gel.

Chapter 4: Myoelectric patterns within the group of patients with iSCI

In the second publication titled “Prediction of isometric motor tasks and effort levels based on high-density EMG in patients with incomplete spinal cord injury”, the similarity of patterns in intensity and spatial distribution of intensity was investigated in a group of patients with incomplete spinal cord injury. The results show that the repeatable pattern exists between different patients and, moreover, for patients with similar level of injury this patterns are more similar.

Chapter 5: A Novel feature for task identification

This chapter summarizes the third publication of the compendium titled “A Novel Spatial Feature for the Identification of Motor Tasks Using High-Density Electromyography”. A novel feature was proposed for the task identification. It is based on the probability density function of HD-EMG activation maps. Classifier based on this new feature shows a higher identification rate, as well as a higher fidelity during fatiguing tasks.

Chapter 6: Conclusions

In the last chapter, the conclusions and main contributions of the thesis are provided. Also, the guidelines for the future work are stated, as well as a list of publications derived from the thesis.

Chapter 2

Problem statement

Extraction of information on motor task intention can be used in many different applications from assistive devices, prosthetics, and rehabilitation robots to leisure and gaming equipment. This information can be extracted at any point of the system for motor control: from the brain centers controlling the movement to the muscles performing the movement. The central nervous system is organized in multiple levels, from simple connections between cells to coordinated cell populations, building a complex architecture of interconnected brain regions, including the centers for motor control. All this brain activity is summed together and its electromagnetic field can be measured on the scalp surface (electroencephalography, EEG). If this information is used as an interface between the subject and the computer, it is called the *brain-computer-interface* (BCI). Although this approach is being extensively researched and the possibilities and achievements are rising rapidly, it is not an easy task. The problem is that the activity of the entire brain is superimposed to the motor control activity, such as emotions and memory.

On the other hand, EMG records electrical activity of many muscle units that carry similar information. The ratio of power of a useful signal, compared to the interference of other sources is much higher in the EMG recordings. Moreover, by recording myoelectrical activity over muscle surface with high spatial sampling (HD-EMG), even higher SNR can be achieved and more information can be extracted. Therefore, this doctoral thesis investigates the possibilities of extraction of motor control information from multichannel sEMG during voluntary contractions.

2.1 Motivation

Voluntary movements are achieved by the contraction of skeletal muscles controlled by the Central and Peripheral Nervous system. The contraction is initiated by the release of a neurotransmitter that promotes a reaction in the walls of the muscular fiber, producing a biopotential known as the Motor Unit Action Potential (MUAP) that travels from the neuromuscular junction to the tendons. The surface electromyographic signal records the continuous activation of such potentials over the surface of the skin and constitutes a valuable tool for the diagnosis, monitoring and clinical research of muscular disorders. Moreover, the use of electrode arrays facilitates the investigation of the peripheral properties of the active motor units such as: conduction velocity and fatigue (Soares et al., 2015); anatomical characteristics in terms of location of the innervation zones (Beck et al., 2012), the spatial composition of the muscle, that is, muscle compartmentalization (Vieira et al., 2010); estimation of number, type and spatial distribution of muscle fibers (Marateb et al., 2016); and change in spatial distribution of MUAPs with exercise and pain (Madeleine et al., 2006). This last property of the muscles has proven to be very useful to infer motion intention not only regarding the direction of the movement but also its force (Rojas-Martínez et al., 2013). The advantages of the HD-EMG lie in the large amount of recorded information, which enables minimizing the effect of electrodes shift and allows choosing an appropriate subset of channels for further analysis.

In this thesis muscle co-activation patterns will be analyzed both in healthy subjects, and in patients with incomplete spinal cord injury (iSCI). In these types of neuromuscular impairments, patients often have residual motor capabilities and can weakly activate their muscles. However, although muscle is contracting and generating myoelectrical activity, the contraction is sometimes insufficient to generate joint movement. In this situation, it is likely that the rehabilitation will not be successful and the patient could develop compensatory movements to replace the lost functionality, either by himself, or by following the therapist's advice. Moreover, rehabilitation robots are widely used in this type of rehabilitation care. However, robots most often have only force sensors and can adjust the trajectory depending on the force that the patient is producing in order to assist/resist his efforts. Although it is well known that rehabilitation robots have a positive effect on the therapy, their effect on the rehabilitation could be greatly improved if the

robots would adjust the force and trajectory based on the patient's capabilities and efforts. A patient's effort to achieve the movement could be extracted by a HD-EMG myocontrol system, which would be connected into the feedback loop of the robot to personalize the rehabilitation. It has been proven already that simple movement of a patient's limb along a set trajectory has a minimal effect on the outcome of the therapy and that the therapy can be greatly improved if the patient is actively trying to achieve a movement. Therefore, a personalized therapy system that responds to the patient's movement intention could bring recovery and patient's independence.

To achieve the accurate identification of motion intention using pattern recognition, a repeatable co-activation pattern should be present among the patients with neurologically disabling diseases. Therefore, the reproducibility of specific muscular activation patterns was investigated in patients with incomplete spinal cord injury during four isometric tasks of the upper limb, paying close attention to the spatial activation patterns. Moreover, activation patterns were also analyzed during different levels of effort.

Muscular pattern reproducibility can be evaluated using a pattern recognition techniques for task identification. In other words, results of task identification can be used as a figure of merit for muscular pattern quality. If the features extracted from the HD-EMG signal form a distinct pattern for each of the tasks, and if patterns for different tasks are different, identification performance will be high, that is, recognizable and distinct patterns will yield high identification results.

Task identification using pattern recognition consists in classification of the recorded sEMG signal segments into one of predefined classes based on a set of characteristics, i.e., pattern, extracted from the recorded EMG signal. These extracted features should ideally form a repeatable and distinct pattern for each class, and should be different between classes. A variety of classifiers (e.g. hidden Markov models, support vector machine, artificial neural network, fuzzy logic and linear discriminant analysis) (Oskoei and Hu, 2007) have already been employed in myocontrol research. Nevertheless, multiple authors agree that the identification does not depend much on the classifier type (Hargrove et al., 2007; Zhang and Zhou, 2012; Hakonen et al., 2015). Therefore, simple and easy to train classifiers like linear discriminant analysis are preferred (Li et al., 2010; Englehart et al., 1999; Tkach et al., 2010; Li et al., 2014; Hakonen et al., 2015).

On the other hand, finding an appropriate set of features is challenging (Englehart et al., 1999; Tkach et al., 2010; Liu and Zhou, 2013).

Through this thesis, the linear discriminant analysis (LDA) was used as a pattern recognition classifier, whereas the support vector machine (SVM) was used for the comparison in only one publication. LDA is a computationally simple and efficient classifier with linear decision boundary and it is based on the Bayesian equation (?). It is a *parametric classifier*, i.e., it estimates statistical probability of classes by estimating the probability density function of each class from the available data, which is not a simple task and can often be erroneous. On the other hand, SVM (?) is nowadays known as a very powerful classifier with a lot of different applications. The big advantage over LDA is the fact that it is a *non-parametric classifier*. The model of the classifier is not obtained using assumptions of the form of the class density function and estimation of it's parameters, which is inevitably a source of error. Instead, SVM forms the decision boundary using the samples (not their density estimates) by maximizing the distance between samples and the boundary. This was the idea Vladimir Vapnik, the inventor of this method stood for. It is better to try to solve the problem directly and simply, without many intermediate steps that can often be complicated and inaccurate. Detailed explanation and the working principle of these two classifiers are provided in the appendix B.

The challenges faced in pattern recognition in electromyography include many factors, such as electrode shift (Hargrove et al., 2008; Young et al., 2011), change in arm posture (Fougner et al., 2011), and slow time dependent changes (Farina et al., 2014a). This thesis addresses the challenges caused by slow time-dependent changes like fatigue (Tkach et al., 2010), and change in electrode-skin impedance (Clancy et al., 2002) on highly controlled isometric tasks. A patient's limb was held in place using a mechanical brace in order to restrict joint movement. Therefore, effects accounted for limb movement, that is, electrode shift and change in arm posture, were minimal.

2.2 Objectives

Main objective

This doctoral thesis addresses the problem of extraction of information from muscular patterns obtained from multichannel surface electromyography and associates them with different motor tasks. The aim of the thesis is to analyze the muscular pattern of the upper-limb muscles during isometric contractions and its relationship to neuromuscular disorders, namely to incomplete spinal cord injury. This information can be useful for the identification of motion intention, i.e. identification of the intended motor task and force based on the sEMG, and could provide a control signal to interfaces that control external devices, like exoskeletons or rehabilitation robots, particularly for patients with neuromuscular disorders including spinal cord injury.

Specific objectives

To achieve the main objective, this thesis strives for the following specific objectives:

- I To investigate muscle co-activation patterns extracted from multichannel sEMG in patients with incomplete spinal cord injury during isometric contractions, as well as to evaluate the repeatability of the muscular patterns for different motor tasks, and for different effort levels. The patterns related to intensity and spatial distribution of intensity were evaluated.
- II To investigate the effects of myoelectric fatigue on the obtained patterns.
- III To investigate how these patterns change during recording time due to non-physiological parameters like drying of conductive gel.
- IV To search for the similarity in multichannel sEMG activation patterns between different patients with incomplete spinal cord injury using the pattern-recognition approach.
- V To investigate new spatial features that can be used for the task identification.
- VI To test the capability of the proposed features in the identification of task and force of isometric contractions using pattern recognition, and to test the stability and robustness of such features to physiological and non-physiological changes.

2.3 Thesis framework

This thesis and the published articles that provide its content as a compendium were developed in the *Department of Automatic Control (ESAII)* of the *Universitat Politècnica de Catalunya (UPC)* under the framework of the muscular research line of the *BIOsignal Analysis for Rehabilitation and Therapy Research Group (BIOART)*, that is part of the *Biomedical Signals and Systems* division of the *Biomedical Engineering Research Centre (CREB)* of UPC and the Biomedical Research Networking Center in Bioengineering, Biomaterials and Nanomedicine (CIBER-BBN). The research was done in collaboration with the *Institut Guttman in Badalona* (Spain) and the *Laboratory of Engineering of Neuromuscular System and Motor Rehabilitation* at the *Politecnico di Torino*.

Furthermore, this work has been supported by multiple funding projects and grants:

1. Ayudas para la contratación de personal investigador novel (FI-DGR 2014). *Agencia de Gestión de Ayudas Universitarias y de Investigación (AGAUR) - Generalitat de Catalunya.*
2. Sistemas multicanal de análisis y sensorización para rehabilitación y monitorización clínica. (DPI2011-22680) *Ministerio de Economía, Industria y Competitividad (MINECO)*
3. Design of methods for assessing processes of neurological and neuromuscular decline associated with aging. (DPI201459049R) *Ministerio de Economía, Industria y Competitividad (MINECO)*

Chapter 3

Spatial distribution of HD-EMG improves identification of task and force in patients with incomplete spinal cord injury

Published as: Jordanić, M., Rojas-Martínez, M., Mañanas, M.A., Alonso J.F. Spatial distribution of HD-EMG improves identification of task and force in patients with incomplete spinal cord injury *Journal of NeuroEngineering and Rehabilitation* 13(1):41, 2016

doi: 10.1186/s12984-016-0151-8

Impact Factor: 3.222; Position: 3 of 65 (Q1) REHABILITATION, 12 of 77 (Q1) BIOMEDICAL ENGINEERING.

Abstract: *Background.* Recent studies show that spatial distribution of High Density surface EMG maps (HD-EMG) improves the identification of tasks and their corresponding contraction levels. However, in patients with incomplete spinal cord injury (iSCI), some nerves that control muscles are damaged, leaving some muscle parts without an innervation. Therefore, HD-EMG maps in patients with iSCI are affected by the injury and they can be different for every patient. The objective of this study is to investigate the spatial distribution of intensity in HD-EMG

recordings to distinguish co-activation patterns for different tasks and effort levels in patients with iSCI. These patterns are evaluated to be used for extraction of motion intention. *Method.* HD-EMG was recorded in patients during four isometric tasks of the forearm at three different effort levels. A linear discriminant classifier based on intensity and spatial features of HD-EMG maps of five upper-limb muscles was used to identify the attempted tasks. Task and force identification were evaluated for each patient individually, and the reliability of the identification was tested with respect to muscle fatigue and time interval between training and identification. *Results.* Three feature sets were analyzed in the identification: 1) intensity of the HD-EMG map, 2) intensity and center of gravity of HD-EMG maps and 3) intensity of a single differential EMG channel (gold standard). Results show that the combination of intensity and spatial features in classification identifies tasks and effort levels properly ($Acc = 98.8\%$; $S = 92.5\%$; $P = 93.2\%$; $SP = 99.4\%$) and outperforms significantly the other two feature sets ($p < 0.05$). *Conclusion.* In spite of the limited motor functionality, a specific co-activation pattern for each patient exists for both intensity, and spatial distribution of myoelectric activity. The spatial distribution is less sensitive than intensity to myoelectric changes that occur due to fatigue, and other time-dependent influences.

Keywords: Myoelectric control, Pattern recognition, High-density electromyography, Incomplete spinal cord injury

3.1 Background

Surface electromyography (sEMG) is commonly used in noninvasive extraction of motor control information and identification of motion intention. Therefore, it has a wide practical application in rehabilitation engineering, e.g., prosthetics (Li et al., 2010; Young et al., 2013; Stango et al., 2015), exoskeletons (Vaca Benitez et al., 2013) and rehabilitation robots (Dipietro et al., 2005; Marchal-Crespo and Reinkensmeyer, 2009).

Conventional myocontrol is based on non-pattern recognition strategies. In a classical example of a single joint prosthesis (one degree of freedom), sEMG signals are recorded on two independent muscles. EMG of one muscle controls the intensity in one movement direction, and the EMG of another muscle in the opposite direction. The output force is proportional to EMG power

of the controlling muscle. This strategy is simple, computationally efficient, robust, and does not need training, which makes it suitable for unsupervised, everyday use. However, it allows control only in one degree of freedom (DoF) at a time. Although this approach can provide intuitive interface with fewer commands (Hakonen et al., 2015), in case of a prosthetic device with multiple degrees of freedom (e.g. hand prostheses), switching between DoFs is impractical and requires a long time to complete a complex task (Farina et al., 2014a).

On the other hand, pattern recognition-based control strategy enables usage of multiple DoFs without switching, which significantly improves task completion time (Hakonen et al., 2015). Although a variety of classifiers (e.g. hidden Markov model, support vector machine, artificial neural network, fuzzy logic) have been evaluated for task identification (Oskoei and Hu, 2007), multiple authors agree that the identification does not significantly depend on the classifier type (Hakonen et al., 2015; Hargrove et al., 2007; Zhang and Zhou, 2012). Therefore, simple and easy to train classifiers, e.g. linear discriminant analysis (LDA), are preferred (Scheme and Englehart, 2013; Boschmann and Platzner, 2013; Young et al., 2012; Li et al., 2014). Conversely, finding an appropriate set of features is challenging (Tkach et al., 2010; Liu and Zhou, 2013; Englehart et al., 1999; Oskoei and Hu, 2006). Time-domain features are commonly used because they can achieve high identification results and are computationally efficient (Hakonen et al., 2015).

The technological advancement of EMG acquisition systems (Merletti et al., 2009, 2010) enables the use of high-density electromyography (HD-EMG). By using an array of closely spaced electrodes organized in a quadrature grid, a wide muscle area is recorded. This technology allows insights into the spatial distribution of the myoelectric intensity of a muscle. The spatial distribution allows monitoring the activation of different muscle regions, which depends on joint position (Vieira et al., 2010), contraction level (Holtermann et al., 2005), and duration of movement (Tucker et al., 2009). In addition, it has already been reported that spatial features can be used in task identification in normal subjects (Stango et al., 2015; Rojas-Martínez et al., 2013).

In patients with neurological disorders (e.g., stroke, spinal cord injury) motor control is impaired and some muscle parts can be left without innervation. As a result, patients often have problems with uncoordinated movements, lack of force, and spasticity. Rehabilitation and therapy can partially regenerate motor control, and either the affected muscles can recover partial function-

ality or other muscle groups can replace the functionality of a dysfunctional part. Therefore, the spatial distribution of motor unit action potentials is different from subject to subject and depends on the injury. But is it task-specific? And a more interesting question: is it force-specific? Liu and Zhou already proved that an intensity-related muscle co-activation pattern exists and that different hand tasks can be successfully identified in patients with incomplete spinal cord injury (iSCI) (Liu and Zhou, 2013). But can spatial distribution of myoelectric intensity help in identification of task and level of effort in patients with iSCI?

In this work, a method for the identification of different tasks and effort levels in patients with iSCI is proposed. High density EMG was measured on muscles participating in the analyzed contractions. By using different feature sets and an LDA classifier, we demonstrate that a specific co-activation pattern exists in patients with iSCI not only for a certain task, but also for a contraction intensity. Furthermore, the influence of time-dependent changes in EMG signal (due to muscle fatigue and drying of conductive gel) on the reliability of identification was evaluated. It was demonstrated that features related to spatial distribution not only improve the identification, but they are also more robust to time changes. What is more, they are helpful when identifying both the task and the desired force, indicating that spatial activation of motor units depends on the type of exercise and the contraction level in patients with iSCI.

3.2 Method

3.2.1 Measurements

Instrumentation

For the recording of HD-EMG signals, 2-D electrode arrays were fabricated in our laboratory (see Figure 3.1c). They were designed as silver-plated eyelets (5 mm external diameter), embedded in a hydrophobic fabric in a quadrature grid with 10 mm inter-electrode distance. When positioned and fixed with elastic straps, fabric follows the contour of the muscle enabling a constant electrical contact between subject's skin and eyelets.

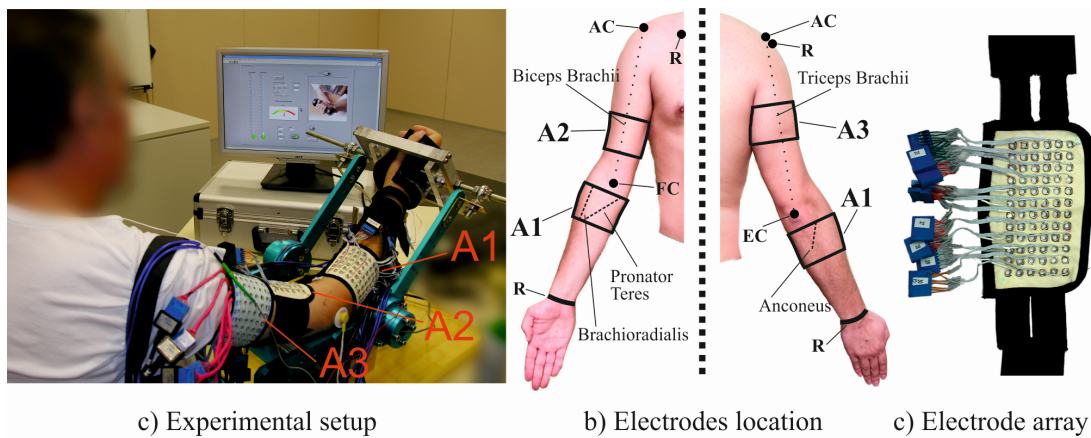


Figure 3.1: Experimental setup. **a)** Positioning of the electrode arrays A1-A3 during the recording. **b)** Anatomical landmarks and paths used for the positioning of the arrays: A1 (6 rows, 16 columns) was placed over the forearm covering Anconeus, Brachioradialis and Pronator Teres muscles, where the most proximal row of electrodes was placed 2 cm bellow the elbow crest (EC) covering all three muscles, according to Kendall et al. (1993); A2 (6 rows, 12 columns) was placed in the distal part of the upper arm with respect to the center of the line connecting fossa cubit (FC) and acromion (AC), and covering Biceps Brachii muscle; A3 (6 rows, 12 columns) was placed in the proximal part with respect to the center of the line connecting EC and AC, over Triceps Brachii. Both A2 and A3 arrays were located in accordance with SENIAM recommendations (Hermens and Freriks, 1999). Reference electrodes (R) were placed on the clavicle, wrist and shoulder of the active arm. **c)** Detail of the electrode arrays used in the experiment

In total, 240 monopolar EMG channels were recorded for each patient using three electrode arrays. A “driven right leg” circuit (Merletti and Hermens, 2004) was used to reduce the common mode interference by feeding the common mode voltage with opposite phase to the patient.

Monopolar EMG signals were digitized using two amplifiers with synchronized sampling (EMG-USB- 128 channels, sampling frequency 2048 Hz, 3 dB bandwidth 10–750 Hz, programmable gains of 100, 200, 500, 1000, 2000, 5000, 10000, manufactured by LISiN-OT Bioelettronica).

In order to perform isometric contractions at the desired force, a mechanical brace was used and torque transducers (OT Bioelettronica, range 150 Nm, resolution 2.5 mV/V) were placed on each joint to record the exerted torque (Figure 3.1c). During the measurements, patients were sitting upright in front of the brace with their dominant arm immobilized at the wrist to avoid hand grip. The forearm was in the sagittal plane, halfway between pronation and supination. The elbow was flexed at 45° and the shoulder was adducted at 90° in the horizontal plane and flexed at 45° in the sagittal plane. The exerted force level was displayed online to patients during the exercise for visual feedback.

Experimental setup

Nine patients (four male, five female; age: 47 ± 18 years; body mass index: 28.2 ± 4.2) diagnosed with iSCI at C4-C6 levels participated in the study. Patients were rated C or D according to the ASIA scale and were injured at least 1 month before the experimental session. The study was conducted in accordance with the Declaration of Helsinki and subsequent amendments concerning research in humans and was approved by the Hospital Ethics Committee and the Local Government. All volunteers gave their written informed consent to participate.

HD-EMG was recorded during four isometric upper-limb tasks, i.e. flexion/extension of the elbow and supination/pronation of the forearm, on five superficial muscles involved by these tasks: Biceps Brachii, Triceps Brachii, Anconeus, Brachioradialis, and Pronator Teres. Prior to positioning of the electrode arrays, skin was cleaned, shaved, and treated with abrasive gel.

Three electrode arrays were used during the experiment: array A1 was placed over the forearm covering Anconeus, Brachioradialis and Pronator Teres muscles, and arrays A2 and A3 were placed over the upper arm covering Biceps Brachii and Triceps Brachii muscles. Reference electrodes were placed on the clavicle, wrist and shoulder of the active arm. After placing the arrays, each eyelet was filled with $20 \mu\text{l}$ of conductive gel using a gel dispenser (Multipette Plus, Eppendorf, Germany). The experimental setup can be seen in Figure 3.1.

HD-EMG recordings

Before signal recording, the maximal voluntary contraction (MVC) was measured for each task as a maximum of three consecutive trials. To prevent fatigue, each trial was followed by a three minute rest (Pizzigalli et al., 2014; Holobar et al., 2010). Patients were trained to keep their fingers and wrist relaxed in order to minimize the activity of forearm muscles that do not participate in the intended tasks.

The measurement protocol was composed of two parts. In the first part, contractions at three levels of effort (10%, 30% and 50% MVC) were measured for each task in randomized order. Visual feedback of the level of effort was provided in real time and subjects were asked to maintain the target level as precise as possible. Patients were instructed to remain at rest for three seconds followed by a contraction at a predefined force level for 10 s. There were three-minute breaks between consecutive recordings to prevent cumulative fatigue.

The second part of the measurement protocol began approximately half an hour (27.0 ± 9.8 min) after the end of the first part of the protocol. Each measurement started with a three-second rest period after which patients performed contraction at 50% MVC until failure. The procedure was repeated for each task and between recordings there were three-minute breaks. The recorded signals were divided into three sets for the subsequent analysis: the first set (submaximal set) was composed of the signals recorded in the first part of the protocol. The second set (time-effect set), used to test the time effect on the identification, was extracted from the beginning (up to 20% of the total duration of the contraction, TDC) of the signals recorded in the second part of the protocol. Finally, the third set (endurance set) was used to test the effect of myoelectric fatigue on the identification, and was composed of the totality of the signals recorded in the second part of the protocol. The flow chart of the recording protocol can be seen in Figure 3.2.

3.2.2 HD-EMG maps and feature extraction

HD-EMG maps calculation

Low quality channels, a common issue in HD-EMG measurements, were identified by an expert system proposed by Rojas-Martínez et al. (2012). The system is based on thresholds associated

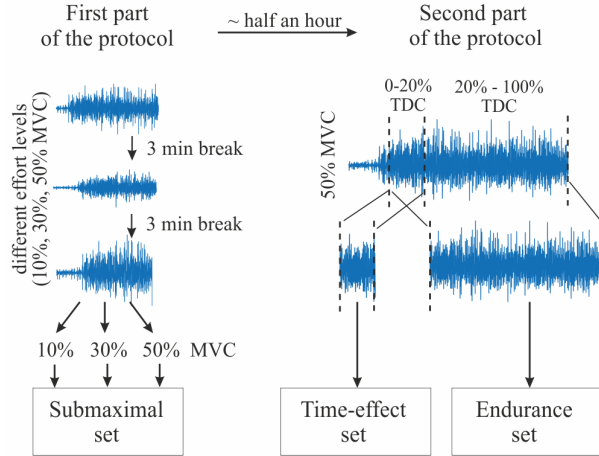


Figure 3.2: HD-EMG recording flow chart: Flow chart describes recording protocol of each task. Note that the recordings order was randomly selected in each part of the protocol.

with the following three features: 1) relative power of low frequency components (from 0 to 12 Hz); 2) relative power of power-line components (50 Hz and first four harmonics); and 3) power calculated from RMS value of the signal. EMG channels without measurement artifacts were zero-phase filtered between 15 Hz and 350 Hz (Butterworth bandpass filter, 4th order), and the first 6 harmonics of power line coupling were suppressed by using the adaptive transversal filter, whose weights were estimated by a least mean squares algorithm (Mañanas et al., 2001).

HD-EMG maps represent the spatial distribution of intensities of active motor units over the surface of the muscle:

$$HM_{i,j} = RMS(sEMG_{i,j}) \quad (3.1)$$

where HM is an activation map and each pixel in a map ($HM_{i,j}$) corresponds to an RMS value of a channel in an electrode array (position i, j). Maps were calculated on non-overlapping time windows of 250 ms to ensure an acceptable response time in applications directed to myoelectric control (Oskoei and Hu, 2007), and channels previously identified as artifacts were replaced by triangle-based cubic interpolation (Rojas-Martínez et al., 2012).

Feature extraction

Two types of features related to HD-EMG maps were extracted: intensity and center of gravity. They were used in classification individually or combined in order to compare their performance. Additionally, the intensity of a single differential channel, i.e. traditional bipolar recordings usually employed in pattern recognition as a “gold standard”, was compared to other features. In any case, the feature set was composed of features extracted from all 5 monitored muscles. Multiple studies suggest that the relationship between EMG amplitude and generated force is not linear (Staudenmann et al., 2010; De Luca, 1997). Accordingly, the intensity features were calculated as a common logarithm of the mean intensity of the HD-EMG maps, which proved to achieve higher classification results than a linear measure (Rojas-Martínez et al., 2013):

$$I = \log_{10} \frac{1}{N} \sum_{i,j} HM_{i,j} \quad (3.2)$$

where I is an intensity feature calculated from the HD-EMG intensity map HM with a total number of N channels, and HM_{ij} is the intensity of a channel located at position i, j .

The center of gravity of an HD-EMG map (CG) was calculated as:

$$CG = \frac{1}{\sum_{i,j} HM_{i,j}} \sum_{i,j} HM_{i,j} \begin{bmatrix} i \\ j \end{bmatrix} \quad (3.3)$$

where (i, j) represents a channel position in the HD-EMG map HM .

The intensity of a single differential channel (Diff) was calculated as a common logarithm of an RMS value of difference of two consecutive channels in the direction of muscle fibers:

$$Diff = \log_{10} \left(RMS(sEMG_{i,j} - sEMG_{i+1,j}) \right) \quad (3.4)$$

where the locations of channels (i, j) and $(i + 1, j)$ are selected following SENIAM recommendations (Hermens and Freriks, 1999). Diff was calculated on the same 250 ms time epoch as the HD-EMG map.

3.2.3 Identification of motion intention

Classification

Three LDA classifiers based on different feature sets extracted from all five monitored muscles were evaluated in the study:

1. Classifier based on the intensity of the HD-EMG map (I)
2. Classifier based on the intensity and center of gravity of the HD-EMG map (I + CG)
3. Classifier based on the intensity of a single differential channel (gold standard) (Diff)

These classifiers were evaluated in the identification of task and level of contraction in patients with iSCI. Furthermore, the reliability of the classifiers was tested with respect to the slow time-dependent changes occurring in myoelectric signals, like those associated with gel drying or those related to changes at the physiological level (myoelectric fatigue).

Available observations were divided into a training group, which was used to train the classifier, and a validation group, which was used to evaluate classifier's performance. Both groups were balanced, i.e. there was an equal number of observations of each class in the training group, as well as in the validation group, and data were split into training and validation sets using a 50% / 50% ratio (Wang et al., 2015). To confirm the model was not overfitted, the results of classification of both sets were compared and were found similar. To achieve the statistical stability of results, each classifier was trained and evaluated in one thousand iterations, which are enough to avoid the potential error due to bad data partitioning (Zimmer and Sahle, 2016), and then classification results were averaged. In every iteration, observations in the training and validation groups were assigned randomly.

The performances of the classifiers were expressed in terms of accuracy (Acc), sensitivity (S), precision (P) and specificity (SP) (Farina et al., 2001), as described in the following equations:

$$Acc = \frac{TP + TN}{TP + FP + TN + FN} \quad (3.5)$$

$$S = \frac{TP}{TP + FN} \quad (3.6)$$

$$P = \frac{TP}{TP + FP} \quad (3.7)$$

$$SP = \frac{TN}{TN + FP} \quad (3.8)$$

where true positives (TP) is the number of samples correctly appended to a certain class; true negatives (TN) is the number of samples that do not belong to a certain class and were not classified to that class; false positives (FP) is the number of samples not belonging to a certain class, but wrongly classified into that class; and false negatives (FN) is the number of samples belonging to a certain class, but wrongly classified into another class.

Short-term identification

Classifiers with different sets of features (I, I + CG, and Diff) were tested on the submaximal set. Signals belonging to this set were recorded in a short time interval and, consequently, in the same conditions.

Two types of identification were considered: **1) Identification of tasks** and **2) Identification of tasks and effort levels**. Identification of tasks had 4 classes corresponding to the type of the task (flexion, extension, supination, and pronation) and an additional fifth class that corresponds to the rest period – no activity class (NoAct). Observations of no activity were extracted from the first three seconds of each recording, where subjects were asked to maintain at rest. Activity classes consisted of a mixture of all effort levels. On the other hand, identification of tasks and effort levels had 13 classes: 4 tasks with 3 levels of effort for each task (10% MVC, 30% MVC and 50% MVC) and NoAct class.

Considering that patients were not always able to maintain the target level of contraction given their condition, the torque signal was used to select only time segments where the measured force

remained within a threshold of $\pm 5\%$, $\pm 10\%$ and $\pm 10\%$ MVC for target contractions at 10%, 30% and 50% MVC. From every submaximal contraction 20 non-overlapping, 250 ms time epochs, closest to the target force were selected. This procedure ensured 20 observations for each task with differentiation on the level of effort, or 60 samples for each task, without differentiation on the effort level. Consequently, 60 observations without muscle activity were selected for NoAct class from the beginnings of exercises (rest period).

Influence of time- progress on identification

Wet electrodes with conductive electrolytic gel are commonly used for sEMG recording. However, these electrodes are not good for long-term monitoring (Searle and Kirkup, 2000). Gel drying increases skin-electrode impedance, affecting amplitude and spectral content of the recorded signal. Moreover, skin perspiration is enhanced under the electrode array, which also affects the skin-electrode impedance and, consequently, the characteristics of the recorded signal. To compare the performances of the different features, task identification was tested in these conditions.

Classifiers were trained on the submaximal set and validated on the time-effect contractions recorded in the second part of the protocol. As in the previous section, 20 time epochs for each task and level of effort were identified from the submaximal set based on the torque signal. Half of the extracted observations of all levels of effort were used for training, following the recommendations of Scheme and Englehart (2013), where it was noticed that a mixture of effort levels in the training group yields a more robust classifier. NoAct observations for the training group were extracted from recordings in the first part of the measurement protocol, whereas observations for the validation group were extracted from recordings in the second part of the protocol.

For comparison, the same classifier was used to validate contractions recorded at the first part of the protocol, i.e. using samples of the submaximal set. Since the classifier was trained on just the half of the available observations from the submaximal set, the remaining observations were used for validation. But considering that time-effect set was composed of contractions recorded at 50% MVC effort level, the validation group was also composed only of 50% MVC contractions

from the submaximal set.

The classifier was trained and evaluated over 1000 iterations with observations selected randomly both in the training and validation sets to avoid bias in the performance.

Influence of muscle fatigue on identification

Muscle fatigue is a slow change that occurs in contracting muscles. It alters the characteristics of recorded sEMG signal (i.e. amplitude and frequency content) (De Luca, 1984) and, inherently, alters the extracted classification features (Wan et al., 2010). To test the effect of fatigue on identification, each recording in the endurance set was divided into five equal time segments, i.e. 0–20% TDC, 20–40% TDC, 40–60% TDC, 60–80% TDC, and 80–100% TDC. The first segments (0–20% TDC) were used as a training group and the identification was carried out on all segments. The classification indices (accuracy, sensitivity, precision and specificity) were calculated for each segment in order to monitor performance during fatigue. The number of observations of each class was the same in the training group, as well as in the validation group.

Statistical methods

A repeated measures analysis of variance (ANOVA) was applied to the different performance indices using each type of task and effort level as measures and features used in the classification as factors. Both, within-subject and between-subject effects were considered in the analysis. In the case of endurance analysis, the repeated measures test was applied to account for differences attributed to the factor time, that is, duration of the contraction. In addition, differences between means were assessed through Student's t-test for paired samples. Effects and differences were considered significant at $p = 0.05$.

3.3 Results

3.3.1 Short-term identification

The different combinations of feature sets extracted from the five recorded muscles (I, I + CG, Diff) were evaluated in non-changing conditions, i.e. training and validation groups were extracted from the same contractions (submaximal set). Features were evaluated in 2 types of identification: 1) identification of tasks and 2) identification of tasks and effort levels.

The results of task identification are shown in Figure 3.3. Adding spatial features to the classification improves the results and decreases the standard deviation. This is especially pronounced in sensitivity of flexion ($88,8\% \pm 12,6\%$ and $96,7\% \pm 5,5\%$ in mean and standard deviation for I and I + CG features, respectively) and extension ($89,6\% \pm 12,1\%$ and $98,7\% \pm 2,0\%$ for I and I + CG features, respectively) as well as in precision of pronation ($89,9\% \pm 12,5\%$ and $96,6\% \pm 6,3\%$ for I and I + CG features, respectively), and NoAct ($85,6\% \pm 15,3\%$ and $94,8\% \pm 6,5\%$ for I and I + CG features, respectively). When evaluating differences in the performance of features through the repeated measures ANOVA, the within-subject effect was not significant when comparing indices obtained with the feature I or with the combination of features I + CG (either for accuracy, sensitivity, precision or specificity). However, the between subject effect was significant ($p < 0.05$ in all cases), showing that performance obtained for the combination of features I + CG was higher than that obtained when using the features I in the classification, independently of the evaluated task. Similar results were obtained when comparing performance of features Diff and I + CG: the within-subject effect showed no significant differences, that is, similar indices were obtained for all tasks (flexion, extension, supination, pronation and no activity), while the between-subjects effect was significant for all indices ($p < 0.05$) except for precision ($p = 0.07$), showing a higher performance for the features I + CG. No significant effects were observed when comparing the performance indices obtained with the features I with those obtained with the features Diff (*p.n.s.*).

Figure 3.4 shows the results of identification of tasks and effort levels. It can be noticed from the results that the identification based on intensity and spatial features displayed, in average, higher performance and lower standard deviation than the other two classifiers. Like in the

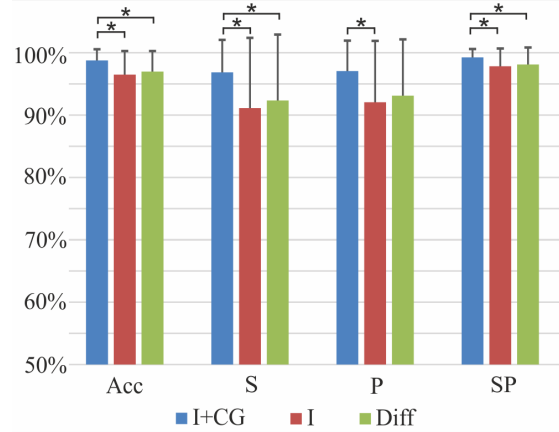


Figure 3.3: Identification of tasks: Average classification indices (Acc, S, P, SP) are shown for classifiers based on different sets of features (I + CG, I, and Diff). Symbol “*” indicates statistical significance ($p < 0.05$).

previous case, the within-subject effect when comparing either between performance indices of I and I + CG or between performances of Diff and I + CG was not significant, showing similar results for all 13 classes (tasks and effort levels and no activity). However, the between-subjects effect was significant in both analyses ($p < 0.001$ when comparing I and I + CG; $p < 0.02$ when comparing Diff and I + CG), showing a higher performance for the case of the combination I + CG. Finally, when comparing performances between features I and Diff, no significant effects were observed (*p.n.s.*).

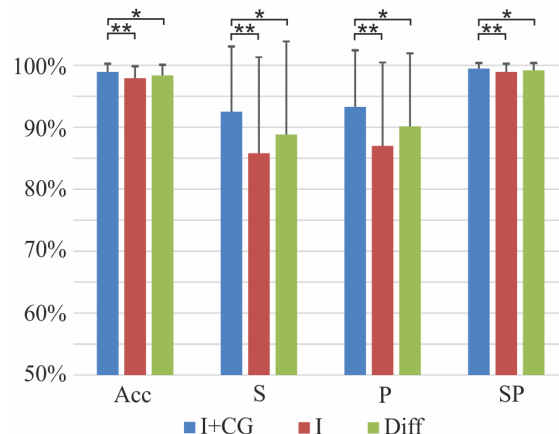


Figure 3.4: Joint identification of tasks and effort levels: Average classification indices (Acc, S, P, SP) are shown for classifiers based on different sets of features (I + CG, I, and Diff). Symbols “*” and “**” indicate statistical significance $p < 0.05$ and $p < 0.01$, respectively.

Figure 3.5 shows the performance of identification of tasks performed at a specific effort level. In this case, the classifier was trained using a mixture of all effort levels. The training group and

the validation group were both extracted from the submaximal set. It can be noticed that all feature sets performed well when identifying tasks corresponding to high levels of contraction, but only the identification with spatial distribution maintained high performance and low standard deviation even at low contraction levels, i.e. 10% MVC, where paired t-tests showed that the identification based on intensity and spatial features significantly outperforms the other two types of features ($p < 0.04$).

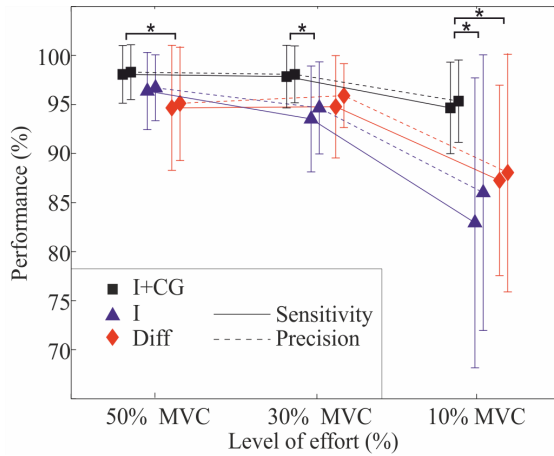


Figure 3.5: Identification of tasks at specific levels of effort: Sensitivity and precision are shown for classifiers based on different sets of features (I + CG, I, Diff). Each classifier was trained using contractions of all effort levels, and evaluated on contractions of specific effort levels. Symbol “**” indicates statistical significance ($p < 0.05$).

3.3.2 Influence of time on identification

For the purpose of evaluation of the effect of time on identification, a classifier based on I + CG was trained using the submaximal set, and the identification was tested both on the submaximal set, and the time-effect set. Results are shown in Figure 3.6, where it is possible to observe that the average performance significantly decreased with time (paired samples t-test showed $p < 0.05$) whereas the standard deviation increased.

Figure 3.7 shows performances of the different feature sets when the validation group was recorded after the training group, i.e. the classifier was trained on the submaximal set and recorded on the time-effect set. It can be noticed that the identification based on Diff features exhibited a significantly lower performance than the identifications based on I or I + CG features (paired samples t-test showed $p < 0.05$), while the identification based on I features performed

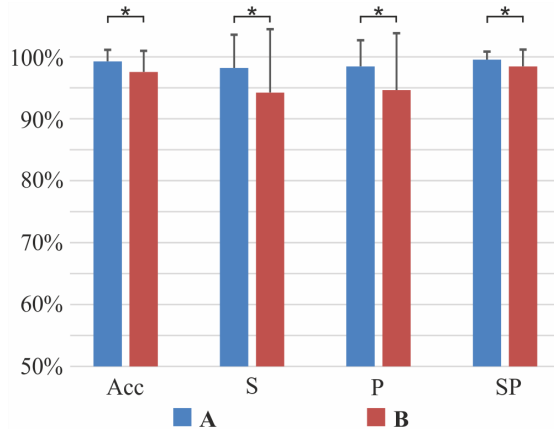


Figure 3.6: Time influence on the identification of tasks: Average classification indices (Acc, S, P, SP) are shown for the classifier based on the I + CG features. In blue bars "A", training and validation sets were recorded during the first part of the protocol, whereas in red bars "B" training and validation sets were recorded during first and second part of the protocol, respectively. Symbol "*" indicates statistical significance ($p < 0.05$).

similarly to the identification based on I + CG features (*p.n.s.*). This last can be understood in light of the results presented in the previous section, where the identification performances using these feature sets were similar at high-middle levels of effort, but I + CG outperformed I features at low effort levels (see Figure 3.5).

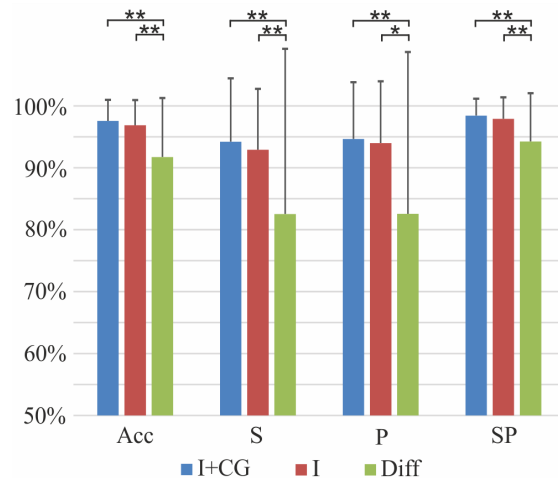


Figure 3.7: Influence of time effect on the identification: Figure shows average classification indices (Acc, S, P, SP) for classifiers based on different feature sets (I + CG, I, Diff). Training set was recorded during the first part of the protocol, and the validation set was recorded during the second part of the protocol. Symbols "*" and "**" indicate statistical significance $p < 0.05$ and $p < 0.01$, respectively.

3.3.3 Influence of time on identification

Figure 3.8 shows the influence of muscle fatigue on the identification based on intensity and center of gravity of the HD-EMG maps. It can be observed that average classification indices gradually decrease with fatigue. When evaluating differences in the performance of these indices, the within-subject effect given by the repeated measures analysis was significant ($p < 0,001$ in all indices). This result relies on the assumption of sphericity, that is, variances of the differences between all pairs of the repeated measurements should be equal; otherwise, the result is positively biased. The conservative Greenhouse-Geisser correction method for the lack of sphericity (Greenhouse and Geisser, 1959) was applied to adjust the degrees of freedom (Landa and Everitt, 2004; Loftus and Masson, 1994) when the assumption of sphericity was violated. As suggested by Landa and Everitt (Landa and Everitt, 2004), Mauchly's test was used to test the sphericity.

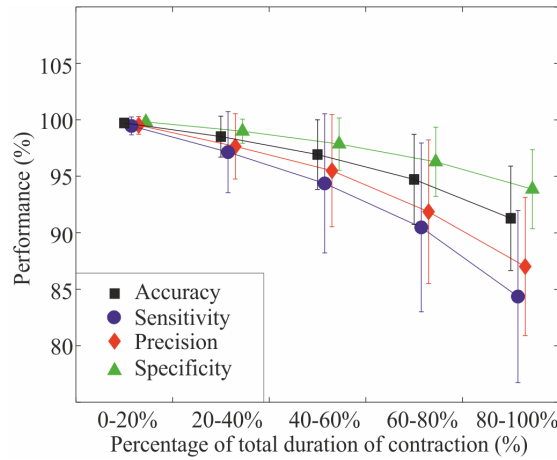


Figure 3.8: Fatigue influence on identification based on I + CG feature set: Average classification indices (Acc, S, P, SP) are shown along the endurance contraction for the classifier based on the I + CG feature set.

Figures 3.9 and 3.10 display the influence of muscle fatigue on sensitivity and precision of the identification based on different feature sets. It can be noticed that all classifiers achieved high sensitivity and precision at the beginning of the endurance contractions, however, as the manifestations of myoelectric fatigue became more evident, the classifier based on intensity and spatial features outperformed the other two, both in average performance and variability.

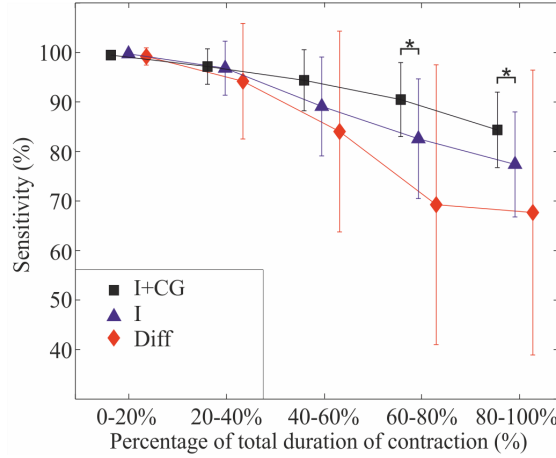


Figure 3.9: Fatigue influence on sensitivity using different sets of features: Average sensitivity along the endurance contraction is shown for classifiers based on different sets of features (I + CG, I, Diff). Symbol “*” indicates statistical significance $p < 0.05$.

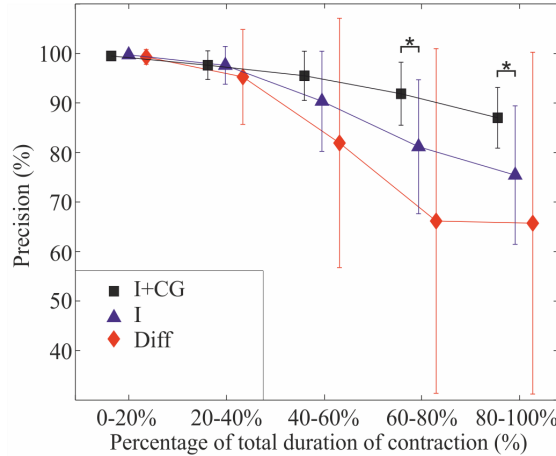


Figure 3.10: Fatigue influence on precision using different sets of features: Average precision along the endurance contraction is shown for classifiers based on different sets of features (I + CG, I, Diff). Symbol “*” indicates statistical significance $p < 0.05$.

3.4 Discussion

Nine subjects with iSCI performed four isometric forearm tasks (flexion, extension, supination, and pronation) at three levels of effort (10% MVC, 30% MVC, and 50% MVC). High density EMG was measured on five muscles of forearm and upper arm in monopolar configuration. Intensity maps were calculated for each muscle and three different feature sets were extracted: the average intensity of a HD-EMG map (I), the intensity and center of gravity of a HD-EMG map (I + CG), and the intensity of a single differential channel (Diff) (gold standard). Using the extracted feature sets and LDA-based classification, both the task and the effort level

were identified, and the influence of fatigue and other time-dependent changes (e.g. drying of conductive gel) on the identification was evaluated. Since the goal of this study was to analyze different feature sets rather than classification methods, LDA was utilized given that this method is the most commonly used, and is generally recommended for myoelectric interfaces (Hakonen et al., 2015). Although it assumes normal distribution of patterns in each class, it has proven to have good performance even when the normality assumption does not hold (Grouven et al., 1996).

When identification using the different features was tested on signals recorded in short time intervals, the combination of I + CG outperformed the other feature sets. The results show that a muscular co-activation pattern exists not only for the task intention ($Acc = 98.7\%$; $S = 96.8\%$; $P = 97.0\%$; $SP = 99.2\%$), but also for the force intention ($Acc = 98.8\%$; $S = 92.5\%$; $P = 93.2\%$; $SP = 99.4\%$).

Although the identification based on the features Diff has slightly better performance in average than the identification based on the features I, a repeated measures ANOVA showed that there is no significant difference in their distributions. Moreover, a small displacement in the position of bipolar electrodes can have a great effect on signal intensity, as well as on spectral content. Consequently, if using Diff as features in classification, a small displacement can have a high influence on the identification performance. This effect does not exist in feature I, making it more robust to small changes in the position of the electrodes. On the other hand, the identification based on the combination of intensity and spatial features significantly outperforms both of them. This result was obtained both for identification of tasks and identification of tasks and effort levels. Furthermore, it has been shown that the classifier based on I + CG discriminates between types of tasks at low levels of effort (10% MVC) significantly better than the classifiers based on the other feature sets (Figure 3.5).

The impedance between the electrodes and the skin changes during time on account of several causes, e.g., drying of conductive gel and sweating. Consequently, the identification performance deteriorates as the time between the training of the classifier and the identification increases. When the identification is performed long after the training of classifier, the results show that the identification based on I + CG performs just slightly better than the identification based

on I features, while the identification based on Diff features is much worse ($S_{I+CG} = 94\%$, $P_{I+CG} = 95\%$; $S_I = 93\%$, $P_I = 94\%$; $S_{Diff} = 83\%$, $P_{Diff} = 83\%$). Although it may seem that, in average, spatial features do not improve the classification with respect to using only the intensity of an HD-EMG map, it is important to outline that these results were obtained on contractions of high levels of effort (50% MVC), where performances were similar even when contractions were recorded at the same time (see figure 3.5).

Muscle fatigue also affects the recorded EMG signal both in the time and spectral domains and therefore the identification performance deteriorates with fatigue. The results of this work show that the classifier based on intensity and spatial features is less sensitive to fatigue than classifiers based on the other feature sets. The proposed classifier shows a very good performance in task identification even at the final stage of fatigue ($Acc = 91.3\%$, $S = 84.3\%$, $P = 87.0\%$, $SP = 93.5\%$).

The proposed method could significantly improve the human-machine interface technology and can be used in numerous applications: computer games, exoskeletons, automatic wheelchairs, rehabilitation robots, prostheses, etc. As suggested by Muller-Putz et al. (2015), non-invasive hybrid brain-computer interfaces (BCI) can be designed as EEG-based BCI supplemented with other biological and mechanical signals.

Furthermore, compared to inertial signals, which are also used as input to control devices, EMG has a major advantage because myoelectric activation precedes the actual movement, which can save valuable response time.

However, it should be noted that although this study represents an improvement in the identification of motion intention, additional experiments should be considered in the future. Firstly, HD-EMG recordings were carried out during controlled isometric submaximal contractions, i.e. patient's arm was fixed and supported by a mechanical brace. Since the methodology was capable to successfully and automatically differentiate between none, very low, low and medium effort levels, we might hypothesize that the method can be useful in prediction without the support of the brace. However, more experiments without the brace and the analysis of the recorded HD-EMG signals would be necessary to confirm and quantify this hypothesis.

3.5 Conclusion

In this study, the spatial distribution of EMG intensity was evaluated for identification of tasks and different levels of effort in patients with iSCI. Results show that the spatial activation of motor units is dependent on the type of exercise and contraction intensity, and that related features can improve identification performance.

Although results show that spatial features also enhance the robustness of the identification to time effect and fatigue, additional experiments need to be performed to test robustness to temporal dependent changes more thoroughly and to determine when the classifier fails by further tests done on fatigue.

The center of gravity was used as a figure of merit to describe the spatial distribution. Although it shows a significant improvement in classification, by definition it is insensitive to fine changes in the distribution of muscle units. Therefore, in future works, more appropriate measures of spatial distribution should be analyzed in order to better describe the spatial distribution of muscle intensity. Also, additional features as those related to the frequency content could be considered to improve even more the classification performance.

3.6 Declarations

3.6.1 Acknowledgements

We are grateful to Ursula Costa and Josep Medina as assistant and Head of the Functional Rehabilitation Service, respectively, of the Neurorehabilitation Hospital Institut Guttmann for their collaboration in the recruitment of patients and clinical support during the experiments carried out at the same Hospital.

This work has been partially supported by the Spanish Ministry of Economy and Competitiveness-Spain (project DPI2014-59049-R). MJ is supported by the grant for the recruitment of early-stage research staff (FI 2014) from the AGAUR, Generalitat de Catalunya, Spain.

3.6.2 Open Access

This article is distributed under the terms of the Creative Commons Attribution 4.0 International License, which permits unrestricted use, distribution, and reproduction in any medium, provided you give appropriate credit to the original author(s) and the source, provide a link to the Creative Commons license, and indicate if changes were made. The Creative Commons Public Domain Dedication waiver applies to the data made available in this article, unless otherwise stated.

3.6.3 Competing interests

The authors declare that they have no competing interests.

3.6.4 Authors' contributions

MRM and MAM implemented the experimental protocol and conducted the experiments. MJ, MRM, and MAM designed the study and interpreted the results. MJ was in charge of the implementation of signal processing and machine learning methods and the analysis of the data. JFA aided in the analysis of the data and in the interpretation of results. All authors read and approved the final manuscript.

Chapter 4

Prediction of isometric motor tasks and effort levels based on high-density EMG in patients with incomplete spinal cord injury

Published as: Jordanić, M., Rojas-Martínez, M., Mañanas, M.A., Alonso J.F. Prediction of isometric motor tasks and effort levels based on high-density EMG in patients with incomplete spinal cord injury *Journal of Neural Engineering* 13(4):46002, 2016

doi: 10.1088/1741-2560/13/4/046002

Impact Factor: 3.465; Position: 13 of 77 (Q1) BIOMEDICAL ENGINEERING, 90 of 258 (Q2) NEUROSCIENCES.

Abstract: *Objective.* The development of modern assistive and rehabilitation devices requires reliable and easy-to-use methods to extract neural information for control of devices. Group-specific pattern recognition identifiers are influenced by inter-subject variability. Based on high-density EMG (HD-EMG) maps, our research group has already shown that inter-subject muscle activation patterns exist in a population of healthy subjects. The aim of this paper is to analyze muscle activation patterns associated with four tasks (flexion/extension of the elbow, and

supination/pronation of the forearm) at three different effort levels in a group of patients with incomplete Spinal Cord Injury (iSCI). *Approach.* Muscle activation patterns were evaluated by the automatic identification of these four isometric tasks along with the identification of levels of voluntary contractions. Two types of classifiers were considered in the identification: linear discriminant analysis and support vector machine. *Main results.* Results show that performance of classification increases when combining features extracted from intensity and spatial information of HD-EMG maps (*Accuracy* = 97.5%). Moreover, when compared to a population with injuries at different levels, a lower variability between activation maps was obtained within a group of patients with similar injury suggesting stronger task-specific and effort-level-specific co-activation patterns, which enable better prediction results. *Significance.* Despite the challenge of identifying both the four tasks and the three effort levels in patients with iSCI, promising results were obtained which support the use of HD-EMG features for providing useful information regarding motion and force intention.

Keywords: Myoelectric control, pattern recognition, high-density electromyography, incomplete spinal cord injury

4.1 Introduction

Myoelectric signals have been extensively studied for more than half a century to understand muscle control strategies and to build rehabilitation and assistive devices. Surface electromyography (sEMG) is preferably used for monitoring because it is a non-invasive, easy-to-use method, rich in neural information, and has relatively high signal-to-noise ratio. It can be used in many and different applications: artificial limbs in prosthetics technology (Li et al., 2010; Huang et al., 2005), exoskeletons in assistive devices (Young et al., 2013), rehabilitation robots that stimulate neuroplasticity (Marchal-Crespo and Reinkensmeyer, 2009; Dipietro et al., 2005), and other human-machine interfaces.

Neuromuscular intention has lately often been identified using a pattern-recognition approach. Although many classifier types have been evaluated for the identification (support vector machine, k-nearest neighbor, hidden Markov models, artificial neural networks) (Oskoei and Hu, 2007), fast-to-train and computationally-efficient classifiers are preferable, e.g., linear discrim-

inant analysis (Hakonen et al., 2015; Hargrove et al., 2007). On the other hand, the choice of features used in classification is very delicate. In literature, a lot of features have been considered in the time, frequency, and time-frequency domains as well as spatial features (Hakonen et al., 2015). Time domain features are commonly used because they are effective and easy to calculate (Hakonen et al., 2015).

Spatial features emerged with the appearance of high-density EMG systems (HD-EMG). Multiple EMG channels are recorded using a 2D array of closely spaced electrodes placed over the wide area of the muscle or group of muscles. This procedure allows the calculation of two-dimensional activation maps where the intensity of each pixel represents the intensity of a corresponding EMG channel. Consequently, the information on spatial distribution of EMG intensity over the muscle is provided. Recent studies show that changes in the spatial activation pattern are related to the duration of movement and fatigue (Tucker et al., 2009; Staudenmann et al., 2014), the position of the joint (Vieira et al., 2010) and the level of contraction (Holtermann et al., 2005). Since the spatial distribution contains a lot of information about the muscle, it is acknowledged as a valuable feature in the identification of motion intention (Hakonen et al., 2015; Stango et al., 2015; Rojas-Martínez et al., 2013).

Most pattern-recognition identification methods are subject-specific. This could be avoided by building a single identifier for a group of patients, i.e. group-specific identifier. However, inter-subject variability is a big concern when designing a group-specific pattern recognition-based identifier. Individuals differ from each other when referring to physiological parameters, e.g., conductivity of subcutaneous tissue and limb dimension. Nevertheless, by comparing HD-EMG activation maps, inter-subject activation patterns for different tasks and levels of contraction were demonstrated to exist in a population of healthy subjects (Rojas-Martínez et al., 2012). Furthermore, by using intensity and spatial features extracted from activation maps it is possible to construct an inter-subject identification method not only for different tasks, but also for different effort levels (Rojas-Martínez et al., 2013). The authors also reported that in healthy subjects the performance improved by adding spatial features in the identification, proving that spatial distribution is less sensitive to inter-subject variability.

Unfortunately, in patients with incomplete spinal cord injury (iSCI) and other neurological

disorders (e.g. stroke), motor control is impaired as a result of damaged nerves. Patients can have uncoordinated movements and lack of force, or, in more difficult cases, they can weakly activate their muscles, but cannot perform the movement. If motion intention could be extracted from muscle activity, that is, EMG, in real time, it would allow them to control external devices even without kinematic sensors. This technology could be helpful during therapy (e.g., Hogan et al. (2006) reported that robotic rehabilitation can be improved by patients' active participation), as well as in everyday life after the injury by using exoskeleton systems. It has already been shown that intensity-related and task-specific activation patterns exist in patients with neuromuscular impairment and that motion intention can be extracted; e.g. using time domain and autoregressive model features Liu and Zhou (2013) were able to perform patient-specific identification of tasks with high performance in patients with iSCI, Zhang and Zhou (2012) in stroke patients, whereas Geng et al. (2014) in mildly-impaired traumatic brain injury patients. However, all of these studies considered subject-specific patterns, that is, the identification was trained and validated individually for each subject in the databases.

To our best knowledge, no studies have evaluated group-specific identification of motion intention in patients with iSCI so far. It is a particularly difficult task because of the diverse nature of injuries among patients, which can result in high variability among activation maps. The objective of this study is twofold: firstly, to analyze patterns in the activation maps associated with four movement directions at the elbow joint and with different strengths in a group of patients with iSCI; and secondly, the automatic identification of these four isometric tasks and the differentiation between levels of voluntary contraction at low-medium efforts. For this purpose, HD-EMG was recorded on patients with iSCI while performing the following motor tasks: flexion, extension, supination and pronation of the forearm at three different effort levels. HD-EMG activation maps were calculated and variability was measured between maps of different patients. Furthermore, inter-subject identification of tasks and effort levels was performed using intensity and spatial features calculated from activation maps.

4.2 Methodology

4.2.1 Experimental protocol

Nine patients (age: 45 ± 20 years; body mass index: 27.1 ± 5.2 ; five male and four female) participated in the experiment. They were all diagnosed with incomplete spinal cord injury (rated C or D according to ASIA scale) and they were injured at least 1 month before the experiment. There were six patients with injury at C4 vertebra and three patients with injuries at C3, C5 and C6 vertebrae. The study was approved by the local ethics committee and all patients gave their written consent. Subjects performed four isometric upper-limb tasks following the same experimental protocol carried out in (Rojas-Martínez et al., 2013): flexion and extension at the elbow and supination and pronation of the forearm. High-density EMG was recorded on five superficial muscles of the upper-arm and forearm, which are dominantly involved in these tasks: Biceps Brachii, Triceps Brachii, Brachioradialis, Anconeus and Pronator Teres.

During the experiments, patients were sitting upright in front of a table with their dominant arm fixed using a mechanical brace to perform isometric contractions at the elbow (Figure 4.1). The forearm was in the sagittal plane, halfway between pronation and supination. The elbow was flexed at 45° and the shoulder was adducted at 90° in the horizontal plane and flexed at 45° in the sagittal plane. Two torque transducers (OT Bioelettronica, range 150 Nm, resolution 2.5 mV/V) were installed in the brace to measure the force exerted at the elbow, which was displayed to patients during the exercise as visual feedback. HD-EMG monopolar signals were recorded using electrode arrays manufactured in our laboratory. They were designed as silver-plated eyelets (5 mm external diameter) embedded in hydrophobic, non-conductive fabric in a $10\text{ mm} \times 10\text{ mm}$ quadrature grid. Elastic straps were used to fix the arrays to the patient's skin.

Three electrode arrays were used to gather a total of 240 monopolar EMG signals for each patient. The first array (6 rows \times 16 columns) was used to record HD-EMG of forearm muscles (Brachioradialis, Anconeus and Pronator Teres) and was placed so that the most proximal row of electrodes was 2 cm below the elbow crease. The locations of the muscles were previously marked on the skin surface according to (Kendall et al., 1993) and the array was placed to cover

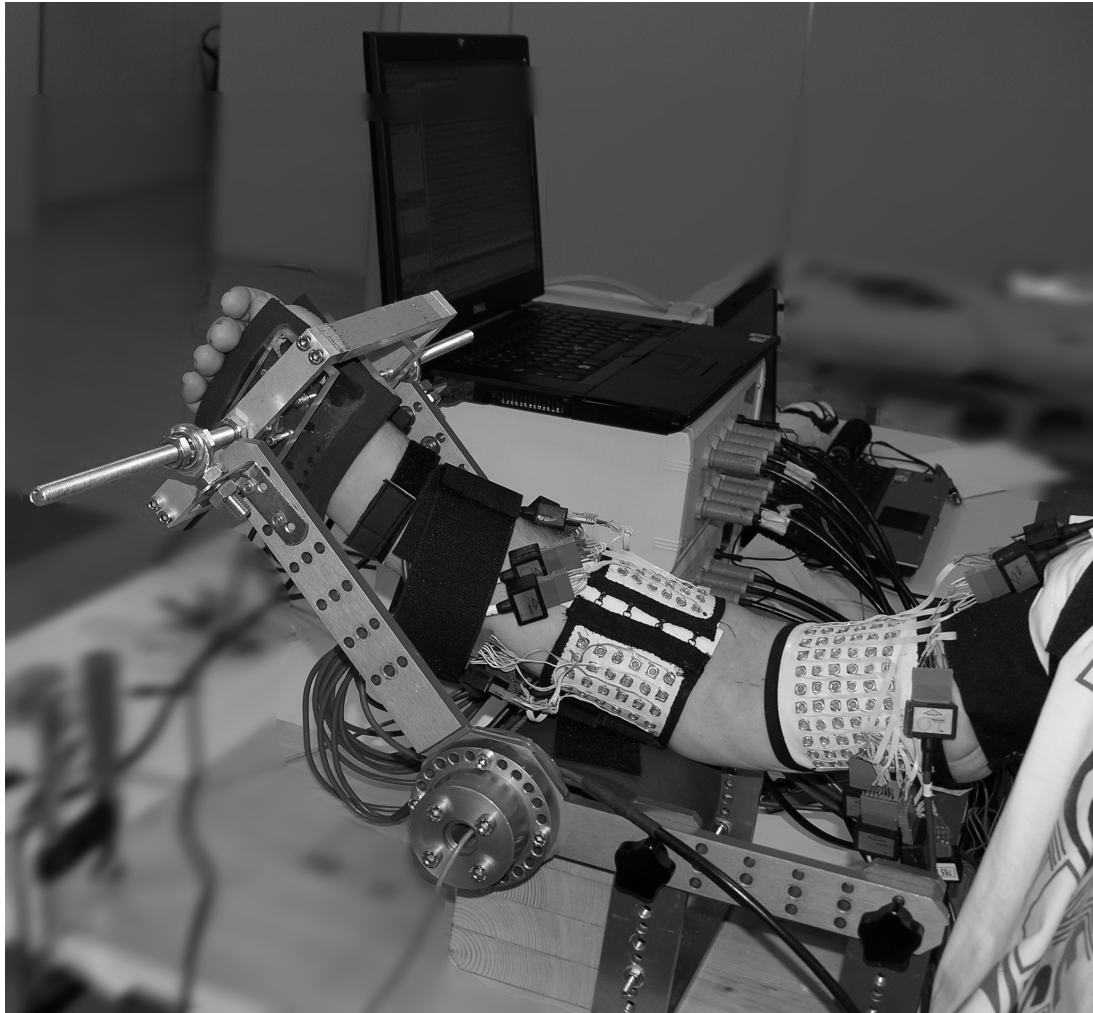


Figure 4.1: Experimental protocol

all three of them. The second and third array (6 rows \times 12 columns each) were placed following the recommendations of the SENIAM project (Hermens and Freriks, 1999) and they covered the Biceps Brachii (distal part of the upper-arm) and Triceps Brachii (proximal part of the upper-arm) respectively. The reference electrodes were placed on the clavicle, wrist, and shoulder of the active arm. When placed, each eyelet was filled with 20 μ l of conductive gel using a gel dispenser (Multipette Plus, Eppendorf, Germany). Signals were recorded using two commercial EMG amplifiers with synchronized sampling (EMG-USB- 128 channels, sampling frequency 2048 Hz, 12-bit A/D converter, 3 dB bandwidth 10-750 Hz, programmable gains of 100, 200, 500, 1000, 2000, 5000, 10000, manufactured by LISiN-OT Bioelettronica). At the beginning of the experimental protocol, the maximal voluntary contraction (MVC) was measured for each task, obtained as the maximum of three consecutive trials. Between each trial there was a three

minute rest to prevent cumulative fatigue. Afterwards, submaximal contractions for the four tasks at three different levels of effort (10% MVC, 30% MVC and 50% MVC) were measured. Patients were asked to maintain the target force as precisely as possible for 10 seconds while the exerted level was displayed to them. Recordings were performed in randomized order and between consecutive recordings there were three minute breaks to prevent muscle fatigue.

4.2.2 HD-EMG activation maps

In order to increase *signal-to-noise ratio* (SNR), the obtained HD-EMG signals were zero-phase filtered between 15 Hz and 350 Hz using a Butterworth band-pass filter of 4th order. Additionally, the power line interference was suppressed using the adaptive filter described in (Mañanas et al., 2001). Channels containing measurement artifacts were identified and removed following the procedure described in (Rojas-Martínez et al., 2012). Based on the torque measurements, 20 time epochs of 250 ms were selected for every recording during which patients were able to maintain the torque level within a range of $\pm 5\%$, $\pm 7.5\%$, and $\pm 10\%$ MVC for the targets of 10%, 30%, and 50% MVC respectively. On the selected epochs, HD-EMG maps, HM , were calculated as:

$$HM_{i,j} = \sqrt{\frac{1}{N} \sum_{n=0}^{N-1} sEMG_{i,j}^2[n]} \quad (4.1)$$

where HM was calculated for $N = 512$ samples corresponding to 250 ms. Maps were calculated as the RMS values obtained from myoelectric signals ($sEMG$), where the position (i, j) of a channel in the array was equivalent to the position of a pixel in the map. Channels identified as artifacts were substituted using a triangular-based cubic interpolation (Rojas-Martínez et al., 2012).

To reduce crosstalk activity of adjacent muscles that can occur on the borders of the map, maps were segmented according to (Rojas-Martínez et al., 2012). This procedure ensured that maps were localized and represented only regions of the associated muscle activity.

To calculate comparable activation maps among patients, spatial coordinates were normalized with respect to limb dimensions and position of an electrode array for every patient. A coordinate

system was built for each muscle where the x -axis was parallel to the medial-lateral direction, whereas the y -axis was parallel to the proximal-distal direction. The x -axis was normalized with respect to the upper-arm circumference measured at the muscle belly of either Biceps Brachii or Triceps Brachii for their corresponding maps, and with respect to the forearm circumference measured at the muscle belly of Brachioradialis for all three forearm muscle maps (Brachioradialis, Anconeus and Pronator Teres). Similarly, the y - axis was normalized with respect to the distance between the Acromion and the Fossa Cubit for Biceps Brachii, the distance between the Acromion and the Olecranon for Triceps Brachii map and the distance between the medial Epicondyle and the Apofysis of the Radius for forearm muscles (Brachioradialis, Anconeus and Pronator Teres).

The origins of these coordinate systems for muscles of upper-arm were set following SENIAM recommendations (Hermens and Freriks, 1999), that is, the point located at $3/4$ of the distance between Acromion and the Fossa Cubit for Biceps Brachii and $1/2$ of the distance between Acromion and the Olecranon for Triceps Brachii. The origin of the coordinate system for each muscle of the forearm was located on the line that connects the origin and insertion of the muscle (Kendall et al., 1993) 2 cm bellow the elbow crease.

Representative activation maps for each patient and recording were obtained by averaging 20 activation maps HM (Eq. 4.1). These maps were then averaged between individuals to obtain activation maps for the group of patients. Since tissue conductivity and electrode-skin impedance is different from patient to patient, the recorded sEMG amplitude can vary a lot between patients. To compensate this effect, the dispersion of each pixel was expressed in terms of relative standard deviation (RSD), i.e. standard deviation between representative maps of different patients was calculated for each pixel in the map, and was then divided by the intensity value of the corresponding pixel in the average activation map. Finally, the average RSD of a map was calculated as the mean value of RSD of all pixels in a map.

4.2.3 Identification

Two types of classifiers were evaluated: linear discriminant analysis (LDA), and support vector machine (SVM) with a radial kernel. Classification was performed in MATLAB (version 2015a)

using the Statistics and Machine Learning Toolbox (mat). Although when using LDA it is assumed that the patterns in each class are multivariate normally distributed with different means and identical covariance matrices, it is shown to be robust against deviations from the multivariate normality assumption (Grouven et al., 1996).

The features used in identification were the intensity and the center of gravity of HD-EMG maps calculated over 250 ms epochs.

Intensity was calculated as the common logarithm of the mean intensity of the map:

$$I = \log_{10} \frac{1}{N} \sum_{i,j} HM_{i,j} \quad (4.2)$$

where I is the intensity feature calculated for an N -channel HD-EMG map (HM). The center of gravity was calculated as:

$$CG = \frac{1}{\sum_{i,j} HM_{i,j}} \sum_{i,j} HM_{i,j} \begin{bmatrix} i \\ j \end{bmatrix} \quad (4.3)$$

where CG is the center of gravity of the HD-EMG map HM , and (i, j) represents position of the channel in the map.

Two types of identification were performed: **1) identification of tasks** and **2) identification of tasks and effort levels**. In identification of tasks, four types of contraction were identified: flexion, extension, supination and pronation. Performances were compared between using only intensity features and using the combination of intensity and spatial features of all five monitored muscles. In this sense, the possible improvement of pattern recognition was evaluated when adding spatial information.

A conjoint identification of tasks and effort levels was constructed as classification in two steps (Rojas-Martínez et al., 2013) (Figure 4.2). In the first step, the identification of tasks was performed, while in the second step, the level of effort of the identified task was determined. The second step was organized as 4 different classifiers, i.e. a single classifier for the identification of the effort level for each task (Figure 4.2). The features used in the identification of level of

effort were the intensity and the center of gravity of the agonist-antagonist muscle pair involved in the task (Rojas-Martínez et al., 2013): Biceps Brachii and Triceps Brachii both for flexion and extension, Biceps Brachii, Brachioradialis and Anconeus for supination, and Pronator Teres and Anconeus for pronation. Two different approaches were used: the identification of three effort levels (10% MVC, 30% MVC, and 50% MVC) and the identification of two effort levels (low, corresponding to 10% MVC, and moderate, corresponding to 30% and 50% MVC). Thus, a total of 12 different classes for the first approach and 8 classes for the second were considered, and accordingly, a confusion matrix of 12 or 8 classes was formed at the output of the second step of the classifier for the evaluation of the identification. Therefore, if a task was misclassified in the first step but the level of effort was correctly classified in the second step, this observation counted as a misclassification.

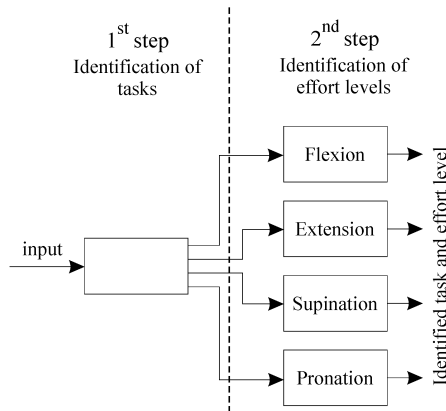


Figure 4.2: Schematic diagram of identification

Observations from all patients were pooled together and the identification was tested using the holdout method where 60% of the data were used for training and 40% for validation. Results were expressed in terms of accuracy (Acc), sensitivity (S), precision (P), and specificity (SP) (Farina et al., 2001):

$$Acc = \frac{TP + TN}{TP + FP + TN + FN} \quad (4.4)$$

$$S = \frac{TP}{TP + FN} \quad (4.5)$$

$$P = \frac{TP}{TP + FP} \quad (4.6)$$

$$SP = \frac{TN}{TN + FP} \quad (4.7)$$

where TP (true positive) is the number of samples belonging to a certain class and classified to that class, TN (true negative) is the number of samples not belonging to a certain class and not classified to that class, FP (false positive) is the number of samples not belonging to a certain class and classified to that class, and FN is the number of samples belonging to a certain class and classified to another class.

To reduce bias, a repeated holdout testing method was performed, i.e. the identification results were averaged over 20 iterations with randomized grouping for training and validation sets.

4.3 Results

4.3.1 Activation maps

Activation maps were calculated and averaged among patients to obtain general activation maps for tasks and levels of effort in order to observe the activation pattern of the muscles.

Table 4.1 presents the relative standard deviation (RSD) between representative activation maps of individual patients. Results are shown for all patients in the database and also only for patients injured at the C4 level. It can be seen that the variability of the group increased notably when patients with injury different to C4 were included. Thus, patients with the C4 level of injury can be considered as a homogenous group.

The activation maps averaged among patients with lesion at the C4 level are displayed in Figure 4.3. The maps were interpolated by factor 20 in both directions and cropped to the active regions for display purposes only. In addition, the spatial distribution of RSD for the same group of patients and for the same level of effort is shown in Figure 4.4. It can be seen that RSD was lower for Biceps Brachii and Triceps Brachii during their main tasks (flexion and extension,

Table 4.1: Relative standard deviation of activation maps for each muscle and effort level averaged between the group of all patients (top) and group of patients with C4 level of injury (bottom).

	Group of all patients			
	10% MVC	30% MVC	50% MVC	All effort levels
Biceps	49.7%	54.6%	57.3%	53.9%
Triceps	65.4%	65.5%	64.5%	65.1%
Brachioradialis	59.9%	67.6%	67.1%	64.9%
Anconeus	39.0%	40.6%	40.7%	40.1%
Pronator Teres	54.2%	58.3%	57.6%	56.7%
Average	53.6%	57.3%	57.4%	56.1%
	Group of patients with C4 level of injury			
	10% MVC	30% MVC	50% MVC	All effort levels
Biceps	38.1%	39.9%	41.7%	39.9%
Triceps	48.7%	47.2%	50.1%	48.6%
Brachioradialis	25.5%	28.1%	31.1%	28.2%
Anconeus	32.9%	32.9%	35.8%	33.9%
Pronator Teres	35.6%	36.1%	35.5%	35.7%
Average	36.2%	36.8%	38.8%	37.3%

respectively) indicating that patients had similar activation patterns. On the other hand, the RSD for these muscles was higher during supination and pronation, which indicates different activation strategies among patients. The inter-subject variability was lower for the forearm muscles, especially the Anconeus.

Table 4.2 shows the percentages of the areas of the activation maps used to calculate the features.

Table 4.2: Percentages of the activation maps covered by the electrode arrays in each patient. Results are presented for each muscle as mean and standard deviation within the group of all patients (top) and group of patients with C4 level of injury (bottom).

	Group of all patients				
	Biceps	Triceps	Brachioradialis	Anconeus	Pronator Teres
	50% \pm 7%	42% \pm 7%	36% \pm 8%	25% \pm 9%	37% \pm 12%
	Group of patients with C4 level of injury				
	Biceps	Triceps	Brachioradialis	Anconeus	Pronator Teres
	48% \pm 8%	42% \pm 8%	35% \pm 5%	22% \pm 8%	36% \pm 13%

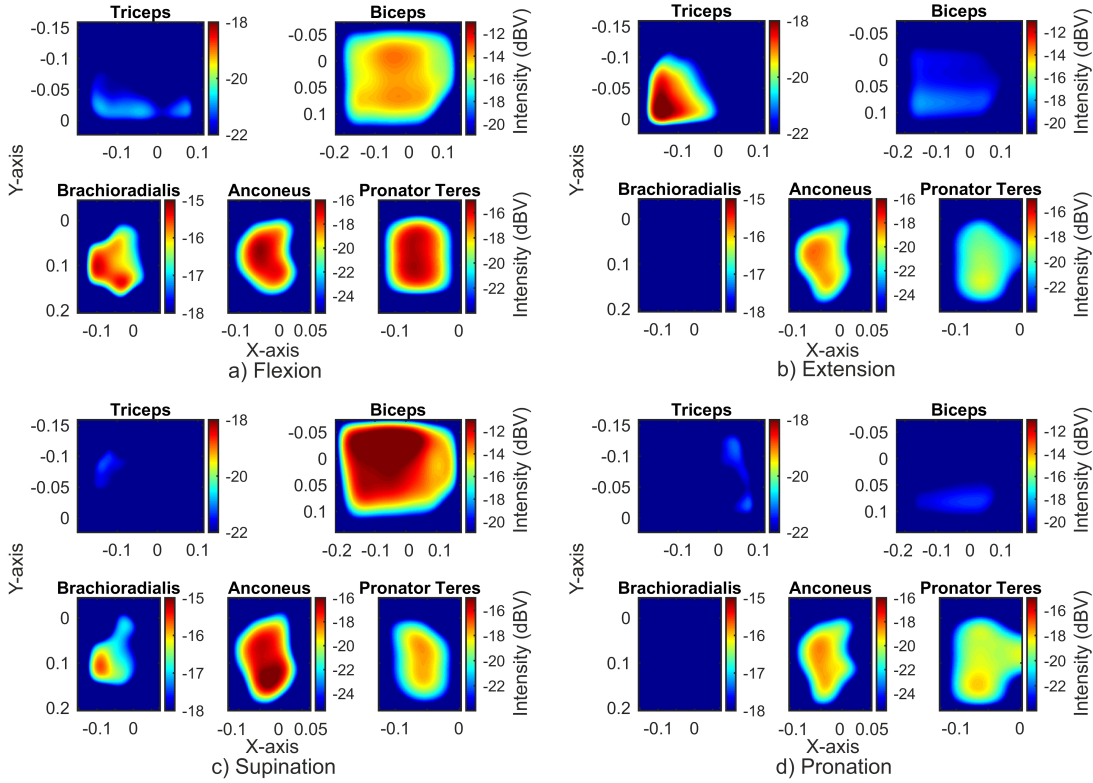


Figure 4.3: Activation maps of different tasks at 50% MVC averaged among patients with C4 level of injury

4.3.2 Identification of tasks

Firstly, the influence of the effort level in the task identification was evaluated. The performance is shown in Figures 4.5 to 4.8 using the LDA classifier while both training and validation sets were composed of recordings at a specific effort level (10%, 30%, or 50% MVC). The task identification improved considerably when adding CG to the intensity features for the classification in both groups: all patients (Figure 4.5 with respect to Figure 4.7) and patients with C4 level of injury (Figure 4.6 with respect to Figure 4.8). In addition, when comparing between the two groups, the identification performance was better in the latter (Figures 4.5 and 4.7 compared to Figures 4.6 and 4.8, respectively). These improvements were observed at all the effort levels. However, when comparing between effort levels, the performance indices (especially sensitivity and precision) were lower at 10% MVC than at 30% or 50% MVC, particularly when combining intensity with spatial features (Figures 4.7 and 4.8). This points out to a lower reliability when identifying tasks at very low levels of contraction.

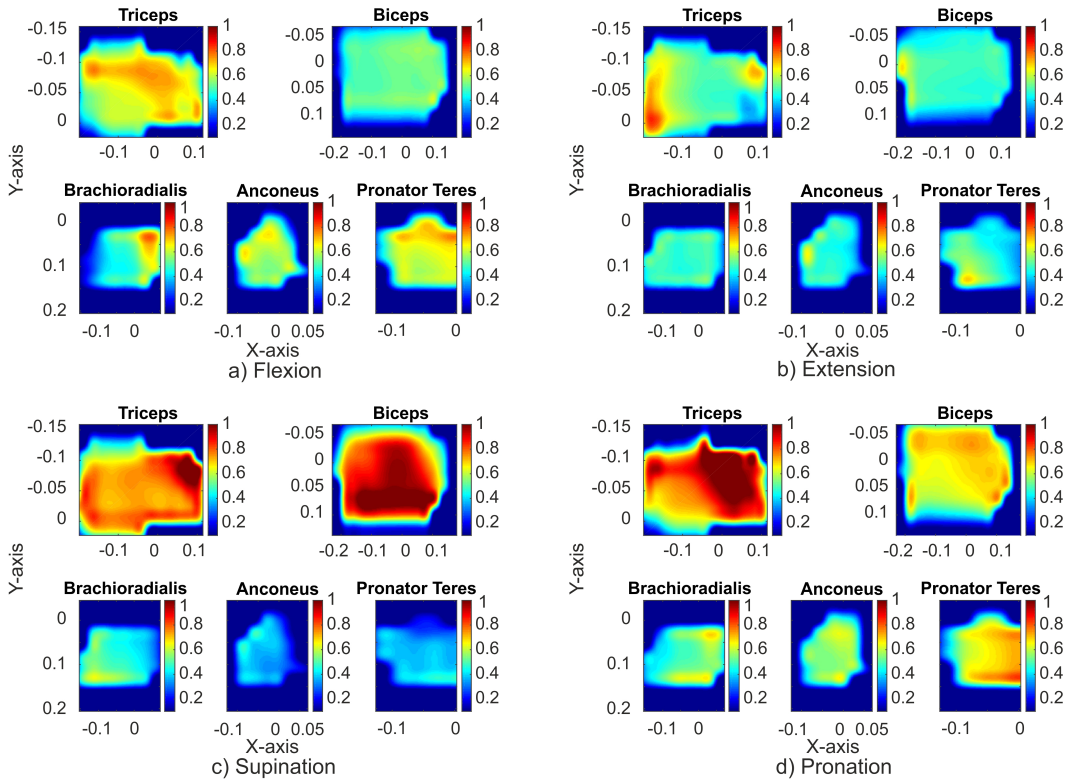


Figure 4.4: Relative standard deviation maps of different tasks at 50% MVC averaged among patients with C4 level of injury

Secondly, the task identification (flexion, extension, supination and extension) based on different sets of features was performed on the pooled data of all three effort levels, using the LDA (Table 4.3) and the SVM (Table 4.4) classifiers. It is shown again that the results for task identification when using the LDA classifier are higher for the group of patients with a C4 level of injury than for the group of patients with all levels of injury. Although this could be noticed from the performance indices when only the intensity features were used ($\Delta Acc = 4.1\%$; $\Delta S = 8.2\%$; $\Delta P = 7.8\%$; $\Delta SP = 2.7\%$), it was more pronounced when spatial features were added to the identification, especially regarding sensitivity and precision ($\Delta Acc = 7.6\%$; $\Delta S = 15.2\%$; $\Delta P = 15.2\%$; $\Delta SP = 5.1\%$). The observed differences between groups could be explained by a lower relative standard deviation between activation maps of patients with C4 level of injury than between maps of all patients). These differences between groups in the automatic identification were removed when using a non-linear classifier, that is, a radial kernel SVM, whose separation power is greater than the higher dispersion of activation maps when the complete group was considered.

Table 4.3: Identification of tasks using LDA classifier

	Intensity features			
	Accuracy	Sensitivity	Precision	Specificity
Flexion	82.6% \pm 1.2%	61.9% \pm 3.3%	66.3% \pm 2.7%	89.5% \pm 1.0%
Extension	79.2% \pm 1.1%	62.6% \pm 4.5%	57.9% \pm 2.1%	84.8% \pm 1.4%
Supination	82.8% \pm 1.1%	61.5% \pm 3.4%	67.0% \pm 2.7%	89.9% \pm 1.1%
Pronation	79.7% \pm 1.1%	62.6% \pm 2.5%	58.9% \pm 2.6%	85.4% \pm 1.8%
AVG all patients	81.1% \pm 1.1%	62.1% \pm 3.4%	62.5% \pm 2.5%	87.4% \pm 1.3%
AVG C4	85.2% \pm 1.0%	70.3% \pm 3.4%	70.3% \pm 2.6%	90.1% \pm 1.4%
	Combination of Intensity and center of gravity features			
	Accuracy	Sensitivity	Precision	Specificity
Flexion	90.7% \pm 0.8%	83.3% \pm 2.1%	80.4% \pm 2.3%	93.2% \pm 1.1%
Extension	84.6% \pm 1.1%	73.3% \pm 2.9%	67.8% \pm 2.8%	88.3% \pm 1.7%
Supination	91.6% \pm 0.9%	84.3% \pm 2.5%	82.6% \pm 1.9%	94.1% \pm 0.7%
Pronation	86.2% \pm 1.0%	65.4% \pm 2.6%	76.2% \pm 2.9%	93.1% \pm 1.1%
AVG all patients	88.3% \pm 0.9%	76.6% \pm 2.5%	76.8% \pm 2.5%	92.2% \pm 1.2%
AVG C4	95.9% \pm 0.9%	91.8% \pm 2.3%	92.0% \pm 2.1%	97.3% \pm 0.8%

Table 4.4: Identification of tasks using SVM classifier

	Intensity features			
	Accuracy	Sensitivity	Precision	Specificity
Flexion	95.9% \pm 0.6%	89.8% \pm 1.6%	93.8% \pm 1.8%	98.0% \pm 0.6%
Extension	95.8% \pm 0.9%	93.2% \pm 3.0%	90.4% \pm 1.7%	96.7% \pm 0.6%
Supination	95.9% \pm 0.6%	90.3% \pm 2.0%	93.2% \pm 1.9%	97.8% \pm 0.6%
Pronation	95.4% \pm 0.8%	92.8% \pm 1.6%	89.3% \pm 2.6%	96.3% \pm 1.1%
AVG all patients	95.8% \pm 0.7%	91.5% \pm 2.0%	91.7% \pm 2.0%	97.2% \pm 0.7%
AVG C4	95.9% \pm 0.7%	91.8% \pm 2.5%	91.9% \pm 2.4%	97.3% \pm 0.9%
	Combination of Intensity and center of gravity features			
	Accuracy	Sensitivity	Precision	Specificity
Flexion	98.8% \pm 0.4%	97.2% \pm 0.9%	97.8% \pm 1.0%	99.3% \pm 0.3%
Extension	99.0% \pm 0.4%	98.1% \pm 1.0%	98.0% \pm 0.9%	99.3% \pm 0.3%
Supination	98.7% \pm 0.4%	98.1% \pm 0.8%	96.8% \pm 1.0%	98.9% \pm 0.4%
Pronation	99.4% \pm 0.3%	98.4% \pm 1.0%	99.2% \pm 0.4%	99.7% \pm 0.1%
AVG all patients	99.0% \pm 0.4%	97.9% \pm 0.9%	98.0% \pm 0.8%	99.3% \pm 0.3%
AVG C4	99.1% \pm 0.4%	98.2% \pm 1.2%	98.2% \pm 1.0%	99.4% \pm 0.4%

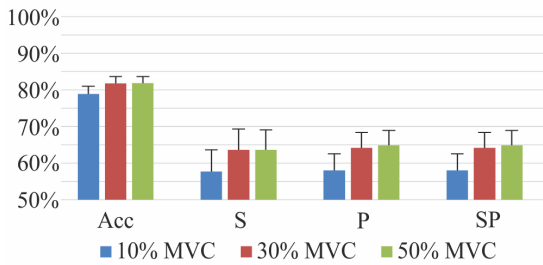


Figure 4.5: LDA classification within a group of all patients using intensity features.

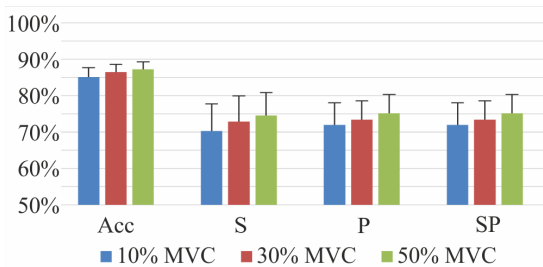


Figure 4.6: LDA classification within a group of C4 patients using intensity features

On the other hand, the performance of both classifiers improved when the center of gravity was added to the intensity features in the classification ($\Delta Acc = 7.2\%$; $\Delta S = 14.5\%$; $\Delta P = 14.3\%$; $\Delta SP = 4.8\%$ for LDA; $\Delta Acc = 3.2\%$; $\Delta S = 6.4\%$; $\Delta P = 6.3\%$; $\Delta SP = 2.1\%$ for SVM). For this reason, the results for the conjoint identification of tasks and effort levels are presented only for the combination of intensity and spatial features in the next Section.

Finally, when comparing the two classifiers, the results showed that the SVM notably outperformed the LDA for both combinations of features ($\Delta Acc = 14.7\%$; $\Delta S = 29.4\%$; $\Delta P = 29.2\%$; $\Delta SP = 9.8\%$ when using only intensity features; and $\Delta Acc = 10.7\%$; $\Delta S = 21.4\%$; $\Delta P = 21.2\%$; $\Delta SP = 7.1\%$ when using the combination of both intensity and center of gravity features).

4.3.3 Identification of tasks and effort levels

The performance indices for conjoint identification of the four tasks and the three effort levels using intensity and spatial features are presented in tables 4.5 and 4.7 for the LDA and SVM classifiers, respectively. Analogously, the joint identification of the four tasks and low and moderate effort levels are presented in tables 4.6 and 4.8 for the LDA and the SVM classifiers, respectively. Similarly to the task identification, improvements considering the group of patients with a C4 level of injury with respect to the whole group were found when using the LDA, but

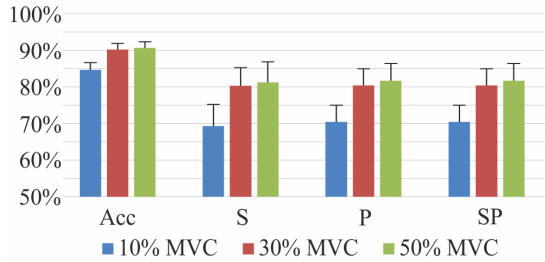


Figure 4.7: LDA classification within a group of all patients using intensity and spatial features

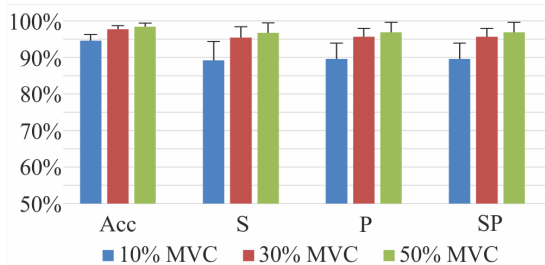


Figure 4.8: LDA classification within a group of C4 patients using intensity and spatial features

not with the SVM classifier ($\Delta Acc = 3.8\%$; $\Delta S = 22.6\%$; $\Delta P = 23.6\%$; $\Delta SP = 2.1\%$ for identification of three levels of effort; $\Delta Acc = 5.8\%$; $\Delta S = 23.1\%$; $\Delta P = 23.4\%$; $\Delta SP = 3.3\%$ for identification of low and moderate effort levels).

Both in the LDA and SVM classifiers the improvement could be seen when identifying low and moderate effort levels instead of three contraction levels ($\Delta S = 14.3\%$; $\Delta P = 15.9\%$ for LDA; $\Delta S = 6.8\%$; $\Delta P = 7.1\%$ for SVM). Note that in this case, when comparing between identifications with different number of classes (12 or 8 classes for three or two effort levels, respectively), accuracy and specificity are not the appropriate indices, as described in (Rojas-Martínez et al., 2013). These two measures are biased by the high number of observations not belonging to a given group and correctly identified as members of the other groups (TN). Thus, because of the higher number of classes, and consequently, higher number of TN observations, these indices tend to have seemingly higher results of identification of tasks and three effort levels. In this comparison, S and P are more appropriate measures because they are not affected by the number of TN (see Eq. 4.4 to Eq. 4.7) but by the number of observations for each group that were correctly classified to that group (TP) with respect to the number of those that were wrongly classified to another group (FN), and with respect to those that were incorrectly classified as members of the group (FP), respectively. Finally, in all cases, the SVM-based identification outperformed the LDA-based both in the conjoint identification of tasks and three effort levels

Table 4.7: SVM identification of tasks and three effort levels

	Accuracy	Sensitivity	Precision	Specificity
Flexion	98.1% \pm 0.4%	88.6% \pm 3.7%	89.5% \pm 3.2%	99.0% \pm 0.3%
Extension	97.6% \pm 0.4%	85.4% \pm 3.7%	85.4% \pm 3.3%	98.7% \pm 0.4%
Supination	97.8% \pm 0.4%	87.5% \pm 3.3%	86.4% \pm 3.9%	98.7% \pm 0.4%
Pronation	96.6% \pm 0.4%	79.3% \pm 5.0%	79.9% \pm 3.8%	98.2% \pm 0.5%
AVG all patients	97.5% \pm 0.4%	85.2% \pm 3.9%	85.3% \pm 3.5%	98.7% \pm 0.4%
AVG C4 patients	97.3% \pm 0.5%	84.1% \pm 5.4%	84.4% \pm 4.5%	98.6% \pm 0.5%

Table 4.8: SVM identification of tasks and low and moderate effort levels

	Accuracy	Sensitivity	Precision	Specificity
Flexion	98.7% \pm 0.4%	94.4% \pm 2.7%	95.6% \pm 2.2%	99.4% \pm 0.3%
Extension	97.9% \pm 0.4%	91.5% \pm 3.7%	92.4% \pm 3.0%	98.8% \pm 0.5%
Supination	97.9% \pm 0.6%	92.8% \pm 2.8%	91.2% \pm 3.2%	98.7% \pm 0.5%
Pronation	97.5% \pm 0.6%	89.5% \pm 3.5%	90.6% \pm 3.1%	98.6% \pm 0.5%
AVG all patients	98.0% \pm 0.5%	92.0% \pm 3.2%	92.4% \pm 2.9%	98.9% \pm 0.5%
AVG C4 patients	97.8% \pm 0.7%	91.4% \pm 3.9%	91.7% \pm 3.6%	98.8% \pm 0.6%

($\Delta Acc = 7.6\%$; $\Delta S = 45.5\%$; $\Delta P = 46.1\%$; $\Delta SP = 4.1\%$) and in the identification of tasks and low and moderate effort levels ($\Delta Acc = 9.5\%$; $\Delta S = 38.0\%$; $\Delta P = 37.4\%$; $\Delta SP = 5.4\%$). The interactions between classifiers, tasks, and effort levels were analyzed using a repeated measures analysis of variance. The post hoc pairwise comparison of means was performed with application of the Bonferroni correction factor. Effects were considered to be significant at p-value $p = 0.01$. The interaction between the classifier and the task, as well as the interaction between the classifier and the effort level were both found significant. However, the post hoc pairwise comparison of means showed no significant differences between the identification results across individual tasks for the SVM classifier, whereas the extension and, especially, the pronation had much lower identification indices than the flexion and the supination for the LDA classifier. When considering the influence of the classifier on the identification of effort level, the detection of 10% MVC had in average the highest performance in both classifiers, but the LDA detected 30% MVC effort level much worse than the 50% MVC effort level, whereas there was no significant difference in detection between 30% MVC and 50% MVC using the SVM.

Table 4.9: Identification of tasks using a subset of electrodes: Classification indices using a 3×3 electrode grid located randomly in each muscle. Results are averaged within the group of all patients (top) and group of patients with C4 level of injury (bottom).

	LDA			
	Accuracy	Sensitivity	Precision	Specificity
AVG all patients	$79.2\% \pm 2.7\%$	$58.5\% \pm 6.5\%$	$58.9\% \pm 5.8\%$	$86.1\% \pm 2.8\%$
AVG C4	$83.5\% \pm 3.2\%$	$67.1\% \pm 7.1\%$	$67.5\% \pm 7.1\%$	$80.0\% \pm 3.1\%$
SVM				
	Accuracy	Sensitivity	Precision	Specificity
AVG all patients	$94.8\% \pm 1.1\%$	$89.7\% \pm 3.3\%$	$89.7\% \pm 2.8\%$	$96.5\% \pm 1.0\%$
AVG C4	$94.8\% \pm 1.4\%$	$89.6\% \pm 3.8\%$	$89.8\% \pm 3.9\%$	$96.5\% \pm 1.5\%$

4.3.4 Classification using smaller arrays of electrodes

Subsets of electrodes (3×3 electrodes) were considered in the identification of tasks and levels of effort to evaluate the classification performance using a lower number of electrodes at different positions. Four different locations within the area covered by the entire array were selected randomly for each muscle to evaluate the impact of their placement on the identification performance. The identification was carried out following the same procedure as considering the entire array but using only the intensity features, because the spatial information could not be measured using these small arrays. The average results of the identification of tasks can be seen in table 4.9, whereas the average results of the identification of tasks and three effort levels can be seen in table 4.10.

Results obtained using 3×3 electrode grids were slightly worse than the results obtained using the entire electrode arrays (see tables 4.3 and 4.4). In addition, the classification indices of conjoint identification of tasks and effort levels were very low, inferring that the results obtained by adding spatial features (see tables 4.5 and 4.7) cannot be reached with a smaller grid of electrodes.

Table 4.10: Identification of tasks and three effort levels using a subset of electrodes: Classification indices using a 3×3 electrode grid located randomly in each muscle. Results are averaged within the group of all patients (top) and group of patients with C4 level of injury (bottom).

	LDA			
	Accuracy	Sensitivity	Precision	Specificity
AVG all patients	$88.1\% \pm 1.3\%$	$28.7\% \pm 7.4\%$	$28.3\% \pm 6.4\%$	$93.5\% \pm 1.5\%$
AVG C4	$89.7\% \pm 1.6\%$	$38.4\% \pm 9.1\%$	$38.8\% \pm 9.1\%$	$94.4\% \pm 1.6\%$
SVM				
	Accuracy	Sensitivity	Precision	Specificity
AVG all patients	$93.8\% \pm 8.5\%$	$62.9\% \pm 7.5\%$	$63.3\% \pm 5.7\%$	$96.6\% \pm 0.8\%$
AVG C4	$93.8\% \pm 1.0\%$	$62.9\% \pm 8.6\%$	$63.6\% \pm 6.9\%$	$96.6\% \pm 1.0\%$

4.4 Discussion

In order to demonstrate the existence of distinguishable group-specific patterns in HD-EMG, the identification of different tasks was performed. Within-group identification of motion intention at different effort levels was tested on nine patients with iSCI performing four upper limb tasks (flexion/extension of the elbow and supination/pronation of the forearm) at three different effort levels (10%, 30%, and 50% MVC).

Although a single type of a classifier would be sufficient to demonstrate the existence of different patterns, for an additional verification two types of classifiers were evaluated in the identification of motion intention: LDA and SVM. The former is a classical, simple, and computationally efficient classification method, whereas the latter is a more powerful classifier that can employ a nonlinear transform of features to improve their separability among classes. In this paper, a SVM with radial kernel was considered. Although the SVM is superior in classification performance, the LDA is commonly used in myocontrol applications because of its simplicity and performance in real-time. However, with the increasing computational power of new computer generations, SVM could become more common in these applications.

The identification of tasks was tested using two feature sets: 1) the average intensities of HD-EMG activation maps (I) of five muscles and 2) the combination of average intensities and centers of gravity ($I+CG$) of the activation maps of five muscles. On the other hand, a conjoint

identification of tasks and effort levels was designed as two-step classifier, following the procedure described by Rojas-Martínez et al. (2013) and tested on a healthy population. The first step comprised the identification of tasks using a combination of intensity and spatial features of all five muscles, whereas in the second step the levels of effort were identified separately for each task. The effort levels were identified using a combination of the intensity and spatial features of agonist-antagonist muscle pairs involved in the task (Rojas-Martínez et al., 2013).

HD-EMG activation maps were calculated for all exercises and compared among patients.

Rojas-Martínez et al. calculated the relative standard deviation between maps within a group of healthy subjects (17.4% in average), reporting an increase in standard deviation between maps with increasing effort levels (12.1%, 16.6%, and 23.6% for 10%, 30%, and 50% MVC, respectively) (Rojas-Martínez et al., 2012). As expected, the dispersion between maps of iSCI patients was considerably higher (56% in average), but the variability was similar in the case of patients with iSCI (table 4.1). However, when maps were compared among patients with the same level of injury, the standard deviation between maps was greatly reduced (19% in average). Moreover, the variability was higher for muscles of the upper-arm (biceps and triceps) than for forearm muscles. This reduction could be either due to a distinct activation, specific to the level of injury, or because during the rehabilitation process patients developed similar activation patterns. This is an important finding that has to be taken into account when training a classifier for a group of patients. Muscle activation patterns in patients differed from those of healthy subjects in (Rojas-Martínez et al., 2012): the Biceps Brachii was more active during supination than during flexion; the Pronator Teres was more active during supination and especially during flexion than during pronation. This could be because both muscles are particularly affected by the iSCI at the level of C4 (Young).

Furthermore, the results using the LDA showed much better identifications within the group of patients with a C4 level of injury than within the group of all patients. These findings could be related to a higher homogeneity among patients with the same level of injury. The combination of intensity and center of gravity performed better than only intensity features. These results showed that similar patterns exist in spite of the diverse nature of their injuries. This correlation exists not only in the average intensity of the HD-EMG activation maps, but also in the spatial

distribution of EMG intensity, which justifies the choice of these intensity and spatial features for automatic identification.

Finally, a considerable improvement was observed when using the SVM instead of the LDA, reaching the following results: 1) excellent automatic task identification even in the group of all patients ($Acc = 99.0\%$, $S = 97.9\%$, $P = 98.0\%$, and $SP = 99.3\%$), 2) a good combined classification of four tasks and three effort levels also in the group of all patients ($Acc = 97.5\%$, $S = 85.2\%$, $P = 85.3\%$, and $SP = 98.7\%$) which is even better in 3) conjoint identification of four tasks and low or moderate effort levels ($Acc = 98.0\%$, $S = 92.0\%$, $P = 92.4\%$, and $SP = 98.9\%$). In spite of the previous reports suggesting the greater importance of selection of the features than the selection of the classifier, our results have shown that both have considerable impact on the identification.

Several array subsets corresponding to 3×3 square grids of channels (IED = 10 mm) located at different positions were also used to evaluate the possibility of task identification using a much smaller number of electrodes. In this case, the results were considerably worse, especially when using the LDA classifier. Due to the small region covered by electrodes in each muscle, the spatial information could not be extracted and it was not possible to increase the performance as in the case of using all the electrodes.

Although this study presents an important improvement in the identification of motion intention, it is important to mention that the recordings were carried out during highly controlled isometric contractions. Therefore, even though the findings are promising, they are only a step towards final real-time applications involving free movements and multiple DoFs.

The results show that the use of a SVM-based classifier is indeed a promising approach in myocontrol-oriented pattern recognition applications. Moreover, even though a different activation pattern can be expected in subjects with neurological impairment, as in the present case, such pattern can still be associated with task and level-dependent changes in the spatial distribution of the intensity, as has been previously observed in non-injured subjects (Rojas-Martínez et al., 2012).

4.5 Conclusions

Group-specific identification of motion intention in impaired patients has a potential to improve the translation of pattern recognition techniques to clinical practice. Unfortunately, group-specific design is a difficult topic because it assumes strong task-related and level of effort-related co-activation patterns among patients, but given the diverse nature of injuries and the high inter-patient variability, co-activation patterns are weak.

This study shows that muscular co-activation patterns in intensity and spatial distribution indeed exist. Furthermore, it shows that stronger co-activation patterns can be found between patients of the same level of injury. Whether because of the rehabilitation process or the level of injury, muscle control strategies are similar for the group of patients with an injury at C4, which makes them a more homogenous population and enables the control of universal assistive devices with higher reliability. In summary, in spite of the difficulty to identify both task and effort level in patients with iSCI, very promising results were found to provide a useful estimation of motion intention.

4.6 Acknowledgements

Special acknowledgement to Ursula Costa and Josep Medina as assistant and Head of the Functional Rehabilitation service respectively, of the Neurorehabilitation Hospital Institut Guttmann for their collaboration in patients recruitment and clinical support during the experiments carried out at the same Hospital.

This work has been partially supported by the Spanish Ministry of Economy and Competitiveness-Spain (project DPI2014-59049-R), and by the FI grant from the AGAUR, Generalitat de Catalunya, Spain.

Chapter 5

A Novel Spatial Feature for the Identification of Motor Tasks Using High-Density Electromyography

Published as: Jordanić, M., Rojas-Martínez, M., Mañanas, M.A., Alonso J.F., Marateb H.R. A Novel Spatial Feature for the Identification of Motor Tasks Using High-Density Electromyography *Sensors* 17(7):1597, 2017

doi: 10.3390/s17071597

Impact Factor: 2.077; Position: 10 of 58 (Q1) INSTRUMENTS AND INSTRUMENTATION.

Abstract: Estimation of neuromuscular intention using electromyography (EMG) and pattern recognition is still an open problem. One of the reasons is that the pattern-recognition approach is greatly influenced by temporal changes in electromyograms caused by the variations in the conductivity of the skin and/or electrodes, or physiological changes such as muscle fatigue. This paper proposes novel features for task identification extracted from the high-density electromyographic signal (HD-EMG) by applying the mean shift channel selection algorithm evaluated using a simple and fast classifier-linear discriminant analysis. HD-EMG was recorded from eight subjects during four upper-limb isometric motor tasks (flexion/extension, supination/pronation of the forearm) at three different levels of effort. Task and effort level identification showed very

high classification rates in all cases. This new feature performed remarkably well particularly in the identification at very low effort levels. This could be a step towards the natural control in everyday applications where a subject could use low levels of effort to achieve motor tasks. Furthermore, it ensures reliable identification even in the presence of myoelectric fatigue and showed robustness to temporal changes in EMG, which could make it suitable in long-term applications.

Keywords: high-density electromyography; pattern recognition; myoelectric control; mean shift; prosthetics

5.1 Introduction

Electromyography (EMG) is a technique for recording the electrical activity produced by skeletal muscles. The EMG signal is a summation of action potentials produced by muscle fibers, directly triggered by the action potentials traveling along motor neurons (Farina et al., 2010). Since EMG is an important source of neural information, it has been extensively studied in the field of human-machine interfacing (Nazmi et al., 2016; Hakonen et al., 2015). Applications of EMG include the control of neurorehabilitation devices such as prostheses (Parker et al., 2006; Li et al., 2010), rehabilitation robots (Marchal-Crespo and Reinkensmeyer, 2009; ?), and identification of muscle anatomical structure (Marateb et al., 2016), but also implementations in leisure activities such as sports (Verikas et al., 2016) and computer games (van Dijk et al., 2016).

EMG signals could be recorded either non-invasively (surface EMG, sEMG) or invasively with needle and wire electrodes (intramuscular EMG, iEMG) (Marateb et al., 1999). Although the iEMG has higher signal-to-noise ratio, both approaches provide a similar quality of identification of upper-arm motor task (Hargrove et al., 2007). Moreover, sEMG is preferred as it is recorded non-invasively.

The pattern recognition approach has been recently used in research laboratories as a state-of-the-art method to decode neural information. Its main advantage over conventional systems is the instant activation of a task belonging to any of the available degrees-of-freedom (DoFs). Many classifiers such as linear discriminant analysis (LDA), support vector machine, and artifi-

cial neural network were successfully employed for this purpose with a high identification fidelity (Oskoei and Hu, 2007), but many authors agree that the choice of the features is more important than the choice of the classifier (Hargrove et al., 2007). Hence, simple and fast classifiers are preferred, among which the LDA is commonly used and has become a general recommendation (Hakonen et al., 2015; Huang et al., 2009). In addition, different studies have focused on pattern recognition from the analysis of isometric contractions for myoelectric control, especially when considering subjects with neuromuscular impairment (in stroke for example) (Celadon et al., 2016) and even for prostheses control for amputees (Ameri et al., 2012). Additional examples can be found in (Li et al., 2013; Jordanic et al., 2016; Jordanić et al., 2016).

Features can be calculated in time, frequency/scale, and time-frequency/scale domain (Nazmi et al., 2016; Hakonen et al., 2015; Oskoei and Hu, 2007). Time domain features are usually used because of their computational simplicity and good performance (Hakonen et al., 2015). Additionally, they can be combined with other features to increase the performance, e.g., autoregressive features (Hargrove et al., 2007).

The influence of the physiological (e.g., muscle fatigue) or non-physiological (electrode-skin impedance) non-stationarity of the EMG features is a big issue in neuromuscular control. As a solution, (Vidovic et al., 2016) and (Hahne et al., 2015) proposed a real-time retraining of the classifier where the parameters are constantly updated. Liu et al. (2016a) proposed a universal LDA classifier which was trained during different days and then combined. Such methods adapt the model to changes in the features, rather than using robust features.

Moreover, the variation of force can affect the identification (Tkach et al., 2010). (Scheme and Englehart, 2013) recommended to train the classifier using all effort levels, whereas (He et al., 2015) tackled the problem using a feature set based on the frequency content of the signal and muscle coordination.

With the recent introduction of high-density EMG (HD-EMG) (Merletti et al., 2009), i.e., multichannel EMG recorded using 2D grids of closely spaced sEMG electrodes, multiple studies have reported improvement in task identification. Stango et al. reported that spatial features extracted from the HD-EMG are robust to the electrodes shift. (Geng et al., 2016) and (Du et al., 2017) exploited the power of deep convolutional network to design gesture recognition

classifier that classifies instantaneous maps, i.e., raw HD-EMG samples. Hahne et al. extracted features using spatial filters optimized to increase separability between different classes (Hahne et al., 2012). These methods exploit the information about the spatial muscle activation pattern extracted from the HD-EMG and the fact that the myoelectric activity over different parts of muscle depends on the various factors (e.g., contraction level (Holtermann et al., 2005), duration of the contraction (Tucker et al., 2009), and joint position (Vieira et al., 2010)) and can be useful in differentiation between tasks.

In our previous work, we used the center of gravity as a feature to describe spatial patterns in HD-EMG (Jordanic et al., 2016; Jordanić et al., 2016; Rojas-Martínez et al., 2013). In this work, we propose a new spatial feature for task identification based on the modified mean shift algorithm. Novel features were evaluated in the identification of four isometric motor tasks of the upper-limb (flexion/extension, supination/pronation of the forearm) using the LDA classifier. The proposed features were tested in three conditions: when the training set and the test set were recorded at the same time (time-dependent changes in the signal are minor), when the test set was recorded after the training set, and during the fatiguing exercise. In addition, features were tested during the identification of the task recorded at different effort levels. The proposed features proved to improve the identification and are especially useful in extreme cases like identification of tasks recorded at very low effort level or identification of tasks during fatigue. These results confirm the usefulness of information of spatial distribution of myoelectric intensity over the muscle in discrimination between tasks. The rest of the paper is organized as follows: in the next section (section 5.2), information about the experimental protocol and the task identification method used in this study is presented. Section 5.3 provides the results of the identification using the proposed features and its comparison with the previously established features. The discussion is provided in Section 5.4 and finally, the conclusions are summarized in Section 5.5.

5.2 Materials and methods

5.2.1 Instrumentation and measurement protocol

Eight healthy subjects (age: 36 ± 5 years; height: 177 ± 5 cm; weight: 75 ± 9 kg; body mass index: 23.7 ± 2.3) participated in the experiment. They reported no pain, and previously had not suffered any injuries or neuromuscular upper limb impairments. The study was conducted in accordance with the Declaration of Helsinki and subsequent amendments concerning research in humans and was approved by the University Ethics Committee and the local government. Recordings and results were documented with the registration number, which corresponded to the Spanish ministry project MICINN (TEC2008-02274): “Analysis of the dynamic interactions in non-invasive multichannel biosignals for rehabilitation and therapy”. All subjects gave their written informed consent to participate in the experimental protocol.

Subjects performed four different isometric upper-limb tasks with two degrees of freedom: flexion/extension and supination/pronation of the forearm. During the experiment they were seated upright with their back being straight. Their dominant arm was positioned in the sagittal plane with the elbow flexed at 45 degrees and the forearm positioned in the middle between supination and pronation, thumb pointing upwards (Figure 5.1a). To avoid muscle activation due to gripping, their hands were fixed at the wrist using a mechanical brace. The brace also contained two torque meters that measured exerted torque at the elbow joint.

HD-EMG was measured on five superficial muscles involved in the presented tasks: biceps brachii, triceps brachii, brachioradialis, anconeus, and pronator teres. Signals were recorded using three two-dimensional electrode arrays manufactured as silver-plated eyelets (2.5 mm radius) positioned in a quadrature grid with a 10 mm inter-electrode distance and embedded in a non-conductive fabric (Figure 5.1b).

After the skin was shaved, cleaned, and treated with abrasive gel, the following electrode arrays were positioned over the upper limb using elastic straps: two electrode arrays (dimensions: 8 rows \times 15 columns) were positioned on the upper arm covering biceps brachii and triceps brachii muscles. The center of each electrode array was placed according to the positions recommended by the SENIAM project (Hermens and Freriks, 1999). The third electrode array was placed over

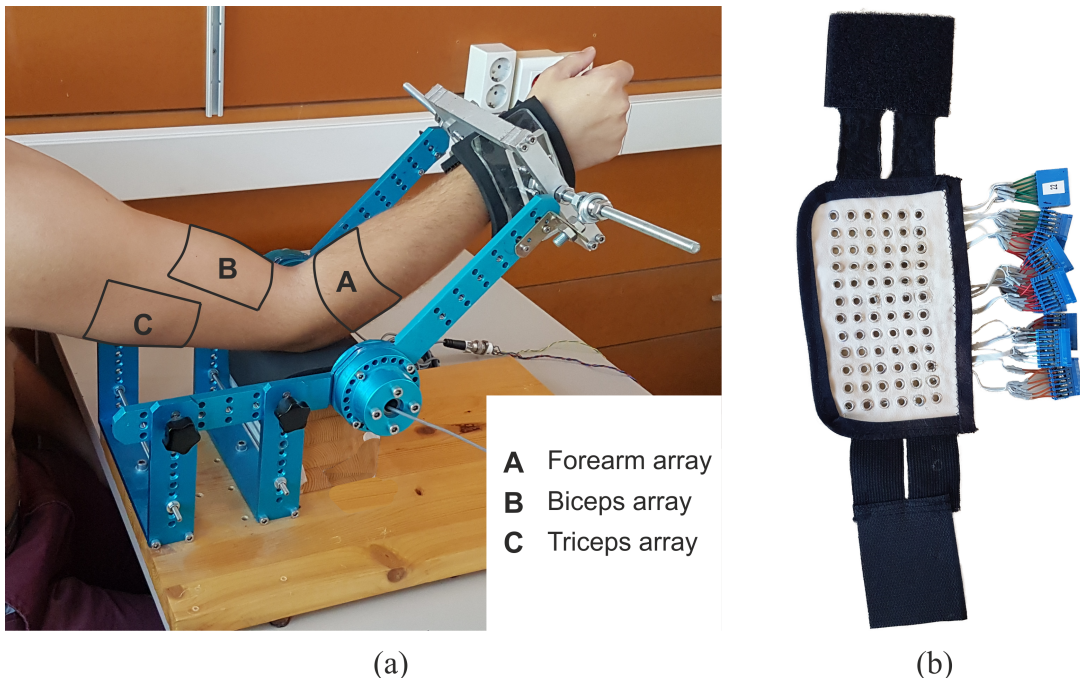


Figure 5.1: Figure shows (a) the position of the arm in the mechanical brace during the recording with the marked outlines of the electrode arrays; and (b) an electrode array.

the forearm, with the first row of electrodes approximately 2 cm below elbow crest, covering brachioradialis, anconeus, and pronator teres muscles. A line connecting the origin and insertion of the targeted muscles were previously marked on the skin and the electrode array was placed to optimally cover these muscles. The forearm electrode array had six rows and between 17 and 19 columns, depending on the forearm circumference. After positioning the electrodes, the conductive gel was applied through the eyelet of each electrode ($20 \mu\text{L}$) using the dosimeter (Multipette Plus, Eppendorf, Germany).

HD-EMG signals were recorded in monopolar mode using three commercially available amplifiers with simultaneous sampling (EMG-USB, 128 channels, 2048 Hz sampling frequency, 10–750 Hz passband, manufacturer LISiN-OT Bioelettronica, Turin, Italy). Torque exerted on the elbow joint was measured using two torque transducers (OT Bioelettronica, range 150 Nm) and was displayed to the patient in real time. The detailed information on the instrumentation settings can be found in (Rojas-Martínez et al., 2012).

Prior to the experiment, the maximal voluntary contraction (MVC) was measured for each task as the maximal of three consecutive trials. In the first part of the experiment subjects were instructed to perform four defined tasks at three randomized different effort levels: 10%

MVC, 30% MVC, and 50% MVC. Having been instructed to maintain the target level for 10 s, the exerted torque was displayed to the subjects. Tasks were performed in random order and between two consecutive recordings there was a two-minute rest to prevent cumulative fatigue.

Approximately 30 min (33 ± 3 min) after the first part of the protocol, endurance measurements were performed. Subjects were instructed to perform each task at 50% MVC until failure. After each measurement, subjects rested for five minutes.

5.2.2 HD-EMG processing

The recorded HD-EMG signals were band-pass filtered using a 4th order Butterworth filter, with the cut-off frequencies of 15 Hz and 350 Hz, in the forward and reverse direction as to minimize the distortions. Outlier channels were automatically identified using a previously described algorithm (Rojas-Martínez et al., 2012). HD-EMG recordings were divided into non-overlapping 150 ms time windows and the average HD-EMG activation maps were then calculated for each window in all three electrode arrays (biceps, triceps, forearm) using the RMS values. Activation maps can be conceptually perceived as images where pixels correspond to channels, and pixel intensities correspond to the muscle activation map in each channel. They were calculated as:

$$AM_{i,j} = \sqrt{\frac{1}{N} \sum_{n=0}^{N-1} EMG_{i,j}^2[n]} \quad (5.1)$$

where AM is the activation map, N corresponds to the number of samples in each window (given a sampling frequency of 2048 Hz, $N = 410$), and $EMG_{i,j}$ denotes the EMG signal recorded by the electrode located at (i, j) position in the recording array. Pixels in AM corresponding to the outlier channels previously identified as artifacts were discarded and substituted using the triangular interpolation (Rojas-Martínez et al., 2012).

5.2.3 Feature extraction

Identification was performed using the combination of intensity features and spatial features (Figure 5.2). Spatial features were extracted using the mean shift algorithm (Comaniciu and

Meer, 2002), a non-parametric approach to estimate modes (local maxima) of the underlying density function by an iterative procedure. The details of the mean shift algorithm are provided in the Appendix A and are briefly discussed here. A centroid point y was positioned at a random point in the space and the mean value was calculated for all points x , which were located within the Euclidean distance, i.e., bandwidth h , from the current centroid. This mean value was assigned as a new position of a centroid y in the next iteration. The procedure can be mathematically defined as:

$$y_{i+1} := \frac{\sum_{j=1}^M x_j}{M} \Bigg|_{\forall x \text{ s.t. } \|x - y_i\| \leq h} \quad (5.2)$$

where x_j ($j = 1, 2, \dots, M$) are samples of the unknown distribution, y_i is the centroid in the i^{th} iteration of the algorithm and the h is a bandwidth parameter. The algorithm stops when the position of the centroid (y) remains constant in consecutive iterations (up to a tolerance). This centroid y is considered to be a mode of the underlying density function. In this study, modes of the density function of RMS activation maps were found using the mean shift algorithm implemented in Python (Pedregosa et al., 2011) and were used as features in the identification.

The bandwidth h was estimated automatically for each map. The maximum Euclidean distance between k nearest neighbors (where k was set to 50% of the total number of elements in the map) was calculated for every sample and the average of the maximum distances was calculated. The bandwidth used in this paper was obtained by multiplying this average distance by a bandwidth factor of 0.5, selected as a tradeoff between the amount of information and the processing time.

Prior to using the mean shift algorithm, each RMS activation map was transformed to a matrix of n rows, each row a channel, by three columns where the first two corresponded to the x , and y location of the channel in the activation map and the third to its intensity as estimated from the RMS of the signal. Since we used the spherical kernel, i.e., the bandwidth h had an equal value in all three dimensions, data was standardized to have zero mean and unity variance in all three dimensions.

A matrix of zeros with the same dimension of the electrode array was then created. Each mode detected by the mean shift algorithm was mapped to the closest location of the electrode in the

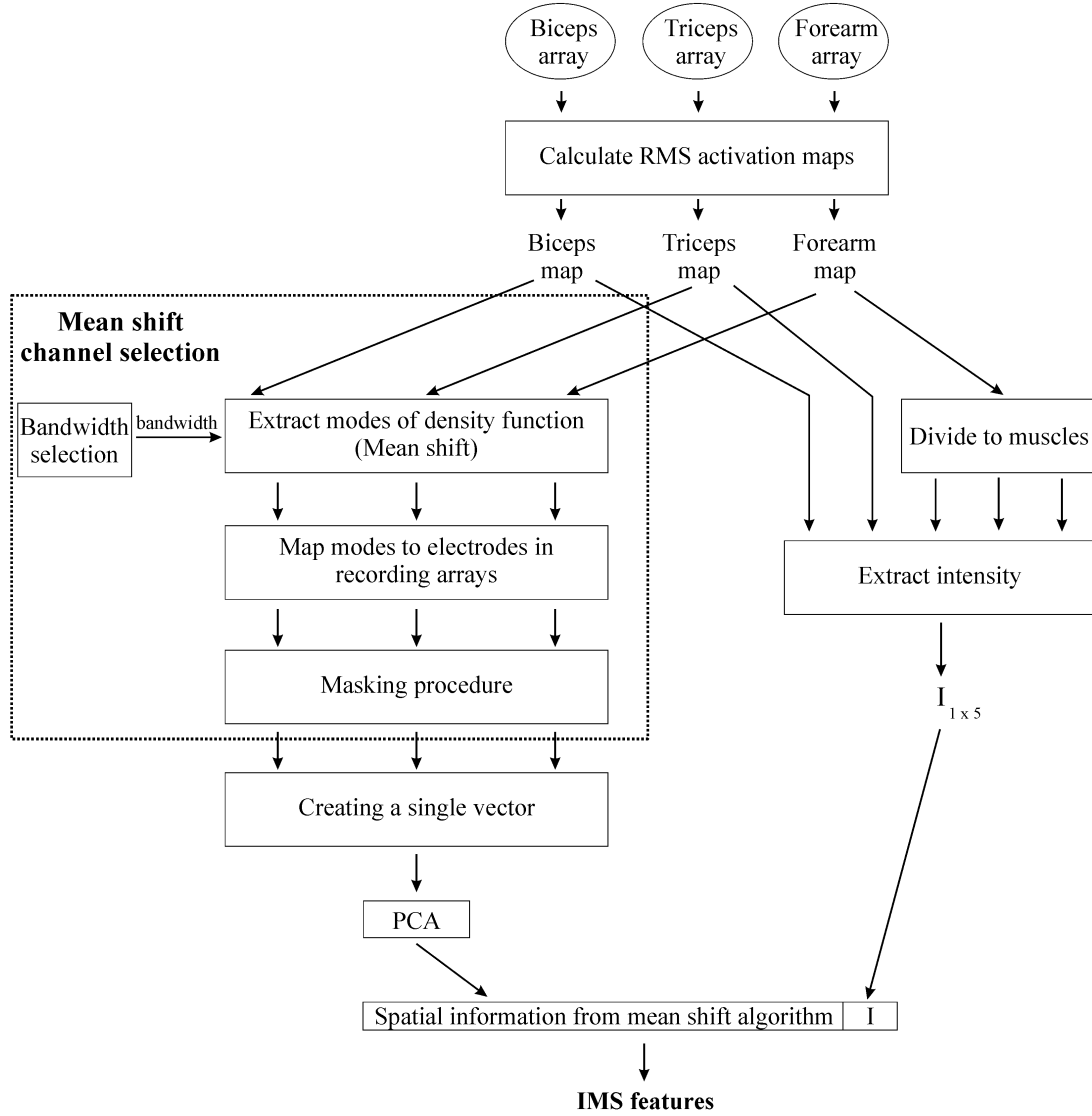


Figure 5.2: Feature extraction flowchart.

array and its value was set to one. The result of this step was a binary image where the number of nonzero elements was equal to the number of detected modes. The procedure was repeated for all three activation maps. The resulting matrices were reshaped as a single $1 - d$ vector in which the number of elements equaled to the total number of recorded EMG channels (for all three electrode arrays).

Principal component analysis (PCA) was then used for reducing the dimensionality of the feature space. A cumulative percentage of variance of 90% was used for dimensionality reduction, i.e., after the transformation to the orthonormal space, features were ordered by variance, and only the features explaining at least 90% of the cumulative variance were kept (Valle et al., 1999).

This reduced spatial feature set was then combined with the intensity features.

For calculation of intensity features, HD-EMG activation maps were segmented into areas covering the targeted muscle following the same procedure described in (Rojas-Martínez et al., 2012) and repeated in (Rojas-Martínez et al., 2013). Segmentation discards the map areas not covering the recorded muscle (e.g., edges of maps), and also divides the forearm map into three different maps which correspond to forearm muscles. From the resulting five segmented activation maps (biceps brachii, triceps brachii, brachioradialis, anconeus, and pronator teres), intensity features (I) were calculated as:

$$I = \log_{10} \frac{1}{N} \sum_{i,j} SAM_{i,j} \quad (5.3)$$

where I is the intensity feature, $SAM_{i,j}$ is the intensity value of the pixel at location (i, j) in the segmented activation map SAM , and N is the total number of pixels in that map. Therefore, this procedure extracts five intensity features, one for each muscle. By concatenation, these intensity features were combined with the reduced spatial features into a single feature vector. These generated features were used in the identification and will be referred to as IMS from now on. Results were compared with the previously proposed feature set: a combination of intensity and center of gravity (ICG) of segmented activation maps (Jordanic et al., 2016; Jordanić et al., 2016; Rojas-Martínez et al., 2013). In this feature set, the center of gravity represents the traditional approach of describing the spatial information of intensity distribution over the muscle. The center of gravity (CG) has two dimensions and was calculated for each of the five muscles as:

$$CG = \frac{\sum_{i,j} SAM_{i,j} \begin{bmatrix} i \\ j \end{bmatrix}}{\sum_{i,j} SAM_{i,j}} \quad (5.4)$$

Therefore, ICG is a feature vector of 15 dimensions. Identification was also performed using only intensity features (I), and two classical features, single differential signal (Diff) and time-domain features (TD). One differential signal was obtained from each of five muscles using a pair of electrodes selected within the electrode arrays. Two adjacent electrodes located over the

location proposed by the SENIAM were used to obtain the differential signal. Feature used in the analysis is RMS value of the differential signal calculated over the 150 ms time window. On the other hand, five TD features were calculated for each recorded channel. These features were firstly proposed by Hudgins (Parker et al., 2006) and used many times in literature (Hakonen et al., 2015). They were: RMS value, mean absolute value, number of zero crossings, waveform length, and number of slope sign changes. To be reduced in number, obtained features were projected to the space of lower dimensionality using PCA. As for the calculation of MS, only projections explaining 90% of variance were kept.

5.2.4 Task identification

LDA was used for the identification of motor tasks. Task identification was evaluated using the repeated holdout method ($N = 20$). Observations were randomly assigned to the training set and the test set (70% to the training set) using stratified sampling. Both the PCA transformation function and the LDA discriminant function were calculated on the training set, and evaluated on the test set. Only the results of the test set are presented. Identification results were expressed in terms of sensitivity (S) and precision (P), defined as:

$$S = \frac{TP}{TP + FN} \quad (5.5)$$

$$P = \frac{TP}{TP + FP} \quad (5.6)$$

where TP (true positive) is the number of samples that were correctly classified, FN (false negative) is the number of samples belonging to a certain class and erroneously classified into another class, whereas FP (false positive) is the number of samples incorrectly classified to a certain class (?).

The identification was evaluated under various conditions:

- Short-term identification

- Long term identification
- Identification during fatigue

In the short term identification, the training and the validation sets were recorded at the same time. These are in fact the “perfect conditions” where the slow time-dependent changes in the sEMG signal associated with the recordings were minor. The dataset was composed of the recordings obtained in the first part of the measurement protocol. Two types of identification were tested: identification of task and identification of task and effort level. In the identification of task, only the task was identified, regardless of the effort level, i.e., recordings of different effort levels were pooled together to form a single class. In this experiment, there were only four classes: flexion, extension, supination, and pronation. Identification of task and effort level was designed as a two-step classifier. In the first step the task was identified, regardless of the effort level, as discussed above. In the second step, classification of three levels of effort was performed for each identified task individually. The second step consisted of four different classifiers, one classifier for the identification of the effort level of each task. For the identification of effort level of a sample, the second step classifier was selected depending on the classified task in the first step (Jordanić et al., 2016). Classifiers in the second step were designed using the reduced feature set, as proposed in (Jordanić et al., 2016), where features were extracted from agonist-antagonist muscle pairs involved in the selected task, i.e., biceps brachii and triceps brachii for identification of the effort level during flexion and extension; biceps brachii, brachioradialis and anconeus for supination; and pronator teres and anconeus for pronation. Since the modes of the density function were calculated for the entire forearm array (not for each muscle separately), modes extracted from the entire forearm array were used in the identification of the effort level during supination and pronation. In the long-term identification, robustness to time effect was tested. In this part of the protocol, the training set was composed of all observations recorded in the first part of the measurement protocol, whereas the test set was composed of the first two seconds of the recordings in the second part of the protocol. Having in mind that there was a time gap between the first part of the protocol and the second part of the protocol (≈ 30 min), using this procedure the influence of different time effects can be evaluated (e.g., drying of conductive gel). On the other hand, to prevent the effect of fatigue, only the first two seconds of the total duration of the exercise were used in the test set. Robustness of the identification was

also tested during endurance tasks recorded during the second part of the recording protocol. Recordings were divided into five equal time epochs. The classifier was trained using the samples extracted from the first 20% of the total duration of recording (TDR), and was evaluated on five equally long segments throughout the exercise: 0–20% TDR, 20–40% TDR, 40–60% TDR, 60–80% TDR, and 80–100% TDR.

5.2.5 Statistical methods

Statistical difference in performance was checked between IMS and other feature sets. The Kolmogorov-Smirnov test showed that the data significantly deviate from a normal distribution, so the non-parametric statistical Wilcoxon signed rank test was used to test for differences between distributions. In addition, the non-parametric repeated measures Friedman test was used to test the differences in identification of the task when the training set was composed of pool of all effort levels, and test set of only 10% MVC, 30% MVC, or 50% MVC. This was repeated for all feature sets. The significance level was set to $p = 0.05$. Statistical tests were performed using the IBM SPSS Statistics software package (IBM SPSS Statistics for Windows, version 20.0, released 2011; IBM Corp.: Armonk, NY, USA).

5.3 Results

5.3.1 Bandwidth and time window selection

Two aspects were considered in the choice of the bandwidth factor: the average execution time of the mean shift algorithm and the amount of information, i.e., number of detected modes (Figure 5.3). The average processing time was measured on a standard desktop computer featuring an Intel® E8400 Core™ 2 Duo CPU (Intel, Santa Clara, CA, USA). Both graphs show that the elbow point was at the bandwidth factor of 0.5. If the bandwidth factor is set to a lower value, both the execution time and the number of modes increase notably. A rapid increase of the number of modes for lower bandwidths implies that the mean shift algorithm is focused on local maxima, whereas the increase of the execution time increases the latency of the system. On the other hand, there was not much difference when the bandwidth factor ranges between 0.5 and 1.0, both in the number of estimated modes, and the execution time. Therefore, the range from 0.5 to 1.0 was considered of interest for the selection of the bandwidth factor.

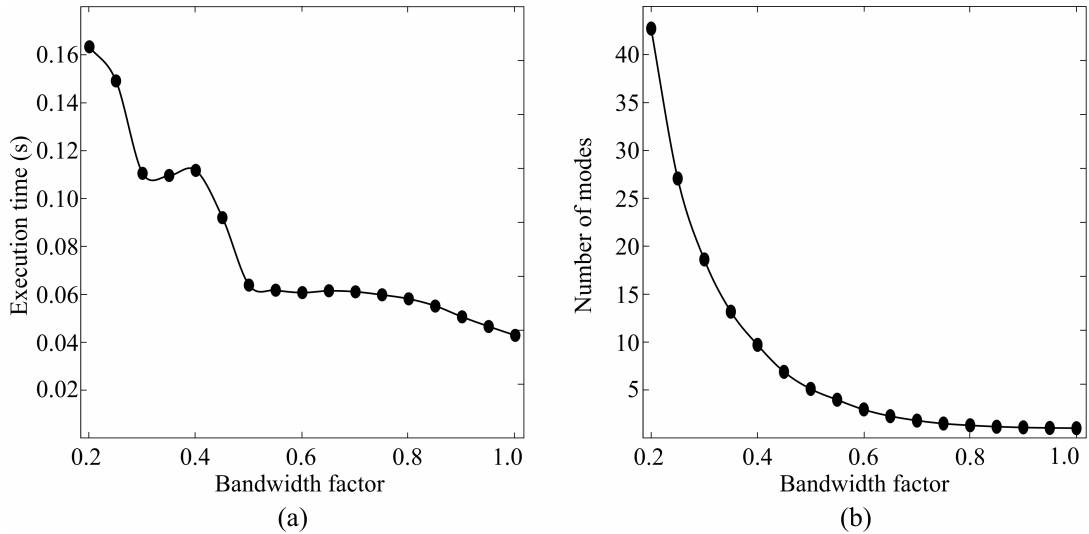


Figure 5.3: Figure shows average processing time (a) and number of estimated modes (b) of mean shift algorithm given the specific bandwidth factor in the range from 0.2 to 1.

The identification of task and the identification of task and effort level (Figure 5.4) were compared using the bandwidth factor of 0.5 and 1.0. The performance of the algorithm was significantly higher when using the bandwidth of 0.5 compared with that of 1 ($p < 0.05$).

On the other hand, the effect of duration of time window in which the features were calculated

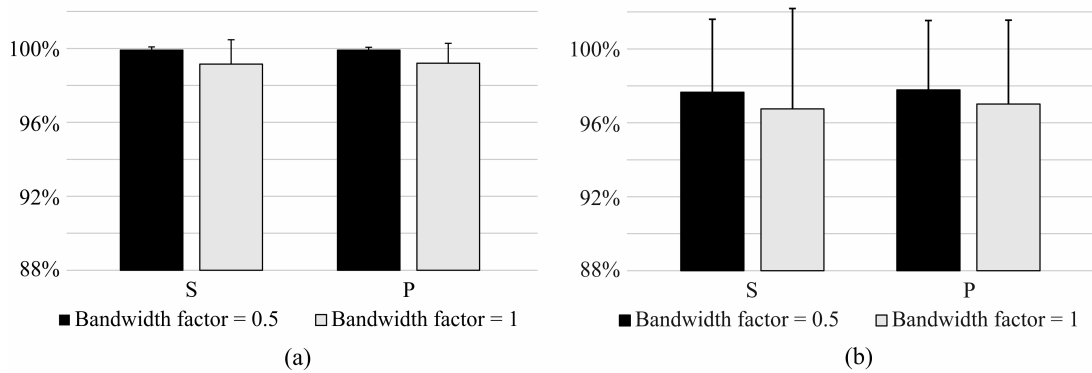


Figure 5.4: Sensitivity and precision of short-term identification of (a) identification of task and (b) identification of task and effort level using bandwidth factors 0.5 and 1.0 in mean shift algorithm.

was analyzed and results are presented in Figure 5.5. Identification based on the IMS features extracted from the 150 ms and 200 ms time windows significantly outperform the identification when features were extracted from shorter time windows, whereas no significant difference was found between results calculated on 150 ms and 200 ms windows.

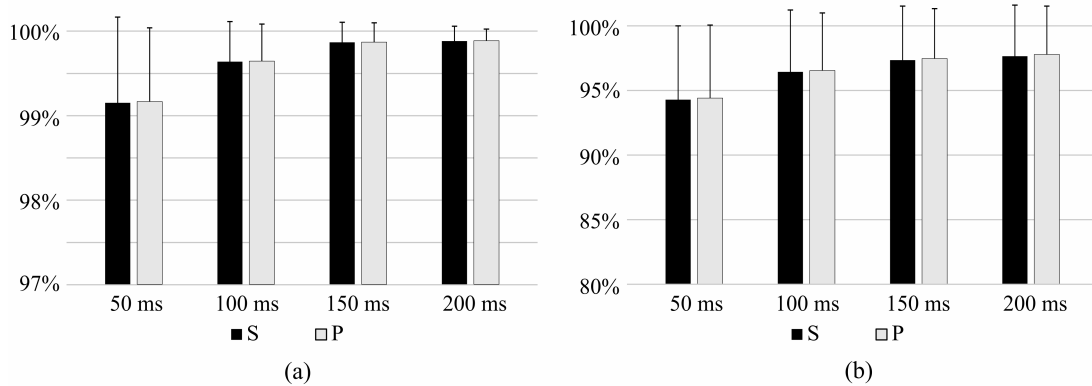


Figure 5.5: Sensitivity (S) and precision (P) of (a) identification of task and (b) identification of task and effort level for time windows of 50 ms, 100 ms, 150 ms, and 200 ms.

Consequently, the bandwidth factor of 0.5 and the time window of 150 ms were used in the rest of the paper.

5.3.2 Short-term identification

Table 5.1 shows the results of the identification of task using the novel features proposed in this paper and Figure 5.6 shows the comparison between IMS, ICG, I, TD, and Diff features in the

identification of tasks. IMS significantly outperformed all of the compared features ($p < 0.05$).

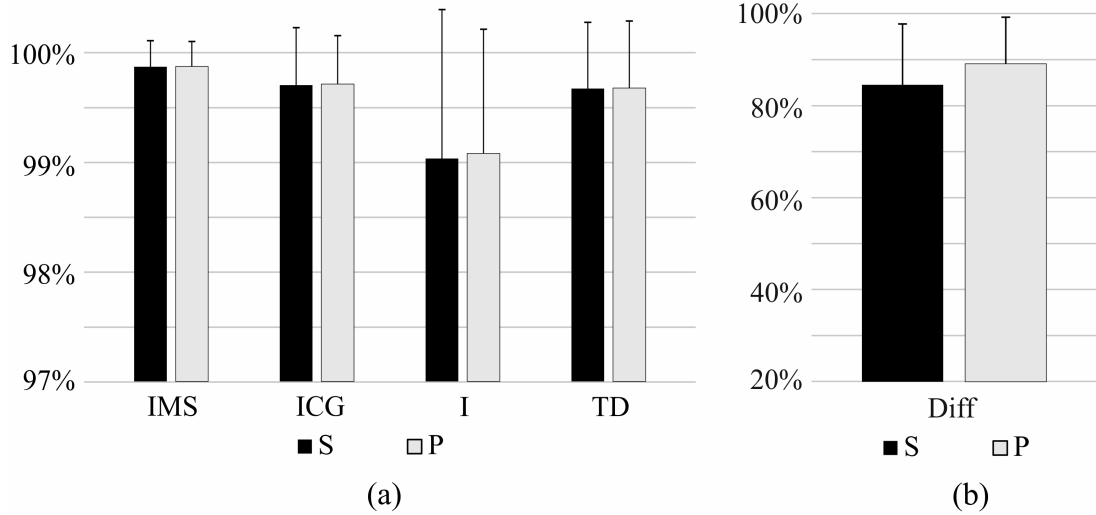


Figure 5.6: Sensitivity (S) and precision (P) of short-term identification of task using (a) IMS, ICG, I, and TD features, and (b) using Diff features. Results of the identification using Diff is showed in a different scale.

Table 5.1: Sensitivity and precision of identification of task using IMS features averaged between patients. Identification Indices for each patient were calculated as an average of hold-out repetitions ($N = 20$) and presented in terms of mean and standard deviation.

Task	Sensitivity (%)	Precision (%)
Flexion	99.7 ± 0.5	99.9 ± 0.2
Extension	99.9 ± 0.1	99.9 ± 0.1
Supination	99.9 ± 0.2	99.7 ± 0.5
Pronation	99.9 ± 0.1	99.9 ± 0.1
Average	99.9 ± 0.2	99.9 ± 0.2

The results of the identification of the task and effort level using IMS features are given in Table 5.2, whereas comparison between IMS and other features is shown in Figure 5.7. IMS features significantly outperform I, TD, and Diff features ($p < 0.05$), whereas the ICG features slightly outperform IMS features ($\Delta S = 0.6\%$, $\Delta P = 0.6\%$; $p < 0.05$).

The sensitivity and precision of the task identification when the classifier was trained using all effort levels (pool of 10%, 30%, 50% MVC) and tested using a specific effort level can be seen in Figure 5.8 and Figure 5.9 for comparison of IMS, ICG, I, and TD features, and for Diff features, respectively. This experiment shows how well each feature set identifies the task of a specific effort level. The difference in performance is especially pronounced in the identification of tasks at very low effort level (10% MVC). IMS significantly outperforms I and Diff features at all

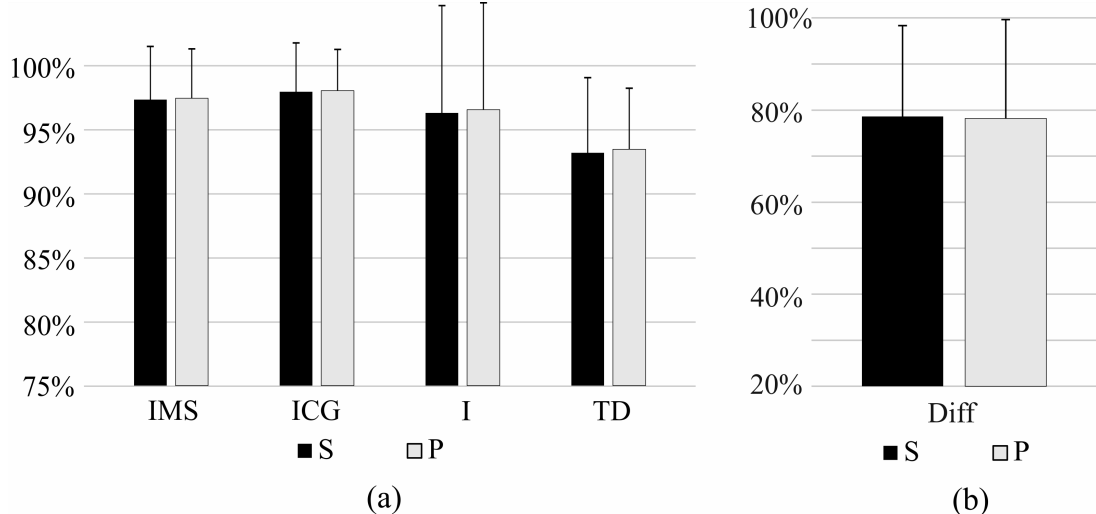


Figure 5.7: Sensitivity (S) and precision (P) of short-term identification of task and effort level using (a) IMS, ICG, I, and TD features, and (b) using Diff features. Results of the identification using Diff is showed in a different scale.

Table 5.2: Sensitivity and precision of identification of task and effort level averaged between patients. Identification indices for each patient were calculated as an average of hold-out repetitions ($N = 20$) and presented in terms of mean and standard deviation.

Task	Sensitivity (%)	Precision (%)
Flexion 10% MVC	98.2 ± 2.8	99.9 ± 0.3
Flexion 30% MVC	98.7 ± 1.1	97.0 ± 3.1
Flexion 50% MVC	97.7 ± 2.9	98.6 ± 1.1
Extension 10% MVC	99.7 ± 0.6	99.6 ± 1.1
Extension 30% MVC	97.4 ± 3.4	97.5 ± 2.1
Extension 50% MVC	97.7 ± 2.3	98.2 ± 2.9
Supination 10% MVC	99.7 ± 0.5	99.9 ± 0.2
Supination 30% MVC	95.2 ± 7.1	96.0 ± 5.1
Supination 50% MVC	96.6 ± 4.9	95.4 ± 6.3
Pronation 10% MVC	99.8 ± 0.2	99.4 ± 1.1
Pronation 30% MVC	93.8 ± 12.3	93.9 ± 11.3
Pronation 50% MVC	93.7 ± 11.9	94.2 ± 11.9
Average	97.4 ± 4.2	97.5 ± 3.9

effort levels, but the difference between IMS and ICG features and the difference between IMS and TD are not significant at moderate effort levels (30% MVC and 50% MVC), whereas IMS features are specifically and significantly better when identifying tasks at low effort levels (10% MVC).

Additionally, no significant difference between task identification at three different effort levels was seen when using IMS features, whereas these differences were significant for other feature sets. This could mean that these novel IMS features are more robust to the variation in the

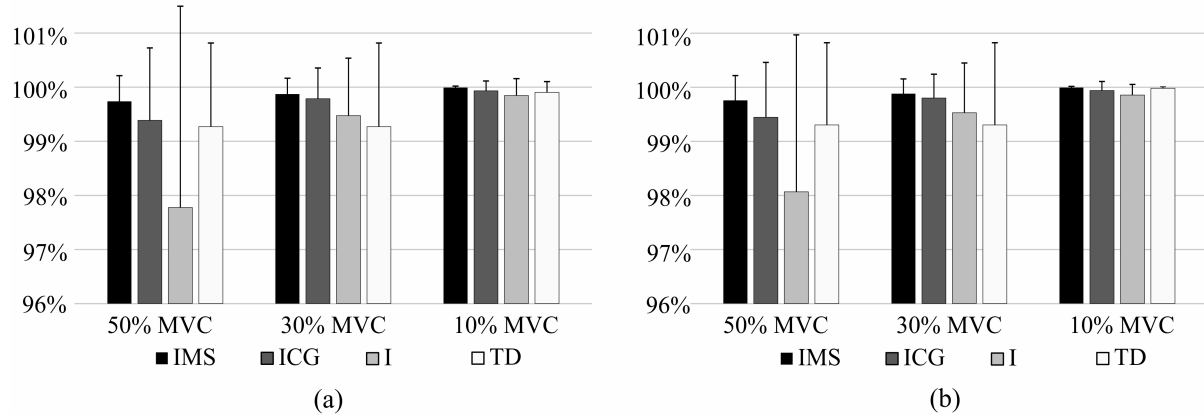


Figure 5.8: Figure shows sensitivity (a) and precision (b) of short-term identification of task recorded at specific effort level using IMS, ICG, I, and TD features.

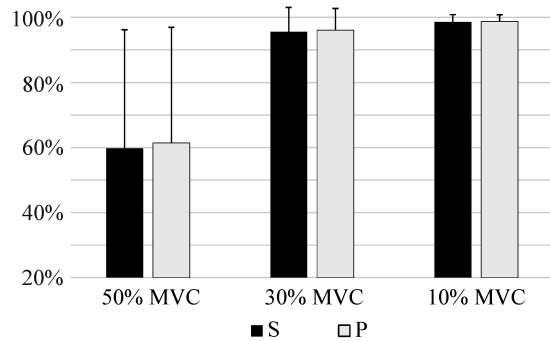


Figure 5.9: Figure shows sensitivity (S) and precision (P) of short-term identification of task recorded at specific effort level using Diff features.

effort level.

5.3.3 Long-term identification

Identification was tested when a significant amount of time passed between the recording of the training and test sets. This allowed an evaluation of influence of slow time-dependent changes in the EMG signal on the robustness of the identification. Figure 5.10 shows the comparison of the intensity features and the combination of intensity and spatial features when these last ones were calculated as the center of gravity or using the mean shift algorithm. There are no significant differences in performances between these IMS, ICG, and I features, whereas IMS feature significantly outperform TD and Diff features ($p < 0.05$). However, it should be noted that the test set was composed only of samples recorded at 50% MVC. And, as previously proven

in literature (Jordanic et al., 2016), and shown in Figure 5.8 and Figure 5.9, the use of spatial information is particularly useful in contractions at low effort levels, whereas only intensity can be sufficient to successfully identify contractions of moderate effort levels (as 50% MVC).

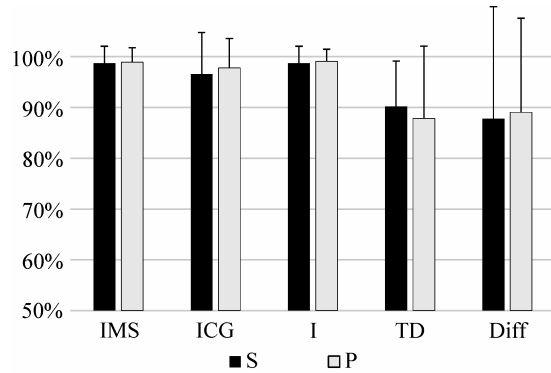


Figure 5.10: Sensitivity (S) and precision (P) of long-term identification of task using IMS, ICG, I, TD, and Diff features.

5.3.4 Identification during fatigue

The influence of fatigue on EMG was evaluated using endurance recordings. Recordings were divided into five equal time epochs. The training set was obtained from the first epoch (0–20% TDR), and the identification was performed on all five time epochs. Changes of sensitivity and precision during the exercise can be seen in Figure 5.11. It can be seen how all feature sets perform similarly at the beginning of the contraction, whereas identification indices decay towards the end as the fatigue accumulates. However at the final stages of fatigue (80%–100% TDR) IMS features significantly outperform other feature sets ($p < 0.05$). These results show the robustness of the IMS features to the fatigue.

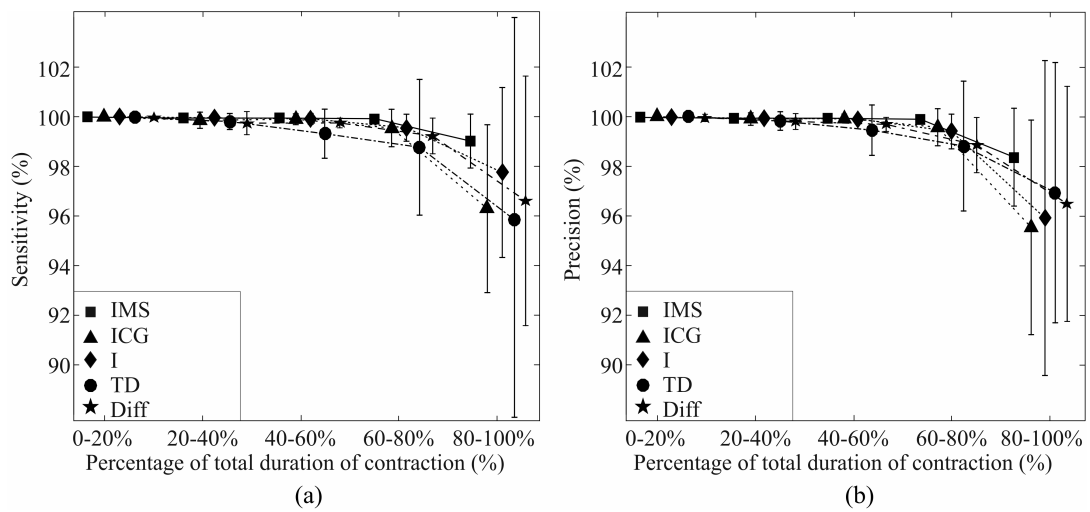


Figure 5.11: Influence of fatigue on (a) sensitivity and (b) precision of the identification of task using IMS, ICG, I, TD, and Diff features.

5.4 Discussion

This study showed that the combination of intensity and spatial information is useful for the extraction of neuromuscular information. The spatial information was calculated from the RMS activation maps using the mean shift algorithm. The results were evaluated using the 70% repeated holdout method and stratified sampling as to have a sufficient number of samples of each class in the sets. To prevent the type III statistical error (Mosteller, 1948; Mohebian et al., 2017), a repeated hold-out was used. Sensitivity and precision, as appropriate unbiased measures in analyzing imbalanced multi-class problems (Jordanić et al., 2016; Rojas-Martínez et al., 2013), were used to quantify the identification.

IMS features achieved very good results compared to other feature sets during task identification when the task was performed at very low effort level. Moreover, the Friedman test showed no significant differences in task identification using IMS when tasks were performed at 10% MVC, 30% MVC, or 50% MVC. This can be a very important quality in everyday applications where subject could not need to contract muscles at moderate effort level to complete the task. It can be a step toward more natural control where even slight contractions can be successfully identified. In fact, only activations with low level of intensity are sometimes possible in patients with neuromuscular impairments.

A high identification rate is not the only factor important in the extraction of neural information from sEMG. The system should also be robust to slow time-dependent changes such as fatigue and electrode-skin contact impedance (Farina et al., 2014a). Therefore, the robustness of the proposed features was tested with respect to time and fatigue. When evaluating the time effect, no significant differences in performance were found between IMS, ICG, and I feature sets and IMS significantly outperformed TD and Diff features. However, time effect was evaluated only when test set was composed of contractions recorded at 50% MVC and, as shown in Figure 5.6, all features perform similarly for the identification of that effort level. This phenomenon was already remarked and described in (Jordanic et al., 2016) where authors noted that adding spatial features to intensity features significantly improved the identification of tasks recorded at low effort levels, whereas improvement is not significant at moderate effort levels. On the other hand, the proposed features are particularly robust in task identification during fatiguing

exercises and show significantly higher identification rate when compared to other features. Further improvements in reliability of the identification during the long-term contractions and fatiguing contractions can be achieved by using adaptive identification models that are being constantly updated during the usage, e.g., (Vidovic et al., 2016; Hahne et al., 2015; Sensinger et al., 2009).

In the current work, features were extracted from the RMS activation maps of the HD-EMG. Although these features proved to be very effective, by describing the EMG signal with its RMS value, i.e., the estimator of variance, the information is partially lost. Since the gradient of the probability density function of raw EMG is a useful feature in task identification, statistical measures (e.g., modes) of the raw HD-EMG, i.e., joint distribution of instantaneous EMG amplitude over the electrode array, could provide valuable information. Moreover, in literature, features were often calculated for each channel separately and selected using the simple sequential method prior to classification (Hargrove et al., 2009; Li et al., 2017). On the other hand, Geng et al. recently proposed a more advanced channel selection method based on common spatial patterns (Geng et al., 2014). Modes of the HD-EMG density function could be correlated with the channels with discriminative information and could be a useful tool in channel selection.

5.5 Conclusions

In conclusion, a new set of features for the identification of isometric motor tasks of upper limb was proposed. It was based on the combination of intensity and the spatial distribution of intensity of HD-EMG. These new features were evaluated using the LDA classifier and the results showed they improve the identification of tasks. Moreover, robustness of the features was tested under the influence of slow time-dependent changes of the EMG. They proved to be particularly useful for task identification when muscles were fatigued. The proposed methods could be used for the design and monitoring of rehabilitation therapies intended for patients with neuromuscular impairment, as well as for the control of external devices like exoskeletons, and prostheses.

5.6 Acknowledgments

Special acknowledgment to Laboratory of Engineering of Neuromuscular System and Motor Rehabilitation at the Politecnico di Torino for the help and collaboration during the experiments. This work has been partially supported by the Spanish Ministry of Economy and Competitiveness (Project DPI2014-59049-R), People Programme (Marie Curie Actions) of the Seventh Framework Programme of the European Union (FP7/2007-2013) under REA grant agreement no. 600388 (TECNIO spring programme), and by the grant for the recruitment of early-stage research staff (FI 2014) from the AGAUR, Generalitat de Catalunya, Spain.

5.7 Author contributions

M.R.-M. and M.A.M. conceived and designed the experimental protocol and conducted the experiments. M.J., M.R.M. and M.A.M. designed the study and interpreted the results. M.J. was in charge of the implementation of signal processing and machine learning methods and the analysis of the data. J.F.A. and H.R.M. aided in the analysis of the data and in the interpretation of results. M.J. wrote the manuscript and all authors contributed to the revising it.

5.8 Conflicts of interest

The authors declare no conflict of interest.

Chapter 6

Conclusion

6.1 Summary

Task identification and movement estimation based on the EMG are popular topics in biomedical engineering involving different areas in machine learning and, particularly, in pattern recognition with many possible applications in assistive and rehabilitation devices. The emergence of the high-density EMG (HD-EMG) opened new possibilities for extracting neural information and it has been reported that spatial distribution of HD-EMG intensity is a valuable feature in the identification of isometric tasks.

This doctoral thesis investigates further the spatial muscle co-activation patterns of myoelectric activity extracted from the HD-EMG activation maps. HD-EMG was measured on five muscles of the forearm and the upper-arm in a monopolar configuration during isometric forearm tasks. Measurements were performed on a group of healthy subjects and on a group of patients with incomplete spinal cord injury.

In chapters 3 and 4, co-activation patterns of patients with incomplete spinal cord injury were analyzed by means of pattern-recognition-based identification of task and effort level. Both intensity related features, and spatial features were analyzed. In chapter 3, co-activation patterns were analyzed for each patient individually, whereas in chapter 4, co-activation patterns were analyzed within the group of patients. In spite of the great diversity between different patients

and their levels and types of injury, similarities between activation patterns were found not only in the intensity of the myoelectric signal, but also in the spatial distribution expressed as center of gravity.

In the chapter 5, a novel feature for task identification was proposed. The feature is based on spatial distribution of the myoelectric activity recorded by the HD-EMG and analyzed by the mean shift algorithm. This new feature was evaluated in identification of task and identification of task and effort level in healthy subjects. The evaluation was performed for each subject individually.

6.2 Main conclusions

In chapter 3, muscle co-activation patterns were analyzed during four isometric tasks and three effort levels in patients with incomplete spinal cord injury. Intensity-based activation maps were calculated for each muscle and different features were extracted: the average intensity of an HD-EMG map, and the center of gravity of an HD-EMG map. Using the extracted feature sets, a successful patient-specific task identification method was designed. It is capable of estimating with high sensitivity and precision not only the motor task, but also the force. This implies that patients with incomplete spinal cord injury have a repeatable co-activation muscular patterns not only in intensity, but also in spatial distribution of intensity over the muscle surface. Moreover, the results lead to the conclusion that the spatial distribution of the myoelectric activity has a significant and discriminative power in classification. Furthermore, adding information on the spatial distribution of myoelectric intensity improves not only the identification result, but also the resilience to fatigue and time effect.

Furthermore, in chapter 4 it was discovered that repeatable patterns in intensity and spatial distribution besides existing for each patient individually, also exist for the entire group of patients. To demonstrate the existence of distinguishable group-specific patterns in HD-EMG, the identification of different tasks was performed, where the classifier was trained and tested using the samples of all patients instead of focusing on individuals, i.e., a group-specific classifier was designed. The existence of the similar patterns in individuals is an interesting result because there should be a high level of variability between patients due to the nature of the injury. Co-

activation patterns were found not only between different tasks, but also between different effort levels. Group-specific identification of motion intention in patients with a neuromuscular impairment could potentially improve the translation of pattern recognition techniques to clinical practice. Also, results show that the similarity is greater between patients with a similar level of lesion (vertebra at which spinal cord injury occurred). This could also have an interesting implication in the translation to the clinical practice because patients with the similar level of injury could be able to use the same assistive/rehabilitation devices with greater ease, avoiding or at least facilitating the calibration process that is intrinsically needed when the training of the system is subject specific. This is an important result because one of the reasons preventing the broad use of pattern recognition approaches for the control of assistive devices is precisely the calibration process that is time-consuming and burdensome for the user.

Finally, in chapter 5, a novel feature for the identification of task and effort level was designed. It is based on the locations of the local maxima of the probability density function of HD-EMG activation maps, and is obtained using the mean shift algorithm. The feature was tested on the population of healthy subjects in a subject-specific approach, that is, the classifier was trained and tested for each subject individually. The feature yields higher identification indices compared to the more classical features, especially in the task identification at very low effort level. By analyzing the influence of fatigue and other time-dependent changes (e.g. drying of conductive gel) on identification, the novel feature had a very good performance. Since the goal of this study was to analyze different feature sets rather than classification methods, LDA was utilized given that this method is the most commonly used, and is generally recommended for myoelectric interfaces (Hakonen et al., 2015).

Density function from which the modes were extracted represents the RMS activation maps of the HD-EMG. Although the feature proved to be useful, by calculating the RMS value, the complexity of the underlying system is reduced, but the information is also partially lost. Therefore, the modes, or other statistical measures of the raw HD-EMG, i.e. joint distribution of instantaneous EMG amplitude over the electrode array, could also be a useful feature in the identification of the motion intention. Furthermore, in the literature, features are often calculated for each channel separately and then the optimal set of channels is selected prior to the classification using the, e.g., sequential method (Hargrove et al., 2009; Li et al., 2017),

selection based on common spatial patterns (Geng et al., 2014), or based on the independent component analysis clustering (Naik et al., 2016). Modes of the HD-EMG density function could be correlated with the channels with discriminative information and could be a useful tool in the channel selection.

Moreover, the mean shift algorithm can be used for clustering and, since it was shown that the algorithm is most effective in the low-dimensional data, image segmentation is one of its most successful applications (Comaniciu and Meer, 2002). A mode of the density estimate, or in this case, a channel selected by the mean shift algorithm, can be considered as a cluster representative (Hennig et al., 2015), related to the possible image segments, where spatial (pixel locations) and range features (the intensity of the grayscale value) are considered. The advantage of the mean shift is that it can be used for clustering non-convex shapes, albeit, it could segment complex non-convex regions in the activation maps. Since segmentation of the muscle activation map can improve the neuromuscular activity estimation (Vieira et al., 2010), this could be a reason why mean shift features improved the performance of the detection system compared to the previously published attributes. In addition, the algorithm only requires setting of one parameter, the bandwidth (h) and, unlike in the similar methods, it is not necessary to define the number of expected clusters. This is a big advantage because it does not require a priori knowledge on the number of clusters.

The proposed motor task identification method based on spatial information of myoelectric distribution could contribute to human-machine interface technology. There are many possible applications for this type of technology, for example computer games, exoskeletons, automatic wheelchairs, rehabilitation robots, prostheses, etc. Nowadays, the field of the brain-computer interface (BCI) technology is advancing very fast with high investments of leading global corporations. However, the non-invasive BCI is still an open problem with a low output rate, which can be greatly improved by using EMG-based identification of motor intention. For example, Müller-Putz et al. suggest non-invasive hybrid brain-computer interfaces (hybrid BCI) designed as EEG-based system, supplemented with other biological and mechanical signals (Muller-Putz et al., 2015). Joining EEG and EMG recordings in the identification of the task intention significantly improves the accuracy of the individual EEG or EMG system. The EMG usually has a higher SNR ratio than the EEG and it is widely used in the identification of the motion

intention, however, it is prone to malfunction due to, e.g. fatigue. When fatigue occurs, the supplemented EEG input keeps the identification stable, and increases the robustness of the system. Thus, advances in obtaining methods more robust to fatigue or time effect are very interesting.

Some patients with neuromuscular impairment can weakly activate their muscles, but insufficiently to generate a movement. In these patients, as well as in patients that can generate only weak movements, HD-EMG maps can still be generated and used in identification of motion intention, as demonstrated in this study. This approach could potentially supplement the existing BCI or inertial sensors based prostheses and result in a device with a better performance. For example, Rohm et al. (2013) performed a very interesting study with a single SCI patient. Their neuroprosthesis consisted of a functional electrical stimulation of the forearm and upper arm muscles, and a semiactive elbow orthosis. Using BCI and a shoulder joystick, the patient was able to perform complex hand and elbow tasks from everyday life (e.g. eating an ice cream cone). The reported performance of that study was 70%, which was remarkable considering the fact that the patient did not have any control over the involved muscles. However, performance of similar patients could be increased by using hybrid BCI if myoelectric activation exists.

As a limitation of the thesis, it should be noted that the proposed features were tested only in highly controlled conditions of isometric contractions. The experiments during non-isometric contractions should be performed in order to validate the quality of the features in dynamic and more natural movements. Also, the experiment included only four tasks related to the elbow joint. Further analysis should include a higher number of more complex tasks related to hand and shoulder. Within the scope of this thesis, advancements have been made in that direction. The experimental protocol was already designed and HD-EMG signal was recorded in healthy subjects during shoulder-related hand movements in horizontal plane, similar to the movements stimulated by rehabilitation robots during the therapy. Identification of non-isometric tasks was performed on that recordings and the results were accepted for publishing (?) and can be found in the appendix C. Moreover, all results in this thesis were obtained during offline analysis. To evaluate practical aspects of the technique, the experiment should be repeated using online identification.

6.3 Main contributions

The original contributions provided by the compendium of publications of this thesis are:

- The definition of a pattern-recognition algorithm for task and force identification. The method was based on the combination of intensity and spatial distribution of intensity of the myoelectric signal, namely center of gravity. The algorithm was validated in the group of patients with incomplete spinal cord injury in terms of robustness during slow time dependent changes, such as fatigue and drying of conductive gel. The results prove the existence of the repeatable co-activation pattern in intensity and spatial distribution for each patient. Furthermore, the pattern exists for different tasks, but also for different effort levels.
- The co-activation pattern in intensity and its spatial distribution of HD-EMG was identified for the group of patients with spinal cord injury. It was proved that there is a coherence between activation patterns of different patients after the injury, both regarding task and force. This coherence can be observed in the intensity of the HD-EMG, but also in the spatial distribution of intensity. Furthermore, a greater similarity was found within the group of patients with a similar level of injury. This result implies the possibility of building assistive/rehabilitation devices for the group of patients with a significantly lower training time.
- Definition of a novel statistical spatial feature derived from the HD-EMG. It was used for the identification of task and effort level in a group of healthy subjects. This feature is based on the probability density function of the HD-EMG activation map.

6.4 Future Work

The work developed in this thesis opens new possibilities in the field of myocontrol in rehabilitation. Some of the most interesting possibilities for future works are the following:

Dynamic contractions

The use of spatial information of myoelectric activity is a novel method which already

showed very good results in the identification of tasks, both in healthy subjects, and in patients with incomplete spinal cord injury during isometric contractions. Isometric contractions are standard to the field of work, that is, pattern recognition for control of human-machine interfaces, and are a good starting point to test new features with respect to more classical features. The recordings during isometric contractions provide measurements with more controlled conditions, i.e., minimized influences related to relative shift of recording electrodes with respect to source of the signal – muscle fiber. Therefore it is a good practice to start using new features in controlled situations in order to establish reliably and precisely the circumstances in which features are useful. However, further studies are necessary to consider non-isometric contractions, which are closer to real conditions. One of these studies was already performed within the scope of the thesis and the results were published (?) and can be found in the appendix C.

Generalized mean shift approach

In chapter 5, the motor task identification algorithm that uses the novel spatial feature is explained. This spatial feature is based on the modes of the probability density function of HD-EMG activation maps. Instead, the viability of features based on the modes of the probability density function of raw HD-EMG signal should be explored. Since the information is partially lost by calculating the RMS value of the signal to obtain the activation maps, using the joint distribution of instantaneous EMG amplitude over the electrode array could provide higher identification results.

Mean shift approach for channel selection

Geng et al. recently proposed a more advanced channel selection method based on common spatial patterns (Geng et al., 2014) and Naik et al. propose channel selection based on independent component analysis (Naik et al., 2016). Modes of the HD-EMG density function, a novel feature proposed in chapter 5, could be correlated with the channels with discriminative information and could be a useful tool in channel selection.

Real time application

The task identification system cannot find an application without the ability of online processing. Therefore, an appropriate recording device along with an optimized processing unit should be built. The device should be able to process the task identification in real

time using an optimized firmware.

Hybrid brain-computer interface

The fusion of EEG and EMG could further improve results of upper-limb task identification, that is, the study performed here using only HD-EMG recordings both in healthy subjects and iSCI patients. This type of study can have an impact on numerous fields of application including brain – computer interfaces (BCI). A goal could be to exploit the fusion of cerebral and neuromuscular information and to quantify the improvements when the innovative technique of HD-EMG is joined with the cerebral activity, what was recently called by the research community a *hybrid BCI* (Muller-Putz et al., 2015; Rohm et al., 2013).

Increase of identification fidelity

Fidelity of the identification could be increased further by using an adaptive model of a classifier that is being constantly updated throughout the exercise in order to compensate for the changes in the myoelectric signal caused by, e.g., fatigue or sweating. There are several recent publications on this subject (Hahne et al., 2015; Vidovic et al., 2016; Sensinger et al., 2009).

Spatial distribution of frequency

Features extracted from frequency/scale domain proved to be very useful in the identification of motor task (Oskoei and Hu, 2007). In future works, it would be interesting to investigate the spatial distribution of frequency over the muscle in search of a discriminative feature.

6.5 Publications derived from the thesis

6.5.1 Journal papers

- Jordanić, M., Rojas-Martínez, M., Mañanas, M.A., Alonso, J.F., Marateb, H.R. A Novel Spatial Feature for the Identification of Motor Tasks Using High-Density Electromyography. *Sensors*, 17(7): 1597, 2017, JCR 2.077, Q1 in Instruments and instrumentation (10/58)

- Rojas-Martínez, M., Alonso, J.F., Jordanić, M., Romero, S., Mañanas, M.A. Identificación de tareas isométricas y dinámicas del miembro superior basada en EMG de alta densidad. *Revista Iberoamericana de Automática e Informática Industrial*, Accepted for publication 2017, JCR 0.390, Q4 in Automation and Control Systems (57/60)
- Jordanić, M., Rojas-Martínez, M., Mañanas, M.A., Alonso, J.F. Prediction of isometric motor tasks and effort levels based on high-density EMG in patients with incomplete spinal cord injury. *Journal of Neural Engineering*, 13(4): 46002, 2016, JCR 3.465, Q1 in Biomedical Engineering (13/77)
- Jordanić, M., Rojas-Martínez, M., Mañanas, M.A., Alonso, J.F. Spatial distribution of HD-EMG improves identification of task and force in patients with incomplete spinal cord injury. *Journal of NeuroEngineering and Rehabilitation*, 13(1): 41, 2016, JCR 3.222, Q1 in Rehabilitation (3/65)

6.5.2 Conference papers

- Jordanić, M., Rojas-Martínez, M., Mañanas, M.A. Muscle pattern from HD-EMG applied to identification of movement intention. Summer School on Neurorehabilitation (SSNR 2015), 2015, Valencia, Spain
- Jordanić, M., Rojas-Martínez, M., Mañanas, M.A., Alonso, J.F. Use of frequency features of HD-EMG in identification of upper-limb motor task. *Cognitive Area Networks*, 4(1): 19:23, 9. Simposio CEA de Bioingeniería: Interfaces Cerebro-Máquina y Neurotecnologías para la Asistencia y la Rehabilitación, 2017, Badalona, Spain
- Jordanić, M., Rojas-Martínez, M., Alonso, J.F., Migliorelli, C. Mañanas, M.A. Identificación de Contracciones Isométricas de la Extremidad Superior en Pacientes con Lesión Medular Incompleta mediante Características Espectrales de la Electromiografía de Alta Densidad (HD-EMG). Jornadas de Automática (Bioingeniería), 2017, Gijon, Spain

Bibliography

- MATLAB and Statistics and Machine Learning Toolbox Release 2015a.
- Ameri, A., Englehart, K. B., and Parker, P. a. A comparison between force and position control strategies in myoelectric prostheses. *Proceedings of the Annual International Conference of the IEEE Engineering in Medicine and Biology Society, EMBS*, pages 1342–1345, 2012.
- Baker, J. J., Scheme, E., Englehart, K., Hutchinson, D. T., and Greger, B. Continuous detection and decoding of dexterous finger flexions with implantable myoelectric sensors. *IEEE Transactions on Neural Systems and Rehabilitation Engineering*, 18(4):424–432, 2010.
- Beck, T. W., DeFreitas, J. M., and Stock, M. S. Accuracy of three different techniques for automatically estimating innervation zone location. *Computer Methods and Programs in Biomedicine*, 105(1):13–21, 2012.
- Boschmann, A. and Platzner, M. Reducing the Limb Position Effect in Pattern Recognition Based Myoelectric Control using a High Density Electrode Array. *2013 ISSNIP Biosignals and Biorobotics Conference (BRC)*, pages 1–5, 2013.
- Boyd, S. and Vandenberghe, L. *Convex optimization*. Cambridge University Press, 2004.
- Cacoullos, T. Estimation of a multivariate density. *Annals of the Institute of Statistical Mathematics*, 18(1):179–189, 1966.
- Celadon, N., Došen, S., Binder, I., Ariano, P., and Farina, D. Proportional estimation of finger movements from high-density surface electromyography. *Journal of NeuroEngineering and Rehabilitation*, 2016.
- Chu, J. U., Moon, I., and Mun, M. S. A Real-Time EMG Pattern Recognition System Based on Linear-Nonlinear Feature Projection for a. *IEEE Transactions on Biomedical Engineering*, 53(11):2232–2239, 2006.
- Cifrek, M., Tonković, S., and Medved, V. Measurement and analysis of surface myoelectric signals during fatigued cyclic dynamic contractions. *Measurement: Journal of the International Measurement Confederation*, 27(2):85–92, 2000.
- Clancy, E., Morin, E. L., and Merletti, R. Sampling, noise-reduction and amplitude estimation issues in surface electromyography. *Journal of Electromyography and Kinesiology*, 12(1):1–16, 2002.
- Comaniciu, D. and Meer, P. Mean shift: a robust approach toward feature space analysis. *IEEE Transactions on Pattern Analysis and Machine Intelligence*, 24(5):603–619, 2002.
- De Luca, C. J. Myoelectrical manifestations of localized muscular fatigue in humans. *Critical Reviews in Biomedical Engineering*, 11(4):251–79, jan 1984.

- De Luca, C. J. The use of surface electromyography in biomechanics. *Journal of Applied Biomechanics*, 13(2):135–163, 1997.
- Dipietro, L., Ferraro, M., Palazzolo, J. J., Krebs, H. I., Volpe, B. T., and Hogan, N. Customized interactive robotic treatment for stroke: EMG-triggered therapy. *IEEE Transactions on Neural Systems and Rehabilitation Engineering*, 13(3):325–334, 2005.
- Du, Y., Jin, W., Wei, W., Hu, Y., and Geng, W. Surface EMG-Based Inter-Session Gesture Recognition Enhanced by Deep Domain Adaptation. *Sensors*, 17(3):458, 2017.
- Duchateau, J. and Enoka, R. M. Human motor unit recordings: Origins and insight into the integrated motor system. *Brain Research*, 1409:42–61, 2011.
- Englehart, K. and Hudgins, B. A robust, real-time control scheme for multifunction myoelectric control. *IEEE Transactions on Biomedical Engineering*, 50(7):848–854, 2003.
- Englehart, K., Hudgins, B., Parker, P. a., and Stevenson, M. Classification of the myoelectric signal using time-frequency based representations. *Medical Engineering and Physics*, 21(6-7):431–438, 1999.
- Englehart, K., Hudgins, B., and Parker, P. A. A wavelet-based continuous classification scheme for multifunction myoelectric control. *IEEE Transactions on Biomedical Engineering*, 48(3):302–11, 2001.
- Englehart, K., Hudgins, B., and Chan, A. D. C. Continuous multifunction myoelectric control using pattern recognition. *Technology and Disability*, 15(2):95–103, 2003.
- Farina, D., Colombo, R., Merletti, R., and Olsen, H. B. Evaluation of intra-muscular EMG signal decomposition algorithms. *Journal of Electromyography and Kinesiology*, 11(3):175–187, 2001.
- Farina, D., Févotte, C., Doncarli, C., and Merletti, R. Blind separation of linear instantaneous mixtures of nonstationary surface myoelectric signals. *IEEE Transactions on Biomedical Engineering*, 51(9):1555–67, 2004.
- Farina, D., Holobar, A., Merletti, R., and Enoka, R. M. Decoding the neural drive to muscles from the surface electromyogram. *Clinical Neurophysiology*, 121(10):1616–1623, 2010.
- Farina, D., Jiang, N., Rehbaum, H., Holobar, A., Graimann, B., Dietl, H., and Aszmann, O. C. The extraction of neural information from the surface EMG for the control of upper-limb prostheses: emerging avenues and challenges. *IEEE Transactions on Neural Systems and Rehabilitation Engineering*, 22(4):797–809, 2014a.
- Farina, D., Merletti, R., and Enoka, R. M. The extraction of neural strategies from the surface EMG: an update. *Journal of applied physiology*, 117(11):1215–30, 2014b.
- Farrell, T. R. and Weir, R. F. F. A comparison of the effects of electrode implantation and targeting on pattern classification accuracy for prosthesis control. *IEEE Transactions on Biomedical Engineering*, 55(9):2198–211, 2008.
- Fougner, A., Scheme, E., Chan, A. D. C., Englehart, K., and Stavdahl, Ø. Resolving the Limb Position Effect in Myoelectric Pattern Recognition. *IEEE Transactions on Neural Systems and Rehabilitation Engineering*, 19(6):644–651, 2011.
- Fougner, A., Stavdahl, Ø., Kyberd, P. J., Losier, Y. G., and Parker, P. a. Control of upper limb prostheses: Terminology and proportional myoelectric control - A review. *IEEE Transactions on Neural Systems and Rehabilitation Engineering*, 20(5):663–677, 2012.

- Freund, H. J., Büdingen, H. J., and Dietz, V. Activity of Single Motor Units from Human Forearm Muscles during Voluntary Isometric Contractions. *Journal of Neurophysiology*, 38(4):933–46, jul 1975.
- Fukunaga, K. and Hostetler, L. The estimation of the gradient of a density function, with applications in pattern recognition. *IEEE Transactions on Information Theory*, 21(1):32–40, 1975.
- Geng, W., Du, Y., Jin, W., Wei, W., Hu, Y., and Li, J. Gesture recognition by instantaneous surface EMG images. *Scientific Reports*, 6(1):36571, 2016.
- Geng, Y., Zhang, X., Zhang, Y.-T., and Li, G. A novel channel selection method for multiple motion classification using high-density electromyography. *Biomedical Engineering Online*, 13:102, 2014.
- Georgakis, A., Stergioulas, L., and Giakas, G. Fatigue analysis of the surface EMG signal in isometric constant force contractions using the averaged instantaneous frequency. *IEEE Transactions on Biomedical Engineering*, 50(2):262–265, 2003.
- Ghaderi, P. and Marateb, H. R. Muscle Activity Map Reconstruction from High Density Surface EMG Signals With Missing Channels Using Image Inpainting and Surface Reconstruction Methods. *IEEE Transactions on Biomedical Engineering*, 64(7):1513–1523, 2017.
- Greenhouse, S. W. and Geisser, S. On methods in the analysis of profile data. *Psychometrika*, 24(2):95–112, 1959.
- Grouven, U., Bergel, F., and Schultz, A. Implementation of linear and quadratic discriminant analysis incorporating costs of misclassification. *Computer Methods and Programs in Biomedicine*, 49(1):55–60, jan 1996.
- Hägg, G. Electromyographic fatigue analysis based on the number of zero crossings. *Pflügers Archiv - European Journal of Physiology*, 391(1):78–80, 1981.
- Hahne, J. M., Graumann, B., and Muller, K. R. Spatial filtering for robust myoelectric control. *IEEE Transactions on Biomedical Engineering*, 59(5):1436–1443, 2012.
- Hahne, J. M., Dähne, S., Hwang, H. J., Müller, K. R., and Parra, L. C. Concurrent Adaptation of Human and Machine Improves Simultaneous and Proportional Myoelectric Control. *IEEE Transactions on Neural Systems and Rehabilitation Engineering*, 23(4):618–627, 2015.
- Hakonen, M., Piitulainen, H., and Visala, A. Current state of digital signal processing in myoelectric interfaces and related applications. *Biomedical Signal Processing and Control*, 18:334–359, 2015.
- Hargrove, L., Englehart, K., and Hudgins, B. A training strategy to reduce classification degradation due to electrode displacements in pattern recognition based myoelectric control. *Biomedical Signal Processing and Control*, 3(2):175–180, 2008.
- Hargrove, L., Li, G., Englehart, K., and Hudgins, B. Principal Components Analysis Preprocessing for Improved Classification Accuracies in Pattern-Recognition-Based Myoelectric Control. *IEEE Transactions on Biomedical Engineering*, 56(5):1407–1414, 2009.
- Hargrove, L. J., Englehart, K., and Hudgins, B. A comparison of surface and intramuscular myoelectric signal classification. *IEEE Transactions on Biomedical Engineering*, 54(5):847–853, 2007.

- He, J., Zhang, D., Sheng, X., Li, S., and Zhu, X. Invariant surface EMG feature against varying contraction level for myoelectric control based on muscle coordination. *IEEE Journal of Biomedical and Health Informatics*, 19(3):874–882, 2015.
- Henneberg, K. Principles of Electromyography. In Bronzino, J., editor, *The Biomedical Engineering Handbook*. CRC Press, Boca Raton, second edition, 1999.
- Henneman, E., Somjen, G., and Carpenter, D. O. Functional Significance of Cell Size in Spinal Motoneurons. *Journal of Neurophysiology*, 28(3), 1965.
- Hennig, C., Meila, M., Murtagh, F., and Rocci, R. *Handbook of Cluster Analysis*. CRC Press, 2015.
- Hermens, H. and Freriks, B. *SENIAM 9: European Recommendations for Surface ElectroMyoGraphy, results of the SENIAM project (CD)*. Roessingh Research and Development, 1999.
- Hogan, N., Krebs, H. I., Rohrer, B., Palazzolo, J. J., Dipietro, L., Fasoli, S. E., Stein, J., Hughes, R., Frontera, W. R., Lynch, D., and Volpe, B. T. Motions or muscles? Some behavioral factors underlying robotic assistance of motor recovery. *Journal of Rehabilitation Research and Development*, 43(5):605–618, 2006.
- Holobar, a. and Farina, D. Blind source identification from the multichannel surface electromyogram. *Physiological measurement*, 35(7):143–165, 2014.
- Holobar, A. and Zazula, D. Multichannel Blind Source Separation Using Convolution Kernel Compensation. *IEEE Transactions on Signal Processing*, 55(9):4487–4496, sep 2007.
- Holobar, A., Minetto, M. A., Botter, A., Negro, F., and Farina, D. Experimental Analysis of Accuracy in the Identification of Motor Unit Spike Trains From High-Density Surface EMG. *IEEE Transactions on Neural Systems and Rehabilitation Engineering*, 18(3):221–229, 2010.
- Holtermann, A., Roeleveld, K., and Karlsson, J. S. Inhomogeneities in muscle activation reveal motor unit recruitment. *Journal of Electromyography and Kinesiology*, 15(2):131–137, 2005.
- Huang, H., Zhou, P., Li, G., and Kuiken, T. Spatial filtering improves EMG classification accuracy following targeted muscle reinnervation. *Annals of biomedical engineering*, 37(9):1849–57, 2009.
- Huang, Y., Englehart, K. B., Hudgins, B., and Chan, A. D. C. A Gaussian mixture model based classification scheme for myoelectric control of powered upper limb prostheses. *IEEE Transactions on Biomedical Engineering*, 52(11):1801–1811, 2005.
- Hudgins, B., Parker, P., and Scott, R. N. A new strategy for multifunction myoelectric control. *IEEE Transactions on Biomedical Engineering*, 40(1):82–94, 1993.
- Jiang, N., Dosen, S., Muller, K.-R., and Farina, D. Myoelectric Control of Artificial Limbs—Is There a Need to Change Focus? [In the Spotlight]. *IEEE Signal Processing Magazine*, 29(5):152–150, 2012.
- Jordanic, M., Rojas-Martínez, M., Mañanas, M. A., and Alonso, J. F. Spatial distribution of HD-EMG improves identification of task and force in patients with incomplete spinal cord injury. *Journal of NeuroEngineering and Rehabilitation*, 13(1):41, 2016.
- Jordanić, M., Rojas-Martínez, M., Mañanas, M. A., and Alonso, J. F. Prediction of isometric motor tasks and effort levels based on high-density EMG in patients with incomplete spinal cord injury. *Journal of Neural Engineering*, 13(4):046002, 2016.

- Kamavuako, E. N., Rosenvang, J. C., Horup, R., Jensen, W., Farina, D., and Englehart, K. B. Surface versus untargeted intramuscular EMG based classification of simultaneous and dynamically changing movements. *IEEE Transactions on Neural Systems and Rehabilitation Engineering*, 21(6):992–998, 2013.
- Kendall, F. P., Kendall McCreary, E., and Provance, P. G. *Muscles: testing and function*. Williams & Wilkins, New York, 4 edition, 1993.
- Knaflitz, M. and Bonato, P. Time-frequency methods applied to muscle fatigue assessment during dynamic contractions. *Journal of Electromyography and Kinesiology*, 9(5):337–50, oct 1999.
- Kupa, E. J., Roy, S. H., Kandarian, S. C., and De Luca, C. J. Effects of muscle fiber type and size on EMG median frequency and conduction velocity. *Journal of Applied Physiology*, 79 (1):23–32, 1995.
- Landa, S. and Everitt, B. S. *A Handbook of Statistical Analyses using SPSS*. Chapman & Hall/CRC, Boca Raton, 2004.
- Li, G., Schultz, A. E., and Kuiken, T. A. Quantifying pattern recognition-based myoelectric control of multifunctional transradial prostheses. *IEEE Transactions on Neural Systems and Rehabilitation Engineering*, 18(2):185–192, 2010.
- Li, X., Samuel, O. W., Zhang, X., Wang, H., Fang, P., and Li, G. A motion-classification strategy based on sEMG-EEG signal combination for upper-limb amputees. *Journal of NeuroEngineering and Rehabilitation*, 14(1):2, 2017.
- Li, Y., Chen, X., Zhang, X., and Zhou, P. Several practical issues toward implementing myoelectric pattern recognition for stroke rehabilitation. *Medical Engineering and Physics*, 36(6): 754–760, 2014.
- Li, Z., Wang, B., Yang, C., Xie, Q., and Su, C. Y. Boosting-based EMG patterns classification scheme for robustness enhancement. *IEEE Journal of Biomedical and Health Informatics*, 2013.
- Liddell, E. G. T. and Sherrington, C. S. Recruitment and some other Features of Reflex Inhibition. *Proceedings of the Royal Society of London B: Biological Sciences*, 97(686):488–518, 1925.
- Lindstrom, L. and Magnusson, R. Interpretation of myoelectric power spectra: A model and its applications. *Proceedings of the IEEE*, 65(5):653–662, 1977.
- Liu, J. and Zhou, P. A novel myoelectric pattern recognition strategy for hand function restoration after incomplete cervical spinal cord injury. *IEEE Transactions on Neural Systems and Rehabilitation Engineering*, 21(1):96–103, 2013.
- Liu, J., Sheng, X., Zhang, D., Jiang, N., and Zhu, X. Towards Zero Retraining for Myoelectric Control Based on Common Model Component Analysis. *IEEE Transactions on Neural Systems and Rehabilitation Engineering*, 24(4):444–454, 2016a.
- Liu, S., Guo, J., Meng, J., Wang, Z., Yao, Y., Yang, J., Qi, H., and Ming, D. Abnormal EEG Complexity and Functional Connectivity of Brain in Patients with Acute Thalamic Ischemic Stroke. *Computational and Mathematical Methods in Medicine*, 2016:1–9, 2016b.

- Loftus, G. R. and Masson, M. E. Using confidence intervals in within-subject designs. *Psychonomic bulletin & review*, 1(4):476–90, 1994.
- Madeleine, P., Leclerc, F., Arendt-Nielsen, L., Ravier, P., and Farina, D. Experimental muscle pain changes the spatial distribution of upper trapezius muscle activity during sustained contraction. *Clinical Neurophysiology*, 117(11):2436–45, 2006.
- Mañanas, M., Romero, S., Topor, Z., Bruce, E., Houtz, P., and Caminal, P. Cardiac interference in myographic signals from different respiratory muscles and levels of activity. *2001 Conference Proceedings of the 23rd Annual International Conference of the IEEE Engineering in Medicine and Biology Society*, 2:1115–1118, 2001.
- Marateb, H. R., McGill, K. C., and Webster, J. G. Electromyographic (Emg) Decomposition. In *Wiley Encyclopedia of Electrical and Electronics Engineering*. John Wiley & Sons, Inc, 1999.
- Marateb, H. R., Farahi, M., Rojas, M., Mañanas, M. A., Farina, D., and Rix, H. Detection of Multiple Innervation Zones from Multi-Channel Surface EMG Recordings with Low Signal-to-Noise Ratio Using Graph-Cut Segmentation. *PLOS ONE*, 11(12), 2016.
- Marchal-Crespo, L. and Reinkensmeyer, D. J. Review of control strategies for robotic movement training after neurologic injury. *Journal of Neuroengineering and Rehabilitation*, 6:20, 2009.
- Merletti, R. and Farina, D. *Surface Electromyography: Physiology, Engineering, and Applications*. Wiley-IEEE Press, Hoboken, New Jersey (USA), 2016.
- Merletti, R. and Hermens, H. Detection and Conditioning of the surface EMG signal. In *Electromyography: Physiology, Engineering, and Noninvasive Applications*, chapter 5, pages 115–120. Wiley, New Jersey, USA, 2004.
- Merletti, R. and Lo Conte, L. R. Surface EMG signal processing during isometric contractions. *Journal of Electromyography and Kinesiology*, 7(4):241–250, 1997.
- Merletti, R. and Parker, P. *Electromyography : physiology, engineering, and noninvasive applications*. Wiley-IEEE Press, 2004.
- Merletti, R., Botter, A., Troiano, A., Merlo, E., and Minetto, M. A. Technology and instrumentation for detection and conditioning of the surface electromyographic signal: State of the art. *Clinical Biomechanics*, 24(2):122–134, 2009.
- Merletti, R., Aventaggiato, M., Botter, A., Holobar, A., Marateb, H., and Vieira, T. M. M. Advances in surface EMG: recent progress in detection and processing techniques. *Critical Reviews in Biomedical Engineering*, 38(4):305–45, 2010.
- Mohebian, M. R., Marateb, H. R., Mansourian, M., Mañanas, M. A., and Mokarian, F. A Hybrid Computer-aided-diagnosis System for Prediction of Breast Cancer Recurrence (HPBCR) Using Optimized Ensemble Learning. *Computational and Structural Biotechnology Journal*, 15:75–85, 2017.
- Mosteller, F. A k-Sample Slippage Test for an Extreme Population on JSTOR. *The Annals of Mathematical Statistics*, 19(1):58–65, 1948.
- Muller-Putz, G., Leeb, R., Tangermann, M., Hohne, J. H., Kubler, A. K., Cincotti, F., Mattia, D., Rupp, R., Muller, K. R., and Millan, J. D. R. Towards Noninvasive Hybrid Brain–Computer Interfaces: Framework, Practice, Clinical Application, and Beyond. *Proceedings of the IEEE*, 103(6):926 – 943, 2015.

- Naik, G. R., Kumar, D. K., and Weghorn, H. Performance comparison of ICA algorithms for Isometric Hand gesture identification using Surface EMG. In *3rd International Conference on Intelligent Sensors, Sensor Networks and Information*, pages 613–618. IEEE, 2007.
- Naik, G. R., Al-Timemy, A. H., and Nguyen, H. T. Transradial Amputee Gesture Classification Using an Optimal Number of sEMG Sensors: An Approach Using ICA Clustering. *IEEE Transactions on Neural Systems and Rehabilitation Engineering*, 24(8):837–846, 2016.
- Nazmi, N., Abdul Rahman, M., Yamamoto, S.-I., Ahmad, S., Zamzuri, H., and Mazlan, S. A Review of Classification Techniques of EMG Signals during Isotonic and Isometric Contractions. *Sensors*, 16(8):1304, 2016.
- Oskoei, M. A. and Hu, H. GA-based feature subset selection for myoelectric classification. *2006 IEEE International Conference on Robotics and Biomimetics, ROBIO 2006*, pages 1465–1470, 2006.
- Oskoei, M. A. and Hu, H. Myoelectric control systems-A survey. *Biomedical Signal Processing and Control*, 2(4):275–294, 2007.
- Park, S. H. and Lee, S. P. EMG pattern recognition based on artificial intelligence techniques. *IEEE Transactions on Rehabilitation Engineering*, 6(4):400–405, 1998.
- Parker, P., Englehart, K., and Hudgins, B. Myoelectric signal processing for control of powered limb prostheses. *Journal of Electromyography and Kinesiology*, 16:541–548, 2006.
- Parker, P. A. and Scott, R. N. Myoelectric control of prostheses. *Critical reviews in biomedical engineering*, 13(4):283–310, 1986.
- Parzen, E. On Estimation of a Probability Density Function and Mode. *The Annals of Mathematical Statistics*, 33(3):1065–1076, 1962.
- Pedregosa, F., Varoquaux, G., Gramfort, A., Michel, V., Thirion, B., Grisel, O., Blondel, M., Prettenhofer, P., Weiss, R., Dubourg, V., Vanderplas, J., Passos, A., Cournapeau, D., Brucher, M., Perrot, M., and Duchesnay, E. Scikit-learn: Machine Learning in Python. *Journal of Machine Learning Research*, 12:2825–2830, 2011.
- Phinyomark, A., Limsakul, C., and Phukpattaranont, P. A Novel Feature Extraction for Robust EMG Pattern Recognition. *Journal of Computing*, 1(1):71–80, 2009.
- Phinyomark, A., Phukpattaranont, P., and Limsakul, C. Feature reduction and selection for EMG signal classification. *Expert Systems with Applications*, 39(8):7420–7431, 2012a.
- Phinyomark, A., Thongpanja, S., Hu, H., Phukpattaranont, P., and Limsakul, C. *Computational Intelligence in Electromyography Analysis - A Perspective on Current Applications and Future Challenges*. InTech, 2012b.
- Pizzigalli, L., Ahmaidi, S., and Rainoldi, A. Effects of sedentary condition and longterm physical activity on postural balance and strength responses in elderly subjects. *Sport Sciences for Health*, 10(2):135–141, 2014.
- Rohm, M., Schneiders, M., Müller, C., Kreilinger, A., Kaiser, V., Müller-Putz, G. R., and Rupp, R. Hybrid brain-computer interfaces and hybrid neuroprostheses for restoration of upper limb functions in individuals with high-level spinal cord injury. *Artificial Intelligence in Medicine*, 59(2):133–142, 2013.

- Rojas-Martínez, M. *Analysis of Forearm Muscles Activity by Means of New Protocols of Multi-channel EMG Signals Recording and Processing*. Phd dissertation, Polytechnic University of Catalonia, 2012.
- Rojas-Martínez, M., Mañanas, M. a., and Alonso, J. F. High-density surface EMG maps from upper-arm and forearm muscles. *Journal of Neuroengineering and Rehabilitation*, 9:85, jan 2012.
- Rojas-Martínez, M., Mañanas, M. a., Alonso, J. F., and Merletti, R. Identification of isometric contractions based on High Density EMG maps. *Journal of Electromyography and Kinesiology*, 23(1):33–42, 2013.
- Scheme, E. and Englehart, K. Training strategies for mitigating the effect of proportional control on classification in pattern recognition-based myoelectric control. *Journal of Prosthetics and Orthotics*, 25(2):76–83, 2013.
- Searle, A. and Kirkup, L. A direct comparison of wet, dry and insulating bioelectric recording electrodes. *Physiological Measurement*, 21(2):271–83, 2000.
- Sensinger, J., Lock, B., and Kuiken, T. Adaptive Pattern Recognition of Myoelectric Signals: Exploration of Conceptual Framework and Practical Algorithms. *IEEE Transactions on Neural Systems and Rehabilitation Engineering*, 17(3):270–278, 2009.
- Sherrington, C. S. Remarks on some Aspects of Reflex Inhibition. *Proceedings of the Royal Society of London B: Biological Sciences*, 97(686):519–545, 1925.
- Simon, A. M., Hargrove, L. J., Lock, B. a., and Kuiken, T. a. A decision-based velocity ramp for minimizing the effect of misclassifications during real-time pattern recognition control. *IEEE Transactions on Biomedical Engineering*, 58(8):2360–2368, 2011.
- Soares, F. A., Carvalho, J. L. A., Miosso, C. J., de Andrade, M. M., and da Rocha, A. F. Motor unit action potential conduction velocity estimated from surface electromyographic signals using image processing techniques. *BioMedical Engineering Online*, 14(1):84, 2015.
- Squire, J. *Muscle: design, diversity, and disease*. Benjamin/Cumnnigs, Menlo Park, CA, USA, 1986.
- Srboj-Egekher, V., Cifrek, M., and Medved, V. The application of Hilbert-Huang transform in the analysis of muscle fatigue during cyclic dynamic contractions. *Medical & biological engineering & computing*, 49(6):659–69, jun 2011.
- Stango, A., Negro, F., and Farina, D. Spatial Correlation of High Density EMG Signals Provides Features Robust to Electrode Number and Shift in Pattern Recognition for Myocontrol. *IEEE Transactions on Neural Systems and Rehabilitation Engineering*, 23(2):189–198, 2015.
- Staudenmann, D., Roeleveld, K., Stegeman, D. F., and van Dieen, J. H. Methodological aspects of SEMG recordings for force estimation - A tutorial and review. *Journal of Electromyography and Kinesiology*, 20(3):375–387, 2010.
- Staudenmann, D., van Dieën, J. H., Stegeman, D. F., and Enoka, R. M. Increase in heterogeneity of biceps brachii activation during isometric submaximal fatiguing contractions: a multichannel surface EMG study. *Journal of neurophysiology*, 111(5):984–90, 2014.

- Stulen, F. B. and De Luca, C. J. Frequency Parameters of the Myoelectric Signal as a Measure of Muscle Conduction Velocity. *IEEE Transactions on Biomedical Engineering*, 28(7):515–523, 1981.
- Tkach, D., Huang, H., and Kuiken, T. a. Study of stability of time-domain features for electromyographic pattern recognition. *Journal of Neuroengineering and Rehabilitation*, 7:21, 2010.
- Tucker, K., Falla, D., Graven-Nielsen, T., and Farina, D. Electromyographic mapping of the erector spinae muscle with varying load and during sustained contraction. *Journal of Electromyography and Kinesiology*, 19(3):373–9, 2009.
- Vaca Benitez, L. M., Tabie, M., Will, N., Schmidt, S., Jordan, M., and Kirchner, E. A. Exoskeleton technology in rehabilitation: Towards an EMG-based orthosis system for upper limb neuromotor rehabilitation. *Journal of Robotics*, 2013:13, 2013.
- Valle, S., Li, W., and Qin, S. J. Selection of the Number of Principal Components: The Variance of the Reconstruction Error Criterion with a Comparison to Other Methods. *Industrial and Engineering Chemistry Research*, 38(11):4389–4401, 1999.
- van Dijk, L., van der Sluis, C. K., van Dijk, H. W., Bongers, R. M., and Scheidt, R. Learning an EMG Controlled Game: Task-Specific Adaptations and Transfer. *PLOS ONE*, 11(8): e0160817, 2016.
- Verikas, A., Vaiciukynas, E., Gelzinis, A., Parker, J., and Olsson, M. Electromyographic Patterns during Golf Swing: Activation Sequence Profiling and Prediction of Shot Effectiveness. *Sensors*, 16(5):592, 2016.
- Vidovic, M. M.-C., Hwang, H.-J., Amsuss, S., Hahne, J. M., Farina, D., and Muller, K.-R. Improving the Robustness of Myoelectric Pattern Recognition for Upper Limb Prostheses by Covariate Shift Adaptation. *IEEE Transactions on Neural Systems and Rehabilitation Engineering*, 24(9):961–970, 2016.
- Vieira, T. M. M., Merletti, R., and Mesin, L. Automatic segmentation of surface EMG images: Improving the estimation of neuromuscular activity. *Journal of Biomechanics*, 43(11):2149–58, 2010.
- Wan, B., Xu, L., Ren, Y., Wang, L., Qiu, S., Liu, X., Liu, X., Qi, H., Ming, D., and Wang, W. Study on fatigue feature from forearm SEMG signal based on wavelet analysis. *2010 IEEE International Conference on Robotics and Biomimetics, ROBIO 2010*, pages 1229–1232, 2010.
- Wang, Y., Li, J., and Li, Y. Measure for data partitioning in m x 2 cross-validation. *Pattern Recognition Letters*, 65:211–217, 2015.
- Widmaier, E. P., Raff, H., and Strang, K. T. *Vander's Human Physiology: The mechanisms of Body Function*. McGraw-Hill Higher Education, 2014.
- Young, A. J., Hargrove, L. J., and Kuiken, T. A. The Effects of Electrode Size and Orientation on the Sensitivity of Myoelectric Pattern Recognition Systems to Electrode Shift. *IEEE Transactions on Biomedical Engineering*, 58(9):2537–2544, 2011.
- Young, A. J., Hargrove, L. J., and Kuiken, T. a. Improving myoelectric pattern recognition robustness to electrode shift by changing interelectrode distance and electrode configuration. *IEEE Transactions on Biomedical Engineering*, 59(3):645–652, 2012.

- Young, A. J., Smith, L. H., Rouse, E. J., and Hargrove, L. J. Classification of simultaneous movements using surface EMG pattern recognition. *IEEE Transactions on Biomedical Engineering*, 60(5):1250–1258, 2013.
- Young, W. Spinal Cord Injury Levels & Classification, W M Keck Center for Collaborative Neuroscience.
- Zardoshti-Kermani, M., Wheeler, B., Badie, K., and Hashemi, R. EMG feature evaluation for movement control of upper extremity prostheses. *IEEE Transactions on Rehabilitation Engineering*, 3(4):324–333, 1995.
- Zhang, X. and Zhou, P. High-Density Myoelectric Pattern Recognition Toward Improved Stroke Rehabilitation. *IEEE Transactions on Biomedical Engineering*, 59(6):1649–1657, 2012.
- Zimmer, C. and Sahle, S. Comparison of approaches for parameter estimation on stochastic models: Generic least squares versus specialized approaches. *Computational Biology and Chemistry*, 61:75–85, 2016.
- Zwarts, M. J. and Stegeman, D. F. Multichannel surface EMG: basic aspects and clinical utility. *Muscle & nerve*, 28(1):1–17, 2003.
- Zwarts, M. J., Lapatki, B. G., Kleine, B. U., and Stegeman, D. F. Surface EMG: how far can you go? *Supplements to Clinical Neurophysiology*, 57:111–9, 2004.

Appendix A

Mean shift algorithm

The mean shift algorithm is a non-parametric approach to estimate the gradient of a density function. It was first proposed by Fukunaga and Hostetler (1975), but did not get a lot of attention of the academic community initially. Although their work was cited more than 1500 times in literature, most of the cites occurred after the famous publication of Comaniciu and Meer in 2002 (counting almost 6000 citations) that revised the method and drew attention of the scientific community to it (Comaniciu and Meer, 2002).

The algorithm is the enhanced version of the Parzen window technique for the estimation of density using a kernel (Parzen, 1962) and its extension to multivariate distributions (Cacoullos, 1966), given that density for the point \mathbf{x} can be estimated based on the observed samples \mathbf{x}_i ($i = 1, 2, \dots, n$) using the kernel function K as:

$$\hat{f}(\mathbf{x}) = \frac{1}{n} \sum_{i=1}^n K_H(\mathbf{x} - \mathbf{x}_i) \quad (\text{A.1})$$

$$K_H = |\mathbf{H}|^{-\frac{1}{2}} K(\mathbf{H}^{-\frac{1}{2}} \mathbf{x}) \quad (\text{A.2})$$

, where $\hat{f}(\mathbf{x})$ is the estimated density, K_H is the normalized kernel function, and H is $d \times d$ bandwidth matrix. The bandwidth matrix H can be fully parameterized, diagonal, or, as in this paper, proportional to identity matrix ($\mathbf{H} = h\mathbf{I}$), which simplifies the expression for the density estimation to:

$$\hat{f}(\mathbf{x}) = \frac{1}{nh^d} \sum_{i=1}^n K\left(\frac{\mathbf{x} - \mathbf{x}_i}{h}\right) \quad (\text{A.3})$$

, where $\hat{f}(\mathbf{x})$ is the estimated density, h is a single bandwidth parameter, d is the number of dimensions, and K is the kernel function. Two commonly used univariate kernel profiles are Epanechnikov (k_E) and Gaussian (k_N):

$$k_N(x) = e^{-\frac{1}{2}x}, \quad x \geq 0 \quad (\text{A.4})$$

$$k_E(x) = \begin{cases} 1-x & 0 \leq x \leq 1 \\ 0 & x > 1 \end{cases} \quad (\text{A.5})$$

, which yield multivariate radially symmetric kernel (K_E) and normal kernel (K_N) respectively:

$$K_N(\mathbf{x}) = \frac{1}{2\pi^{d/2}} e^{-\frac{1}{2}\|\mathbf{x}\|^2} \quad (\text{A.6})$$

$$K_E(\mathbf{x}) = \begin{cases} \frac{1}{2} \frac{d+2}{c_d} (1 - \|\mathbf{x}\|^2) & \|\mathbf{x}\| \leq 1 \\ 0 & \|\mathbf{x}\| > 1 \end{cases} \quad (\text{A.7})$$

, where d is the number of dimension and c_d is the constant that ensures the kernel integrates to one.

Mean shift vector is defined as (Comaniciu and Meer, 2002):

$$\mathbf{ms}(\mathbf{x}) = \frac{\sum_{i=1}^n \mathbf{x}_i g(\|\frac{\mathbf{x}-\mathbf{x}_i}{h}\|^2)}{\sum_{i=1}^n g(\|\frac{\mathbf{x}-\mathbf{x}_i}{h}\|^2)} - \mathbf{x} \quad (\text{A.8})$$

, where $g(x)$ is the negative derivative of the original univariate kernel profile $k(x)$:

$$g(x) = -\frac{dk(x)}{dx} \quad (\text{A.9})$$

Mean shift is a function defined for every point in space. It is a vector of difference between the current position and the weighted mean of all points within its bandwidth h , whose weights are defined by the kernel profile $g(x)$. Therefore, the mean shift vector always points to the direction of maximum increase of the density and can be considered as a function proportional to the gradient of the density function:

$$\mathbf{ms}_g(\mathbf{x}) \propto \nabla \hat{f}_k(\mathbf{x}) \quad (\text{A.10})$$

In addition, mean shift can be effectively used to find modes (local maxima) of the underlying density function by an iterative procedure. Kernel is usually centered at a random point in space and the mean shift vector is calculated. In the next iteration, the kernel is centered at the location pointed by the mean shift vector. The procedure is mathematically defined as:

$$\mathbf{y}_{i+1} := \frac{\sum_{j=1}^n \mathbf{x}_j g(\|\frac{\mathbf{y}_i-\mathbf{x}_j}{h}\|^2)}{\sum_{j=1}^n g(\|\frac{\mathbf{y}_i-\mathbf{x}_j}{h}\|^2)} \quad (\text{A.11})$$

By repeating this procedure, at every step, the center of the kernel is shifted to the direction of maximum increase of the density function until the local maximum is reached. At this location, the difference between two consecutive points is zero (up to a tolerance). These final stationary points are considered to be modes of the probability density function:

$$\mathbf{y}_{i+1} - \mathbf{y}_i = 0 \quad (\text{A.12})$$

$$\mathbf{y}_{i+1} - \mathbf{y}_i = 0 \quad (\text{A.13})$$

$$\mathbf{ms}_g(\mathbf{y}_i) = \nabla \hat{f}_k(\mathbf{y}_i) = 0 \quad (\text{A.14})$$

This algorithm is very useful in image processing and feature space analysis with many applications, of which clustering is the most popular. It only requires setting one parameter, bandwidth

(h). On the other hand, unlike the similar methods, e.g., k -means clustering, it is not necessary to define the number of expected clusters. This is a big advantage because it does not require *a priori* knowledge on the number of clusters. Detailed explanation of the mean shift algorithm can be found in the literature (Comaniciu and Meer, 2002; Fukunaga and Hostetler, 1975).

In this study, modes of the density function of root-mean-square (RMS) activation maps were found using the mean shift algorithm implemented in Python (Pedregosa et al., 2011) and were used as features in the identification. The Epanechnikov kernel profile was employed to describe the density function, which yielded flat kernel profile $g(x)$ in the calculation of the mean shift vector:

$$g(x) = \begin{cases} 1, & \|x\| \leq h \\ 0, & \|x\| > h \end{cases} \quad (\text{A.15})$$

This choice of the kernel profile simplified the update of the mean shift centroid to:

$$\mathbf{y}_{i+1} := \frac{\sum_{j=1}^N \mathbf{x}_j}{N} \Bigg|_{\forall \mathbf{x} \text{ s.t. } \|\mathbf{x} - \mathbf{y}_i\| \leq h} \quad (\text{A.16})$$

In the other words, the new centroid was calculated as the mean value of N points located within the Euclidean distance h from the current centroid.

Appendix B

Pattern recognition

Pattern recognition is a classification technique and the principle by which it is performed is learned independently from the data, i.e., training set. There are two main types of pattern recognition: supervised and unsupervised. Supervised pattern recognition implies that the classes of the training set are known and are used to obtain the model. New inputs are identified as one of the predetermined classes. On the other hand, unsupervised pattern recognition is used when no labels are available and samples are assigned to unknown classes. This technique is more appropriate for the clustering problem because the classes are determined automatically by the system, whereas supervised approach is more appropriate for the classification because classes are defined by the system designer, and, therefore, it is usually used in task identification based on EMG.

In statistical pattern recognition, each sample is composed of m measures that form the pattern, i.e., features $(x_0, x_1, \dots, x_{m-1})$. The objective of the algorithm is to obtain a decision rule, i.e., the decision boundary which separates well samples of different classes. There are many *state-of-the-art* classifiers that use various principles to construct these boundaries. However, many researchers agree that the fidelity of the classification in EMG applications depends mostly on selection of features (Hakonen et al., 2015). In other words, with appropriate selection of features, all classifiers will give similar classification result. A short introduction is provided on the two methods used in the thesis: Linear Discriminant Analysis and Support Vector Machine. Although the SVM is superior in classification performance, the LDA is commonly used in myocontrol applications because of its simplicity and performance in real-time. However, with the increasing computational power of new computer generations, SVM could become more common in these applications.

B.1 Linear Discriminant Analysis

All models are wrong; some models are useful.
George E. P. Box

Linear Discriminant Analysis is a computationally simple and efficient classifier with linear decision boundary and it is based on the Bayesian equation (?). In a classical problem with n

samples in training set, which consist of m features, the dataset of available samples is a matrix of dimension $[n \times m]$, whereas the label that describes the belonging of each sample to one of the classes is y , where $y \in (0, 1, 2, \dots, K - 1)$.

According to Bayesian equation, the probability that a sample \mathbf{x}_0 belongs to a class k is equivalent to the:

$$P(y = k | \mathbf{x} = \mathbf{x}_0) = \frac{P(\mathbf{x} = \mathbf{x}_0 | y = k) P(y = k)}{P(\mathbf{x} = \mathbf{x}_0)} \quad (\text{B.1})$$

, where k represents the class. Term $P(\mathbf{x} = \mathbf{x}_0 | y = k)$ is called the *class-conditional* probability and describes the probability that the sample with exact features \mathbf{x}_0 is encountered within the group of samples belonging to the class k . Term $P(y = k)$ is called the *a priori* probability and describes the probability that the sample belonging to the class k is found within the group of all samples, regardless of the features. Finally, the term $P(\mathbf{x} = \mathbf{x}_0)$ is called the *marginal* probability and describes the probability of finding the sample with exact set of features in the dataset, regardless of the class. Marginal probability can be written as a sum of class-conditional probabilities multiplied by the a priori probabilities for each class:

$$\begin{aligned} P(\mathbf{x} = \mathbf{x}_0) &= P(\mathbf{x} = \mathbf{x}_0 | y = 1) P(y = 1) + \\ &P(\mathbf{x} = \mathbf{x}_0 | y = 2) P(y = 2) + \dots + \\ &P(\mathbf{x} = \mathbf{x}_0 | y = K) P(y = K) \end{aligned} \quad (\text{B.2})$$

Following the Bayesian theory, the hypothesis, i.e., the predicted class of a sample \mathbf{x}_0 is chosen as the class which has the highest probability $P(y = k | \mathbf{x} = \mathbf{x}_0)$:

$$h(\mathbf{x}_0) = \operatorname{argmax}_k P(y = k | \mathbf{x} = \mathbf{x}_0) \quad (\text{B.3})$$

Statistically speaking, this is the best possible classifier. The problem arises in the implementation. The exact probability density functions are unknown and have to be estimated from the available data, which is the source of error. Estimated version of the stated probabilities will be marked with a different symbols to stress out the fact they are just an estimates:

$$p_k(\mathbf{x}) := P(y = k | \mathbf{x}) \quad (\text{B.4})$$

$$g_k(\mathbf{x}) := P(\mathbf{x} | y = k) \quad (\text{B.5})$$

$$\pi_k := P(y = k) \quad (\text{B.6})$$

Linear Discriminant Analysis estimates marginal probability term (π_k) as a ratio of number of samples belonging to class k and the total number of samples, whereas the class-conditional probability term in the Bayesian equation is estimated as a multivariate Gaussian function:

$$g_k(\mathbf{x}) = \frac{1}{(2\pi)^{m/2} |\Sigma_k|^{1/2}} e^{-\frac{1}{2}(\mathbf{x} - \mu_k)^T \Sigma_k^{-1} (\mathbf{x} - \mu_k)} \quad (\text{B.7})$$

, where m is the dimensionality of the feature space, i.e., number of features representing each sample. Function g_k is estimated class-conditional probability of class k , and μ_k and Σ_k are the mean and co-variance matrix for class k , respectively, and they are estimated from the available data as:

$$\mu_k = \frac{1}{n_k} \sum_i \mathbf{x}_i \Bigg|_{\forall \mathbf{x} \in k} \quad (\text{B.8})$$

$$\Sigma_k = \frac{1}{n_k - K} \sum_i (\mathbf{x}_i - \mu_k)(\mathbf{x}_i - \mu_k)^T \Bigg|_{\forall \mathbf{x} \in k} \quad (\text{B.9})$$

, where n_k represents the number of samples belonging to a class k . To simplify the model, LDA assumes that the co-variance matrices Σ_k are the same for all classes:

$$\Sigma_0 = \Sigma_1 = \dots = \Sigma_{K-1} = \Sigma \quad (\text{B.10})$$

and they are usually calculated using the weighted average:

$$\Sigma = \frac{\sum_{k=1}^K n_k \Sigma_k}{\sum_{k=1}^K n_k} \quad (\text{B.11})$$

The consequence of this assumption is the linearity of the decision boundary. Without this assumption the same calculus would lead to quadratic discriminant analysis, which has non-linear boundary.

In a two class example ($y \in \{0, 1\}$), all samples on the decision boundary will have the same probability of belonging to class 0 or 1:

$$D.B. = \left\{ \mathbf{x} \mid P(y = 0 \mid \mathbf{x} = \mathbf{x}_0) = P(y = 1 \mid \mathbf{x} = \mathbf{x}_0) \right\} \quad (\text{B.12})$$

Following this idea, the decision boundary can be estimated by solving the equation:

$$\frac{g_0(\mathbf{x}) \pi_0}{\sum_{k=1}^K g_k \pi_k} = \frac{g_1(\mathbf{x}) \pi_1}{\sum_{k=1}^K g_k \pi_k} \quad (\text{B.13})$$

$$\frac{1}{(2\pi)^{m/2} |\Sigma_0|^{1/2}} e^{-1/2(\mathbf{x}-\mu_0)^T \Sigma_0^{-1} (\mathbf{x}-\mu_0)} \pi_0 = \frac{1}{(2\pi)^{m/2} |\Sigma_1|^{1/2}} e^{-1/2(\mathbf{x}-\mu_1)^T \Sigma_1^{-1} (\mathbf{x}-\mu_1)} \pi_1 \quad (\text{B.14})$$

If making the assumption on the equal co-variance matrices for both classes ($\Sigma_0 = \Sigma_1 = \Sigma$), and taking the logarithm, the equation takes the form:

$$-\frac{1}{2} (\mathbf{x} - \mu_0)^T \Sigma^{-1} (\mathbf{x} - \mu_0) + \log(\pi_0) = -\frac{1}{2} (\mathbf{x} - \mu_1)^T \Sigma^{-1} (\mathbf{x} - \mu_1) + \log(\pi_1) \quad (\text{B.15})$$

, which can be written in the form of the linear function $x^T \beta + \alpha = 0$ as:

$$\mathbf{x}^T (\Sigma^{-1} \mu_0 - \Sigma^{-1} \mu_1) + \frac{1}{2} (\mu_1^T \Sigma^{-1} \mu_1 - \mu_0^T \Sigma^{-1} \mu_0) + \log\left(\frac{\pi_0}{\pi_1}\right) = 0 \quad (\text{B.16})$$

This equation represents the decision boundary between two classes, i.e., all samples lying on this line will have equal probability of belonging to class 0 and class 1. It should be noted that the slope of the line depends only on the class means and co-variance matrix, whereas a priori probabilities (which are the result of number of samples belonging to class 0 or 1) have effect only on the y -intercept term, i.e., the offset of the function. This is an interesting point that demands caution. If groups are unbalanced, that is, number of samples of one group is higher than in the other group, y -intercept of the decision boundary will be affected and the classifier will be biased by this disproportion. If groups are unbalanced because of the incomplete or missing data, whereas in reality they are balanced, this can have a negative effect.

When considering multiclass classification problem, probability of a sample belonging to each class is firstly estimated by the equation:

$$p_k = -\frac{1}{2} \log |\Sigma| - \frac{1}{2} (\mathbf{x} - \mu_k)^T \Sigma^{-1} (\mathbf{x} - \mu_k) + \log(\pi_k) \quad (\text{B.17})$$

and then the class is estimated as the one with the highest probability as:

$$h(\mathbf{x}) = \operatorname{argmax}_k p_k(\mathbf{x}) \quad (\text{B.18})$$

B.2 Support Vector Machine

Try to solve the problem directly and never solve a more general problem as an intermediate step.

Vladimir Vapnik

Support vector machine is nowadays known as a very powerful classifier with a lot of different applications (?). The big advantage over LDA is the fact that it is a *non-parametric* classifier. The model is not obtained using assumptions of the form of the class density function and estimation of its parameters, which is inevitably erroneous. Instead, SVM forms the decision boundary using the samples (not their density estimates) by maximizing the distance between samples and the boundary. This was the idea Vladimir Vapnik, the inventor of this method stood for. It is better to try to solve the problem directly and simply, without many intermediate steps that can be complicated and inaccurate.

In pattern recognition, the decision rule (h) is usually obtained by multiplying the sample (\mathbf{x}) by predefined weights (Θ):

$$\Theta^T \mathbf{x} + \Theta_0 \quad (\text{B.19})$$

, where Θ_0 is a constant. If samples \mathbf{x}_0 and \mathbf{x}_1 lay on the decision boundary, following statements are true:

$$\Theta^T \mathbf{x}_0 + \Theta_0 = \Theta^T \mathbf{x}_1 + \Theta_0 \quad (\text{B.20})$$

$$\Theta^T (\mathbf{x}_0 - \mathbf{x}_1) = 0 \quad (\text{B.21})$$

This result implies that Θ is perpendicular to the boundary:

$$\Theta \perp (\mathbf{x}_0 - \mathbf{x}_1) \quad (\text{B.22})$$

The goal of the SVM is to find the decision boundary between two classes so that the distance between the samples and the decision boundary, i.e., the margin is maximized. The distance (d) from a sample to the decision boundary can be defined as the distance between the sample \mathbf{x} and any point lying on the boundary, \mathbf{x}_0 , projected onto the vector Θ .

$$d = \frac{\Theta^T (\mathbf{x} - \mathbf{x}_0)}{|\Theta|} \quad (\text{B.23})$$

Term $|\Theta|$ is introduced to normalize the vector Θ . Without the normalization the distance would depend on the norm of Θ .

Since \mathbf{x}_0 is on the decision boundary, the expression $\Theta^T \mathbf{x}_0 + \Theta_0 = 0$ is valid, and, therefore, the expression for the distance can be written as:

$$d = \frac{\Theta^T \mathbf{x} + \Theta_0}{|\Theta|} \quad (\text{B.24})$$

Margin (M) can be defined as the distance from the boundary to the closest sample:

$$M = \min_i d_i \quad (\text{B.25})$$

Depending on which side of the boundary the sample is located, the distance can be positive or negative. In order to keep it strictly positive, term y is introduced, where $y \in \{-1, 1\}$:

$$M = \min_i \{y_i d_i\} \quad (\text{B.26})$$

$$M = \min_i \left\{ \frac{y_i (\Theta^T \mathbf{x}_i + \Theta_0)}{|\Theta|} \right\} \quad (\text{B.27})$$

The objective is to maximize the margin M . Since Θ can be rescaled, a certain Θ exists so that $y_i (\Theta^T \mathbf{x}_i + \Theta_0) = 1$, which implies

$$\exists \Theta, y_i (\Theta^T \mathbf{x}_i + \Theta_0) = 1 \Rightarrow M = \min_i \left\{ \frac{1}{|\Theta|} \right\} \quad (\text{B.28})$$

Therefore, to maximize the margin, a separating hyperplane should be found such that a norm of vector orthogonal to the hyperplane (Θ) is minimal.

For every point not on the boundary the following term is valid:

$$y_i (\Theta^T \mathbf{x}_i + \Theta_0) > 0 \quad (\text{B.29})$$

Value C can be selected such that:

$$y_i (\Theta^T \mathbf{x}_i + \Theta_0) > C \quad (\text{B.30})$$

$$y_i \left(\frac{\Theta^T \mathbf{x}_i}{C} + \frac{\Theta_0}{C} \right) > 1 \quad (\text{B.31})$$

Since Θ and Θ_0 can be rescaled, it can be written:

$$\Theta := \frac{\Theta}{C}, \quad \Theta_0 := \frac{\Theta_0}{C} \quad (\text{B.32})$$

, and, therefore:

$$y_i (\Theta^T \mathbf{x}_i + \Theta_0) > 1 \quad (\text{B.33})$$

Finally the optimization problem states:

$$\min \frac{1}{2} |\Theta|^2, \quad s.t. \quad y_i (\Theta^T \mathbf{x}_i + \Theta_0) > 1. \quad (\text{B.34})$$

L_2 norm is preferred because it has continuous derivative, whereas constant $1/2$ is introduced for the mathematical convenience. The optimization is solved using Lagrangian method as:

$$L(\Theta, \Theta_0, \alpha_i) = \frac{1}{2} |\Theta|^2 - \sum_{i=1}^n \alpha_i [y_i (\Theta^T \mathbf{x}_i + \Theta_0) - 1] \quad (\text{B.35})$$

$$\frac{\partial L}{\partial \Theta} = \Theta - \sum_{i=1}^n \alpha_i y_i \mathbf{x}_i = 0 \Rightarrow \Theta = \sum_{i=1}^n \alpha_i y_i \mathbf{x}_i \quad (\text{B.36})$$

$$\frac{\partial L}{\partial \Theta_0} = \sum_{i=1}^n \alpha_i y_i = 0 \quad (\text{B.37})$$

By rewriting the problem in B.35 in terms of dual variable α , the following expression can be obtained:

$$L(\alpha) = \sum_i \alpha_i - \frac{1}{2} \sum_j \sum_i \alpha_j \alpha_i y_j y_i \mathbf{x}_i^T \mathbf{x}_j \quad (\text{B.38})$$

Since this function depends only on dual variable α , the solution can be obtained by maximization:

$$\max L(\alpha) \quad s.t. \quad \begin{cases} \alpha_i \geq 0 \\ \sum_i \alpha_i y_i = 0 \end{cases} \quad (\text{B.39})$$

In this optimization problem, the objective has the form of quadratic function, whereas con-

straints are linear. This problem is typically solved using quadratic programming. Since it is a convex problem, the solution will always be global maximum. Once the dual variable α is found, the primal variable Θ can be calculated using the equation B.36.

In the optimization, Karush-Kuhn-Tucker conditions need to be satisfied (Boyd and Vandenberghe, 2004). One of this condition is *complementary slackness*, stating that in the optimal point (the solution of the problem), the product of dual variable and the constraint must be zero:

$$\alpha_i [y_i (\Theta^T \mathbf{x}_i + \Theta_0) - 1] = 0 \quad (\text{B.40})$$

This condition explains well the principle of SVM. Since the dual variable must be greater or equal to zero ($\alpha \geq 0$), there are two possibilities:

1. If α is greater than zero, $[y_i (\Theta^T \mathbf{x}_i + \Theta_0) - 1]$ must equal one:

$$\alpha_i > 0 \Rightarrow y_i (\Theta^T \mathbf{x}_i + \Theta_0) = 1 \quad (\text{B.41})$$

2. If $[y_i (\Theta^T \mathbf{x}_i + \Theta_0) - 1]$ is greater than zero, α must be zero:

$$y_i (\Theta^T \mathbf{x}_i + \Theta_0) > 1 \Rightarrow \alpha = 0 \quad (\text{B.42})$$

Since for all samples lying on the margin, the statement

$$y_i (\Theta^T \mathbf{x}_i + \Theta_0) = 1 \quad (\text{B.43})$$

holds, α will be greater than zero only for the samples lying on the decision hyperplane, whereas for the samples further away from the hyperplane, α will be zero. Given the fact that Θ depends on linear combination of samples weighted by α (eq. B.36), only the samples lying on the boundary will have effect in the calculation of Θ (where $\alpha > 0$), and they are called *support vectors*. The inconveniency of this approach is the fact that the data need to be linearly separable, i.e., there should not be any data on the other side of the margin, which is rarely the case in practice. For this reason it is called the *hard margin SVM*. Margin has distance one from the boundary and all points have to be distanced more or equal (constraint in eq. B.33).

To relax this constraint, variable β_i is introduced for every sample \mathbf{x}_i , such that $\beta_i \geq 0$:

$$y_i (\Theta^T \mathbf{x}_i + \Theta_0) \geq 1 - \beta_i \quad (\text{B.44})$$

For points lying on the other side of the margin, β will be positive, whereas for the points on the margin or on the correct side of it, it will be zero. This is the ground assumption for *soft margin SVM*. The new optimization problem states:

$$\max \frac{1}{2} |\Theta|^2 + \gamma \sum_{i=1}^n \beta_i \quad s.t. \quad \begin{cases} y_i (\Theta^T \mathbf{x}_i + \Theta_0) \geq 1 - \beta_i \\ \beta_i \geq 0 \end{cases} \quad (\text{B.45})$$

The term $\gamma \sum_{i=1}^n \beta_i$ is introduced to minimize this effect, whereas γ is the constant of penalization. The procedure of solving the problem is the same as in hard margin SVM, using the Lagrangian method:

$$L(\Theta, \Theta_0, \beta_i, \alpha_i, \lambda_i) = \frac{1}{2} |\Theta|^2 + \gamma \sum_{i=1}^n \beta_i - \sum_{i=1}^n \alpha_i [y_i (\Theta^T \mathbf{x}_i + \Theta_0) - 1 + \gamma \beta_i] - \sum_{i=1}^n \lambda_i \beta_i \quad (\text{B.46})$$

$$\frac{\partial L}{\partial \Theta} = \Theta - \sum_{i=1}^n \alpha_i y_i \mathbf{x}_i = 0 \Rightarrow \Theta = \sum_{i=1}^n \alpha_i y_i \mathbf{x}_i \quad (\text{B.47})$$

$$\frac{\partial L}{\partial \Theta_0} = \sum_{i=1}^n \alpha_i y_i = 0 \quad (\text{B.48})$$

$$\frac{\partial L}{\partial \beta_i} = \gamma - \alpha_i - \lambda_i = 0 \quad (\text{B.49})$$

By rewriting the optimization problem in terms of dual variable α , the same term can be obtained as in eq. B.38:

$$L(\alpha) = \sum_i \alpha_i - \frac{1}{2} \sum_j \sum_i \alpha_j \alpha_i y_j y_i \mathbf{x}_i^T \mathbf{x}_j \quad (\text{B.50})$$

, and the new optimization problem states:

$$\max L(\alpha) \quad s.t. \quad \begin{cases} \alpha_i \geq 0 \\ \lambda_i \geq 0 \end{cases} \quad (\text{B.51})$$

However, since objective function $L(\alpha)$ does not depend on dual variable λ_i , the substitution

can be made following the expression in eq. B.49 and the new optimization problem states:

$$\max L(\alpha) \quad s.t. \quad 0 \leq \alpha_i \leq \gamma. \quad (\text{B.52})$$

This is the only difference between hard margin SVM and soft margin SVM.

It is important to state that the optimization problem does not depend on \mathbf{x} , but on $\mathbf{x}^T \mathbf{x}$. This allows the use of *kernel trick* and implicitly enables nonlinear transform of the feature space at little additional cost (?). Usually, non-linear decision boundary can be achieved by nonlinear transform of features:

$$\mathbf{x} \rightarrow \Phi(\mathbf{x}) \quad (\text{B.53})$$

However, this operation is computationally expensive. The solution can be achieved using kernel functions. Kernel is a function $K(x, y)$ for which:

$$K(\mathbf{x}, \mathbf{y}) = \Phi(\mathbf{x})^T \Phi(\mathbf{y}) \quad (\text{B.54})$$

Since in the equation B.37 \mathbf{x} does not appear by itself, but in a form of dot product $\mathbf{x}^T \mathbf{x}$, non-linear transform can be used in a form of kernel trick:

$$L(\alpha) = \sum_i \alpha_i - \frac{1}{2} \sum_j \sum_i \alpha_j \alpha_i y_j y_i K(\mathbf{x}_i, \mathbf{x}_j) \quad (\text{B.55})$$

Most often used kernel is a radial basis kernel ($K_{RBF}(\mathbf{x}_i, \mathbf{x}_j)$):

$$K_{RBF}(\mathbf{x}_i, \mathbf{x}_j) = e^{-\frac{\|\mathbf{x}_i - \mathbf{x}_j\|^2}{2\sigma^2}} \quad (\text{B.56})$$

Although SVM is conceptually designed as a two-class classifier, techniques for multiclass classification also exist, e.g. *one-versus-one* or *one-versus-all* (?).

Appendix C

Identification of isometric and non-isometric upper-limb tasks using HD-EMG

Published as: Rojas-Martínez, M., Alonso, J.F., Jordanić, M., Romero, S., Mañanas, M.A. Identification of isometric and non-isometric upper-limb tasks using HD-EMG *Revista Iberoamericana de Automática e Informática industrial (RIAI)*, Accepted for publication, 2017

doi: _____

Impact Factor: 0.390; Position: 57 of 60 (Q4) AUTOMATION AND CONTROL SYSTEMS; 25 OF 26 (Q4) ROBOTICS.

Abstract: Identification of tasks and estimation of volitional movement based on electromyography (EMG) constitute a known problem that involves different areas in the field of expert systems and particularly pattern recognition, with many possible applications in assistive and rehabilitation devices. The obtained information can be very useful to control exoskeletons or robots used in active rehabilitation processes. The emerging method of high-density electromyography (HD-EMG) opens up new possibilities to extract neural information, and it has already been reported that the spatial distribution of HD-EMG intensity maps is a valuable feature in the identification of isometric tasks.

This study explores the use of the spatial distribution of myoelectric activity and carries out a

task identification during dynamic exercises at different velocities which are much closer to the ones commonly used during therapy. To this end, HD-EMG signals were recorded in a group of healthy subjects while performing a set of isometric and dynamic upper limb tasks. The results show that spatial distribution is a very useful feature in the identification not only of isometric contractions but also of dynamic contractions, so it can be very useful to improve the control of rehabilitation devices, making it more natural and permitting to adapt better to the user.

Keywords: bioengineering; electromyography; neuromuscular; rehabilitation

C.1 Introduction

Every year there are a half million spinal cord injuries and 15 million strokes. These injuries can have an impact on the motor control, resulting in uncoordinated movements, lack of force, and spasticity. In these cases, robot-assisted therapies can be used to stimulate neuroplasticity (?). If the movement intention of a patient could be extracted in the real time, this information could be used to optimally control the assistive device based on the patient's needs, maximizing the benefits of the therapy (Hogan et al., 2006).

The use of the spatial information of the myoelectric activation maps is a novel method that can achieve high results of task identification, both in healthy subjects (Stango et al., 2015), but also in patients with incomplete spinal cord injury (Rojas-Martínez et al., 2013; Jordanic et al., 2016; Jordanić et al., 2016). This study analyses the possibility of using the features extracted from these maps for the identification of set of isometric contractions performed at subjective force levels, and also for the identification of dynamic contractions. Upper-limb motor tasks were recorded in a group of healthy subjects, and were consisted of hand movements in horizontal plane, involving mostly shoulder movements. These tasks were selected because they are usually involved in the therapy with rehabilitation robots (?).

C.2 Methodology

C.2.1 Experimental protocol

Five male subjects participated in the study (age: 24.8 ± 6.1 years, height: 178.6 ± 10.2 cm, weight: 76.8 ± 13.8 kg). They had no neuromuscular or musculoskeletal disorders of the upper limb prior to the recording. HD-EMG signals of muscles associated to the shoulder movement, namely *biceps brachii*, *triceps brachii*, *pectoralis major*, and upper part of the *trapezius*, were recorded on the dominant side using two EMG amplifiers (EMG-USB, OT-Bioelettronica, Turin, Italy) with synchronized sampling (2048 Hz sampling frequency). Using four 2D electrode arrays manufactured in our laboratory, 228 differential EMG channels were measured. Electrode arrays were designed as silver-plated eyelets embedded in the hydrophobic fabric with inter-electrode distance of 10 mm. Arrays were placed so that the center of the array would be positioned following the guidelines of the SENIAM project (Hermens and Freriks, 1999).

Experimental protocol was divided in two parts: a) recording of isometric contractions, and b) recording of dynamic contractions. During the recording of the isometric contractions, subjects were seated upright with their back straight, elbow flexed at approximately 90 degrees, and shoulder in the neutral position (see figure C.1A). Maintaining this position, subjects performed three tasks, pushing a fixed object positioned directly in front of them forward, leftward, and rightward. Each of these tasks was realized at three different effort levels: low, medium, and high. Effort levels were chosen by the subjects following their own perception of the exerted force. In addition, HD-EMG was also recorded during the rest state. Each contraction had the duration of ten seconds with two minute rest period between contractions.

For recording of dynamic contractions, subjects were asked to maintain the previously described posture (straight back and elbow flexed at 90 degrees) and to displace an object over the horizontal plane, following the predefined trajectory (see figure C.1b):

- a) From the center of the plane, located at approximately 30 cm in front of the subject, until the full extension of the shoulder, and return to the center.
- b) From the center to the point located approximately 40 cm leftward, following the trajectory perpendicular to the previous one, and return to the center.

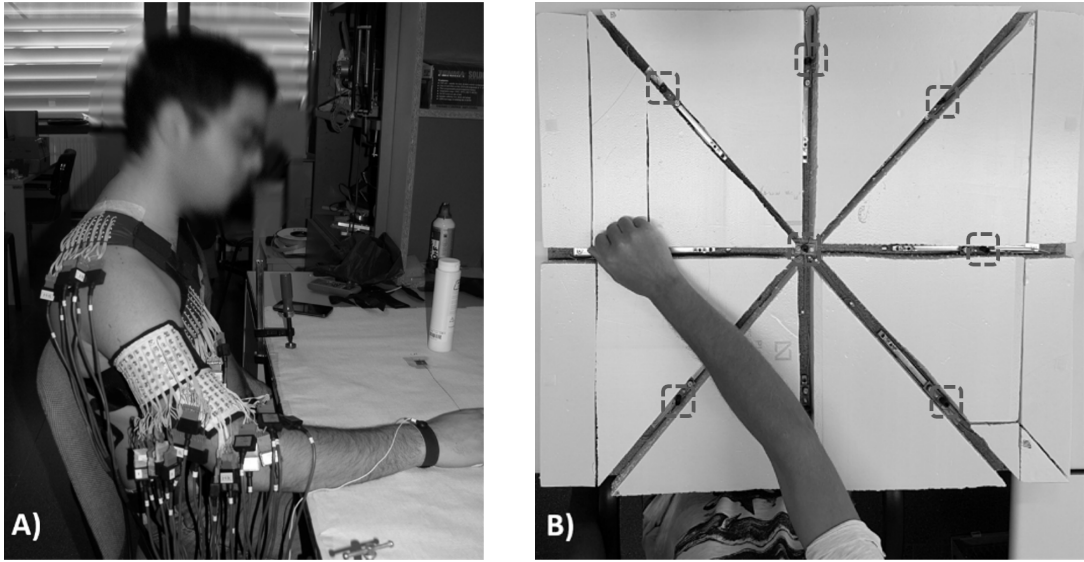


Figure C.1: Figure shows **A**) measurement equipment and the position of the subject during the experimental protocol, and **B**) experimental plane in which the tasks were performed. Position sensors are marked by dashed rectangles.

- c) Repeat the same movement in the other direction, until the point located approximately 40 cm rightward, and return to the center.

Each movement sequence was performed two times at two different velocities, fast and slow, based on the subject's perception, but without change of speed during the sequence. In addition to HD-EMG, positioning signal was also recorded. Proximity sensors were used that generated a signal each time the subject would reach one of the end-points of the trajectory (see figure C.1B).

C.2.2 Signal processing

The recorded signals were filtered using 4th order Butterworth filter with zero-phase. Additionally, signals were filtered using an adaptive filter for reducing the power line interference.

Afterwards, signals were divided in 250 ms time windows without overlapping, and the RMS value was calculated for each channel. Using these values, activation map HM was calculated for each time window as:

$$HM_{i,j} = \sqrt{\frac{\sum_n sEMG_{i,j}^2(n)}{N}} \quad (\text{C.1})$$

, where $N = 512$ samples (corresponding to time window of 250 ms), i and j are positions (row

and column in the electrode array) of the sEMG channel, which correspond to the position (i, j) of the pixel in the activation map HM . The channels identified as artifacts were substituted using the triangle-based cubic interpolation (Rojas-Martínez et al., 2012).

From these activation maps following features were extracted: logarithm of the average intensity of the map (Ilog), and the center of gravity (CG). In the first case, it was already shown that the logarithmic transform is useful in the identification of effort levels (Rojas-Martínez et al., 2012), and in the second case, it was shown that the spatial distribution of myoelectric activity changes with the force level (Holtermann et al., 2005), and with the isometric task intention (Jordanic et al., 2016).

On the other hand, positioning signal recorded during dynamic part of the protocol was used to sort the HD-EMG signal epochs in order to obtain the segments corresponding to each of the movements described in the protocol.

C.2.3 Movement classification

The classification was realized for each subject individually, both for the isometric tasks, and for the dynamic tasks. For the isometric tasks, two types of the classification were considered:

- a) identification of four tasks regardless of the effort level (rest, push forward, push leftward, push rightward)
- b) identification of tasks and effort levels (identification of three tasks at three different effort levels, and the rest state)

The identification of the isometric tasks was performed to validate the experimental protocol. Although in our previous work we managed to identify isometric tasks with high sensitivity and precision, using both intensity and spatial features, the tasks considered in that studies were related to the elbow, and not to the shoulder (Jordanic et al., 2016; Jordanić et al., 2016; Rojas-Martínez et al., 2013).

For the dynamic task, the identification consisted of the classification of each of the following tasks:

- a) move forward

- b) return back to the center
- c) move leftward
- d) return back to the center
- e) move rightward
- f) return back to the center

For the task identification, a classifier based on the linear discriminant analysis (LDA) was used, a technique often used in myoelectric pattern recognition because of the speed and low computational complexity (?).

In the case of isometric contractions, database was separated in two groups, training set, consisting of 60% of the available data, and test set, consisting of 40% of the available data. This data separation, followed by the training and classification was repeated 100 times in order to minimize the possible statistical error (hold-out validation method). The identification results reported in the study are the result averaged over all iterations.

In the case of dynamic contractions, classifier was trained using the observations recorded in one recording sequence (both for slow and fast movements), and validated using the observations recorded in the other sequence. Afterwards, the training set and the test set were swapped and the identification was repeated. The reported results are the average of these two identifications. This type of validation was used to reduce the possible statistical error, although it is possible that in the second recording subject learned how to control the velocity and perform the exercise better.

Finally, the performance of the classification was expressed in terms of sensitivity (S) and precision (P) (Farina et al., 2001), calculated as:

$$S = \frac{TP}{TP + FN} \quad (\text{C.2})$$

$$P = \frac{TP}{TP + FP} \quad (\text{C.3})$$

, where TP is the number of true positives, that is, correctly classified samples, FP is the number of false positives, which indicate the number of wrongly classified samples to a certain class, and

FN is the number of false negatives, that is, the number of samples incorrectly classified to another class. The sensitivity (S) and precision (P) were obtained for each of the classes, and the averaged resultd were calculated.

C.3 Results

C.3.1 Activation maps

In the figure C.2 activation maps of *pectoralis major* are shown. Different activation patterns can be observed during the performance of dynamic tasks. It should be noted that the activation intensity depends on the task, presenting the highest activation (in mV) during the return from full forward extension to the center of the plane, and the reverse. Also, it can be noted that the spatial distribution changes depending on the exercise, for example, during the contraction associated with the forward movement (see figure C.2a), the activation is located at the left side of the map (columns 1 to 3), whereas in the rightward movement (see figure C.2b), the area with higher activity is located in the right part of the map (column 8, rows 2 to 4). Although only maps of *pectoralis major* are shown, the similar differentiation can be found in the remaining three muscles, which is used as a feature in the identification.

C.3.2 Isometric task identification

To test if the spatial distribution of intensity improves the identification, two types of identification were performed: the identification based only on intensity features, and the identification based on the combination of intensity and spatial features. Additionally, identification of task was performed (forward, rightward, leftward, and rest), and the identification of task and effort levels. The results of the task identification, regardless of the effort level are shown in table C.1, whereas the results of the identification of task and effort level are shown in table C.2.

It can be seen that by adding center of gravity to intensity features, results improve for approximately 10% in the case of the task identification and 5% in the case of the identification of task and effort level. Moreover, since when using center of gravity, standard deviation is smaller, it can be concluded that spatial distribution has a positive effect on the identification.

Table C.1: Results of the identification of isometric tasks using the Ilog features and the combination of Ilog and CG features. The results are presented as the mean and the standard deviation calculated across five subjects.

Task	Ilog		Ilog + CG	
	Sensitivity	Precision	Sensitivity	Precision
Forward	73 ± 13	77.1 ± 15	92.1 ± 6.9	93.6 ± 6.4
Rightward	83.5 ± 16	92 ± 9.4	96.2 ± 4.9	95.9 ± 3.9
Leftward	85.8 ± 14	87.3 ± 13	96.1 ± 5.4	97.8 ± 5
Rest	98.7 ± 2.1	87.1 ± 3.2	100 ± 0	98.5 ± 3.4
Mean	85.3 ± 11.2	85.9 ± 10.2	96.1 ± 4.3	96.4 ± 4.7

Table C.2: Results of the identification of isometric tasks and effort levels using the Ilog features and the combination of Ilog and CG features. The results are presented as the mean and the standard deviation calculated across five subjects.

Task	Force	Ilog		Ilog + CG	
		Sensitivity	Precision	Sensitivity	Precision
Forward	low	91.4 ± 14	89.8 ± 12	99 ± 2.3	99.2 ± 1.7
	medium	86.4 ± 25	88.8 ± 16	96.7 ± 7.5	99.4 ± 1.4
	high	87.7 ± 14	89.9 ± 14	95.8 ± 6	98.5 ± 3.4
Rightward	low	98.3 ± 3.7	89.4 ± 11	97.7 ± 3.6	94.6 ± 7.5
	medium	90.4 ± 18	91.3 ± 6.5	98.3 ± 3.7	98.3 ± 3.9
	high	98.3 ± 3.9	100 ± 0	100 ± 0	99.2 ± 1.7
Leftward	low	96 ± 5.1	92.1 ± 8.3	96.9 ± 7	95.2 ± 7.3
	medium	85.7 ± 5.9	85.3 ± 11	94.4 ± 7.8	94.8 ± 7.4
	high	93.9 ± 7.1	96 ± 7.2	98.3 ± 3.7	97 ± 6.6
Rest		97.5 ± 5.6	98.5 ± 3.4	100 ± 0	99 ± 2.2
Mean		92.6 ± 10.2	92.1 ± 8.9	97.7 ± 4.2	97.5 ± 4.3

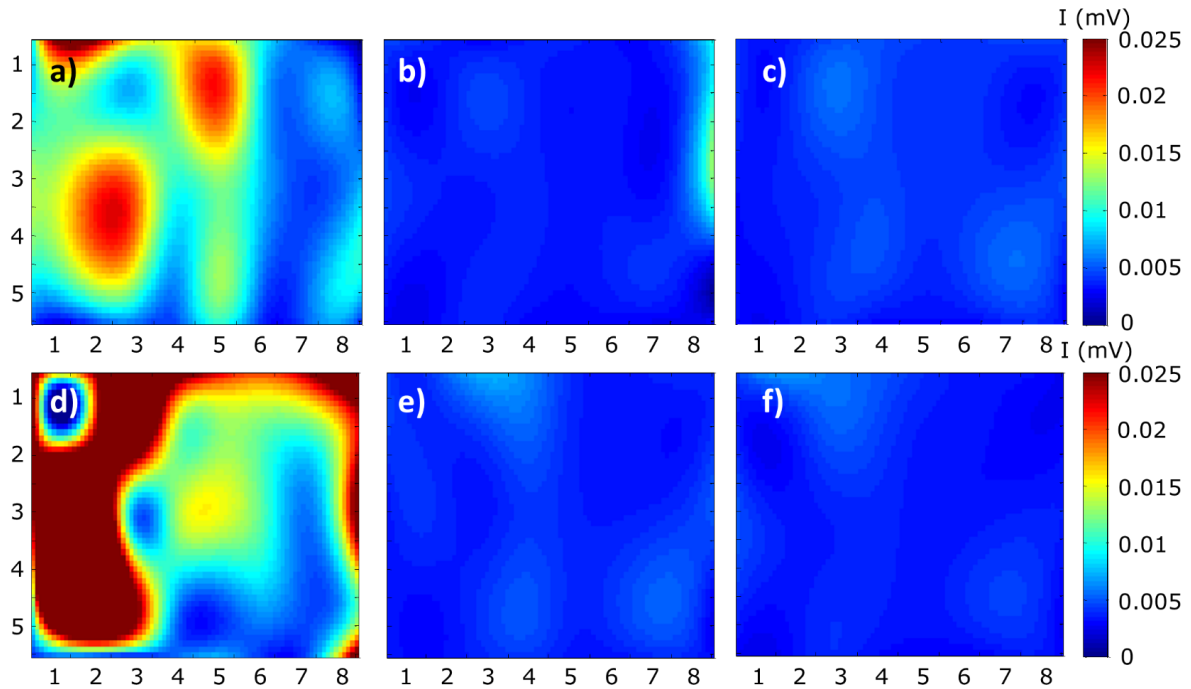


Figure C.2: Activation maps of *pectoralis major* of one of the subjects. Up. Movement from the central point a) forward, b) rightward, and c) leftward. Down. Movement toward the center from d) ahead, e) right, and f) left.

C.3.3 Dynamic task identification

In the case of dynamic task identification, 6 classes were considered: move forward and return, move leftward and return, and move rightward and return.

Tables C.3 and C.4 show the results obtained by averaging the results of each patient, using only intensity features (table C.3), and combination of intensity and spatial features (table C.4). As in isometric contractions, identification results are higher when combining intensity and spatial features.

Higher variability can be observed compared to the isometric task identification, as well as lower sensitivity and precision, as could be expected since the dynamic contractions represent a more complex problem. Finally, it should be noted that although the mean identification results of fast movements are higher than slow movements, the variability is higher in the identification of fast movements. Therefore, it can not be said with certainty that fast movements can be identified with higher identification results.

Table C.3: Identification of six dynamic contractions based on the intensity features, separately for slow movements and fast movements. The results are presented as the mean and the standard deviation calculated across five subjects.

		Slow		Fast	
		Sensitivity	Precision	Sensitivity	Precision
From the center	Leftward	60.7 ± 12.6	68.8 ± 7.9	77.2 ± 14.1	74.9 ± 13.5
	Rightward	87.7 ± 7.8	79.6 ± 8.7	77.2 ± 14.3	75.7 ± 12.0
	Forward	77.9 ± 9.9	74.8 ± 10.1	76.8 ± 13.6	77.0 ± 10.6
Toward center from	Ahead	73.4 ± 11.8	74.7 ± 11.1	80.4 ± 14.2	75.5 ± 9.5
	Right	68.8 ± 11.5	75.7 ± 12.1	85.4 ± 9.3	78.8 ± 10.4
	Forward	71.8 ± 9.0	72.9 ± 8.3	78.3 ± 20.9	71.9 ± 15.6
Mean		73.4 ± 10.4	74.4 ± 9.7	79.2 ± 14.4	75.7 ± 11.9

Table C.4: Identification of six dynamic contractions based on the combination of intensity and spatial features, separately for slow movements and fast movements. The results are presented as the mean and the standard deviation calculated across five subjects.

		Slow		Fast	
		Sensitivity	Precision	Sensitivity	Precision
From the center	Leftward	85.0 ± 13.1	83.1 ± 5.7	94.4 ± 11.4	94.0 ± 13.3
	Rightward	94.8 ± 3.4	91.9 ± 7.9	95.6 ± 9.2	90.6 ± 14.6
	Forward	84.4 ± 11.0	86.7 ± 11.0	95.4 ± 9.2	90.4 ± 13.8
Toward center from	Ahead	92.3 ± 7.1	92.4 ± 12.8	93.7 ± 14.1	93.7 ± 14.1
	Right	85.1 ± 6.2	86.7 ± 6.6	96.6 ± 7.1	92.1 ± 12.1
	Forward	81.0 ± 5.6	89.7 ± 7.4	91.8 ± 11.0	85.5 ± 14.0
Mean		87.1 ± 7.7	88.4 ± 8.6	94.6 ± 10.3	91.0 ± 13.6

C.4 Conclusions

Results show that in all cases identification can be improved by adding spatial features, i.e., center of gravity to the intensity features. This fact implies that the task-dependent patterns exist in the spatial domain, both in the isometric tasks and in the dynamic tasks. Besides improving the average identification results, by adding features based on the spatial distribution, standard deviation of the results is lower, which improves the robustness of the identification.

This results confirm the previous findings in the literature (Hargrove et al., 2007; ?; Jordanic et al., 2016; ?) that there is a neuromuscular compartmentalization within the muscles, and that different muscle areas activate during different tasks.

Moreover, in the case of isometric contractions, besides identifying only task (forward, rightward, and leftward), it is also possible to identify force level, which enables simultaneously controlling task and force, which is an important step towards the control of external devices in a natural way.

On the other hand, identification results of the dynamic contractions are lower than the identification results of the isometric contractions. These results can be expected since the dynamic contractions imply joint movement and shortening of the muscle fibers, which has an effect on the sEMG signal and increases the complexity of the classification problem. Moreover, the velocity of the movement is decided by the subject, which makes it subjective, and more difficult to classify, as would be the case during the rehabilitation. In spite of these difficulties, the obtained results are very promising (sensitivity and precision close to 90%), but should be improved further in terms of identification indices and robustness.

The overall results of the identification of fast and slow movements are similar. Although the identification of fast movements has higher identification indices, the standard deviation is also higher (>10%), and, therefore, it cannot be concluded with certainty that the identification depends on the speed of the movement. To establish this relationship, more tests should be performed on the database containing more subjects.

As a general conclusion, it was demonstrated that the proposed methodology and the obtained results are promising and that the information extracted from the HD-EMG can be useful in controlling of external devices, e.g. rehabilitation robots.

As a future works, the protocol should be extended to the patients with neuromuscular im-

pairments, where the motion intention could be extracted from intensity and spatial domain of HD-EMG recordings in order to control external devices like rehabilitation robots.

C.5 Acknowledgments

The authors are grateful to Ignasi Gallardo for his collaboration in the design of the study.

This work has been partially supported by the project ROBERT of the CIBER-BBN, and by the Spanish Ministry of Economy and Competitiveness (project DPI2014-59049-R).